Novel Intermediate Filament Proteins in *Ramazzottius varieornatus* and *Todarodes pacificus*

Author

Thomas Wilkening

Van Mildert College

Supervisors

Prof. Roy Quinlan

Dr. Martin Goldberg

A thesis submitted in fulfilment for the

degree of Master of Science by Research

Academic Years 2019/2021

at the

Faculty of Science

Department of Biosciences

Durham University

Abstract

Tardigrades are an extremophile invertebrate phylum increasingly popular in astrobiological research and science journalism on account of their extreme resilience. *Ramazzottius varieornatus* possesses three intermediate filament proteins; orthologs of an A-type lamin 2, a B-type lamin 1 and a cytoplasmic intermediate filament called cytotardin found in *H. dujardini*. This project aims to investigate to what extent the molecular similarities between the novel cytoplasmic intermediate filament and its lamin counterparts leads to similar *in vitro* properties. To this end, this protein, mutants thereof and a novel eye lens intermediate filament protein in *Todarodes pacificus* possessing molecular structural similarities to the tardigrade proteins, were produced and examined. Sequence and simulated biochemical analysis, as well as the nature of the rapid *in vitro* assembly of multiple superstructures indicates the lamin-like behaviour of the tardigrade cytoplasmic intermediate filament, whose central rod domain has the proportions of a Type V intermediate filament. Cytotardin is shown by electron microscopy, quantified by sedimentation assay, to be able to form paracrystalline structures across a wide range of pH and ionic strengths with a 24-25nm banding pattern characteristic of lamins. Substitution of an α-helix arginine residue for cysteine in the conserved LNTR motif mimics the keratin-14 mutation first associated with Epidermolysis Bullosa, causing partial loss of function. Deletion of the tail segment of cytotardin removes the ability to form sustainable paracrystals, let alone do so without divalent cations, supporting current models for intermediate filament assembly. Cytotardin and the A-type lamin appear closely related, based on their sequence identity and Western blot analysis and are capable of forming complex paracrystals with mobile structures. The *in vitro* networks of cytotardin and the A-Type lamin create viscous reticuli and gels in the solutions they inhabit. Western blot analysis shows both cytotardin and to a lesser extent the two *R. varieornatus* lamins are recognised by rabbit serum antibodies against *T. pacificus* eye lens protein.

Contents

Acknowledgements

Massive thanks to Professor Roy Quinlan, who believed in me and this research. To Muhammad Al-Ansari, who inspired and taught me with his scientific skill, conscientiousness, and confidence. To Professor David Harper, who inspired me in academia and research.

Special Mentions Also To:

Dr Kathryn Hughes	Jessica Bozak
Dr Natalie Young	Taylor Fitzsimons
Dr Alexia Kalligeraki	Elizabeth Mantle
Dr Alice Uwineza	Gemma Gordon
Dr Kleopatra Papa	Alex Boyadjiev

An amazing cohort of colleagues who have showed me great ways to do science in a myriad of circumstances and occasions.

Oliver Alanis	Vicky Kelly
Christine Richardson	Gillian Summerill
Prof. Iakowos “Akis” Karakesisoglou	Beccy Manning
	Dr Adrian Brown

For keeping the department and lab running during a most challenging situation.

Prof. Heather Kelly	Prof. Paula Chadwick

My undergraduate academic advisors whose support and council they were kind enough to keep me in touch with.

Prof. John Girkin	Dr Chris Saunter
Dr Richard Thompson	Dr Penelope Lawton
Dr Anders Aufderhorst-Roberts	Dr Martin Goldberg

Materials, Biophysics and Microscopy experts of excellent calibre who lent their recommendations / assistance to the biophysical approaches discussed.

Prof. Takekazu Kunieda, Dr Lars Hering and Dr. Slava Tomarev

For work instrumental to the questions we will now be asking.

Declaration of Authorship

I, Thomas Wilkening, declare that this thesis titled, 'Novel Intermediate Filament Proteins in *Ramazzottius varieornatus* and *Todarodes pacificus'* and the work presented in it are my own.
I confirm that:

This work was done wholly or mainly while in candidature for a research degree at this University.
Where any part of this thesis has previously been submitted for a degree or any other qualification at this University or any other institution, this has been clearly stated.
Where I have consulted the published work of others, this is always clearly attributed.
Where I have quoted from the work of others, the source is always given. With the exception of such quotations, this thesis is entirely my own work.
I have acknowledged all main sources of help.
Where the thesis is based on work done by myself jointly with others, I have made clear exactly what was done by others and what I have contributed myself.

Signed: TMWilkening
Date: 24/09/2021

Acronyms and Abbreviations

a.a.	Amino Acid
AKA	Also Known As
bp	Base Pairs [of DNA]
CAHS	Cytoplasmic Abundant Heat Soluble
Cu-P	Copper 1-10 phenanthroline, also known as cupric phenanthroline
DROME	*D. melanogaster*, Abbreviation as found on Uniprot
DTT	Dithiothreitol, reducing agent
EDTA	Ethylenediaminetetraacetic acid, chelating agent
FABP	Fatty Acid Binding Proteins
GuHCl	Guanidine hydrochloride, also known as guanidinium chloride.
HDJD	*H. dujardini*, also known as *Hypsibius exemplaris*
HSP, Hsp	Heat Shock Protein
HPLC	High Pressure/High Performance Liquid Chromatography
IBP	Inclusion Body Preparation
IEC	Ion Exchange Chromatography
IF	Intermediate Filament
IMAC	*Isotomurus maculatus*
kDa	kiloDaltons; approximately equivalent to kg/mol or 1000 C_{12} nucleons
MAHS	Mitochondrial Abundant Heat Soluble
mcl	Microlitres, µl
MWt	MWt
PefaBloc	A commercial name for AEBSF, or 4-(2-aminoethyl)-benzene-sulfonyl fluoride
PMSF	Phenylmethanesulfonylfluoride
POI	Protein Of Interest
RAMVA	*R. varieornatus*, Abbreviation as found on Uniprot
RCF	Relative Centrifugal Force
SDS PAGE	Sodium Dodecyl Sulphate Polyacrylamide Gel
SEM, TEM	Scanning Electron Microscopy, Transmission Electron Microscopy
TEAB	Triethylammonium bicarbonate
TMAE column	Trimethyl aminoethyl column, commonly used for Ion Exchange Chromatography
***T. pacificus*, TPAC**	*Todarodes sloanei pacificus* (Steenstrup, 1880), also known as *Ommastrephes pacificus* (Steenstrup, 1880), *Ommastrephes sloani pacificus* (Sasaki, 1929), or simply *Todarodes pacificus.*
Tris-HCl, Tris Buffer	Tris(hydroxymethyl)aminomethane Buffer, also known as tromethamine or THAM in medical contexts. Paired with HCl for the buffers in this study.
ULF	Unit Length Filament
wt, WT	“wild type”, that is the non-mutated/most common allele form of the protein

List of Figures and Tables

“Cute fat bugs with eight legs and sloth-like claws, that don’t die when dry and like moss have strange Type V cell strings. They look to be in the smart part of cells but are not. Why? Why are they different from other Type V cell strings?”

- Myself, tasked to explain this Thesis in words of one syllable by Prof. J Bothwell, Durham

Part I - Literature Review

I.1 - Intermediate Filaments

Intermediate filament proteins are cytoskeletal components of intermediate width between the 5-7nm wide actin filaments and the 25nm wide microtubules, identifiable through their distinctive α-helical rods and tendency to form filaments (Parry and Steinert, 1999). Alongside actin and microtubules, IFs make up the basic cytoskeletal components of metazoan cells; unlike microtubules, IF distribution in cells is not associated directly with the distribution of the endoplasmic reticulum or mitochondria (Bohdan *et al*., 1992). Microtubules are vulnerable to collapse under pressure, filamentous actin networks need constant reassembly via treadmilling to stay stable, let alone cope with pressures such as osmotic swelling, and both require energy input via nucleoside triphosphates to do so. IF proteins which do neither (Herrmann and Aebi, 2000) and need no energy input, keep steady to ensure critical structural stability in extreme osmotic scenarios like anhydrobiosis, resilience against which tardigrades are known to display in the extreme (Hengherr *et al*., 2007; Møbjerg *et al*., 2011). Over 75 human diseases have been linked to various mutations in IF proteins (Omary *et al*., 2004; Godsel *et al*., 2008). However, incomplete understanding of filament structure limits understanding of IF-related genetic conditions.

All IFs share two major molecular characteristics: first, their capacity to self-assemble, at least in physiological pH buffers in the absence of macromolecular cofactors (Godsel *et al*., 2008; Kelemen, 2017); second, the three section structure, consisting of a conserved α-helix rod domain (itself 3-4 parts with non-coiled coil linker domains) flanked by non–α helical head and tail domains of different size, sequence, and function (Herrmann and Aebi., 2000; Kelemen, 2017). The α-helical rod domain of IF proteins forms coiled-coil units that polymerize into non-polar filaments. It contains a characteristic heptad repeat pattern, denoted a, b, c, d, e, f, and g, with hydrophobic residues usually being in positions a and d, polar residues elsewhere, and positions e and g usually being charged (Parry *et al*., 1977; Quinlan *et al*., 1986). This leads to an α-helical structure with a long hydrophobic region on its surface which is flanked by charged residues and thus suitable for binding to a similar α-helix. This leads to them wrapping around each other in parallel with the hydrophobic side chains of one α-helix interacting with those of the second one, while the more hydrophilic amino acid (a.a.) side

chains are left exposed to the aqueous environment, thus yielding a two-stranded α-helical coiled-coil structure (Herrmann *et al.*, 2009). The basic building block of common to all IF proteins is a dimer, prone to itself dimerising in an antiparallel manner to a create a tetramer (Giesler *et al.*, 1985), which is itself a basic building block for many vertebrate cytoplasmic IFs (Soellner *et al.*, 1985). The driving force of assembly for the resultant dimers involves both the rod and the terminal domains. Chemical cross-linking studies on assembled cytoplasmic IFs show three types of dimer lateral association: this begins with A_{11} interaction between the "knob" and "pocket" regions (Fig. 1.1) of 1B coiled coil segments of opposing dimers (best characterised in canonical IF types II-IV (Eldirany *et al.*, 2019, 2021), and the A_{22} interaction between the coil 2B segments of opposing dimers. These interactions have been linked to the conserved LNDR and TYRKLLEGE at coils 1a and 2 respectively in chicken lamins, although less so in lamin-like chicken eye lens IF CP49 (Quinlan *et al.*, 1996; 1999). What follows in the mature filament is an unstaggered A_{12} interaction between the two coils in a mature filament (Quinlan and Franke, 1982, Steinert *et al.*, 1993b).

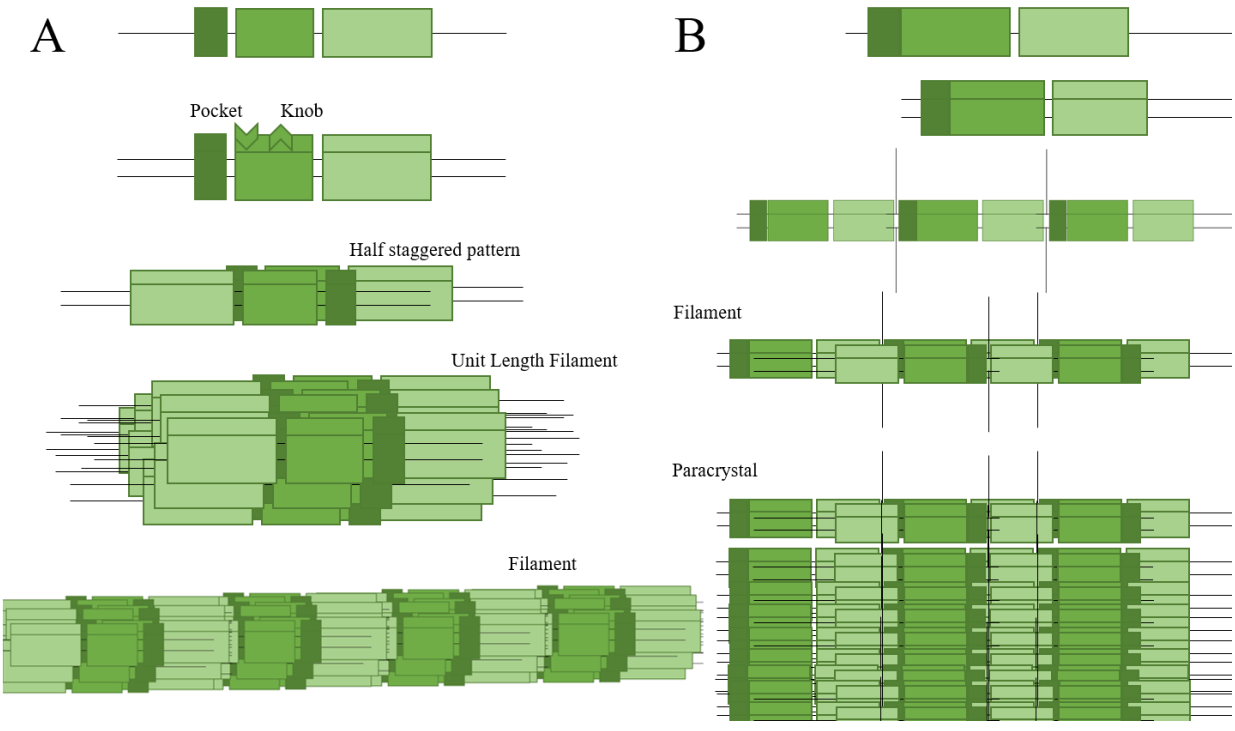

***Fig. 1.1*:** IF Assembly in A: Vertebrate Cytoplasmic IFs and B: Lamins

IF polymerization is a hierarchical process using a combination of lateral and longitudinal, cis and trans associations of IF monomers (Herrmann and Aebi, 2004; Block *et al*, 2015).

Filamentation of vertebrate cytoplasmic IFs such as vimentin, keratin and desmin is has been extensively characterised in three steps: the first step initiates with rapid (within a matter of seconds) lateral association of circa 50nm monomers (for example 50.9nm for keratin; Steinert *et al*., 1993a) into circa 45nm hydrophobically bound dimers (for example 46.2nm for keratin and 43.9 nm for vimentin; Steinert *et al*., 1993b). These form longer non-polar overlapping tetramers via salt bridge interactions (Ahn *et al.*, 2019), with eight tetrameric subunits forming 60–65 nm Unit Length Filaments (ULFs; Herrmann *et al*, 1999); in the second step, filaments grow longer by end-to-end attachment of ULFs (Portet *et al*, 2009); and the third step consists of compaction, resulting in approximately 10 nm thick filaments (Fig. 1.1, Stromer *et al*, 1987). This process does not require a chemical energy source like ATP and does not depend on any co-factors, as evidenced by how *in vitro* it can be induced by simple increases to the ionic strength (Lilina *et al*., 2020).

Lamins also follow a hierarchical polymerization process, but their filament assembly differs from cytoplasmic IFs. Initially, two lamin polypeptide monomers associate laterally into dimers with their domains being parallel. Here, the tetramers are about 75nm long and 3.5nm in diameter (Turgay *et al*., 2017), and instead of lateral assembly from ULFs, (Fig. 1.1) they first form of thinner, highly flexible filaments, which are known as protofilaments (Min *et al*., 1996, Strelkov *et al*., 2004). Head-to-tail attachment, or the A_{CN} interaction, of dimers results in thin protofilaments with a “beaded” appearance because of the immunoglobulin-like tail domain (Ben-Harush *et al*., 2009). Subsequent lateral association of protofilaments is modelled as happening via dynamic grooves within the ends of coil dimers 1B, rather than the knobs and pockets (Eldirany *et al*., 2019) of cytoplasmic IFs leads to thick bundles which compact as a result (Ahn *et al.*, 2019). With the addition of cations to promote charge based adhesion between the tail domains, the lamins self-assemble into characteristic paracrystal with a 25 nm striation pattern (Stuurman *et al*, 1998; Karabinos *et al.*, 2003; Herrmann and Aebi, 2004). *In vivo*, however, they stay at a 3.5nm diameter and instead form a lattice structure called the nuclear lamina (Goldberg *et al*., 2008; Turgay *et al*., 2017).

I.1.1 - Structural Evolution

The IF molecular structure shows significant conservation of sequence, but an even more striking conservation of molecular structure, in the central rod domain. IFs have been

documented in arthropods and other invertebrates, these have extensively diverged from the evolutionary path taken by *Chordata* and do not usually include cytoplasmic IFs (Steinert and Roop, 1988; Weber *et al.*, 1989; Kollmar, 2015). The fact that some did challenged the existing assumption that cytoplasmic IFs were only found in vertebrates, as for example as collembolans and copepods may also have cytoplasmic IFs, as well as the basal chordate *Branchiostoma* (Karabinos *et al*., 1998). The difference between vertebrate and invertebrate cytoplasmic IFs lies in a characteristic 42 a.a. deletion found in vertebrate cytoplasmic IFs on the end of coil 1b. This seems to have occurred entirely in line with the development of the phylum *Chordata* as while the urochordates such as *Ciona* and *Styela* (Wang *et al*., 2000) possesses a lamin much resembling cytotardin, even their cytoplasmic IFs possess the vertebrate-like deletion. Meanwhile, in comparatively close evolutionary distance, the cytoplasmic IFs of the hemichordate *Saccoglossus kowalevskii* and the priapulid *Priapulus caudatus* both retain the full length coil 1B segment characteristic for cytoplasmic IF proteins across protostomic phyla. The hemichordate cytoplasmic IF follows in domain organisation much more closely protostomic IF proteins than true vertebrate IF proteins. This, and the lack of tail motifs also exhibiting homology to lamins is a molecular phenotype of cytoplasmic IFs only so far found in *Chordata*, indicating a single evolutionary event. As such, the canonical IF families I to IV identified in vertebrates almost certainly arose by gene duplications and sequence drift post-deletion in coil 1b very shortly after *Chordata* became a distinct clade (Zimek *et al*., 2002). Invertebrate IFs with lamin-like sequences include the *T. pacificus* squid eye lens protein L10112.1 (Tomarev *et al*., 1993) and cytotardin (Hering *et al*., 2016). Lamins in general, even in vertebrates, are more similar to invertebrate cytoplasmic IF proteins than they are to vertebrate cytoplasmic IF proteins or many invertebrate lamins (Lin and Worman, 1993), implying that an ancestral lamin gave rise to the first cytoplasmic IF proteins in separate events in invertebrates, which retained the 42 a.a. signature (Kaufmann *et al*., 1983; Blumenberg, 1989; Heitlinger *et al*., 1992; Erber *et al*., 1999; Galiova *et al*., 2008). An example of this is the nematodes *C. elegans* and *Ascaris lumbricoides*, in the latter case specialised into forming muscle-like fibres; as has become a characteristic feature of invertebrate IFs, they retained the full-length coil 1b from their lamin ancestor (Weber *et al.*, 1989; Karabinos *et al*., 2001). Consequently, the evolutionary history of IFs backs the hypothesis that lamins are the best model for cytotardin behaviour.

Almost all invertebrate lamins are highly similar to lamin B, often more similar to vertebrate lamin B than any lamin A equivalents they may have, and when there is only one lamin, it is

always a B-type lamin. This, and the intron-exon structure of lamins, for example in *Hydra* (Erber *et al*., 1999) and *Priapulus*, leads current research to believe B-type lamin was the original IF, as all IF proteins share their distinct intron patterns apart from type IVs and VIs; which are believed to have originated from an intron-less RNA intermediate undergoing retrotransposition (Lewis *et al*., 1986; Dahlstrand *et al*., 1992; Lin and Worman, 1993; Riemer and Weber, 1994). *C. elegans* and *Drosophila* Dm0 genes do not share the intron positions of Lamin A, suggesting separate origins for their own developmentally expressed lamin (Blumenberg, 1989). Studies using *Xenopus* lamin and invertebrate cytoplasmic IFs show conserved intron patterns between them and suggest that the nuclear to cytoplasmic evolution of IFs in vertebrates occurred due to loss of nuclear localization and isoprenylation signals (Dodemont *et al*., 1990; Döring and Stick, 1990).

The intron positions in human lamin B1 (LMNB1) are conserved in the lamin A (LMNA) and lamin B2 (LMNB2) genes; whereas LMNB2 contains an intron between coil 1A and coil 1B code that is not present in other IFs (including LMNA), implying that LMNB2 and LMNA both evolved from an LMNB1-like ancestor. This is reflected in the relative importance of lamins in development, where in organisms with both A and B lamins, e.g., mammals, and in very different forms, *Drosophila* (Riemer and Weber, 1994; Lin and Worman, 1993), lamin B is constitutively expressed in all somatic cells, while lamin A is expressed primarily in differentiated tissues, dependent on developmental pathway (Riemer and Weber, 1998; Stick, 1992; Lin and Worman, 1995). This hierarchy is reflected in the structure of the nuclear membranes by Field Emission SEM studies conducted by Goldberg *et al*., in 2008. Here B-type lamins are shown to be the base of the nuclear lamina, on top of which the exogenously expressed A-type lamins formed thicker filaments.

I.1.2 - Lamins

Lamins were first characterized as 60 to 80 kDa major proteins which form the nuclear lamina (Aebi *et al*., 1986) in metazoans, divided into A/C (alternatively spliced mRNA variants, the latter lacking codons for the final 82 a.a., leading to a 62.9kDa (in humans) protein called lamin C, Fisher *et al*., 1986) and B types; eventually identified as IF proteins by sequence homology (McKeon *et al*., 1986). Lamins follow the main order of IF structure, e.g. a central rod domain comprising three α-helical coiled-coil domains, a short amino-terminal globular head domain and a varyingly longer, carboxyl terminal globular tail domain. The ahelical N-terminal end

domain is small compared with most other IF proteins (about 30 residues long), whereas the C-terminal end domain is relatively large; between 187 to 277 residues. Relative to vertebrate cytoplasmic IF proteins, such as vimentin, the central rod domain of lamins has a longer coil 1b, and the non-helical C-terminal tail region contains an additional immunoglobulin-like domain: monomeric lamin is at also its most elementary supramolecular level a dimer rather than a tetramer. Latest research implies the basic lamin structural unit consists of anti-parallel pairs of parallel dimers, leading to the α-helical conformations forming a ~38-nm-long structure, and cryo-electron tomography suggests that lamins can form functioning 3.5-nm-thick protofilaments as well as 10-nm thick IF proteins used as lamin models (Riemer *et al*., 1994; Herrmann *et al*., 2007; Buxboim *et al*., 2014; Ahn *et al*., 2019).

Lamin A, a 70kDa protein has an expanded carboxy-terminal tail domain that is only expressed in differentiated animal cells, and contains a unique 90 a.a. segment relative to Lamin B, which is found in all tissues and has a molecular weight of 65kDa. Generally, lamin A resembles lamin B, which was originally identified in connection with the nuclear envelope, as a potential docking site for vimentin (Aaronson and Blobel, 1975; Georgatos and Blobel, 1987), with a similar amino-terminal head domain, central rod domain and nuclear localisation sequence motif in the tail domain (Loewinger and McKeon, 1988; Stick, 1988; Meier *et al*., 1991). The tail domain CaaX box (C = cysteine, a = aliphatic amino acid, x = any a.a.), which tardigrade lamin-2 also possesses (Hering *et al*., 2016), serves as a localiser for the protein to surface and endomembrane sites, such as the nuclear membrane. This is where the cysteine is farnesylated and the final "-aaX" residues are removed before further methylation and for lamin A, additional 15 residue cleavage after that (Hutchison *et al*., 1994) so as to control membrane binding. Removal of farnesylated and methylated cysteine residues from lamin A, during interphase, is linked to dissociation from the nuclear envelope (NE) at mitosis as soluble dimers and tetramers, whereas lamin B, which retains its modified cysteine residues, remains with NE vesicles upon breakdown, caused by phosphorylation of multiple sites leading to breakdown of filamentation (Torvaldson *et al.*, 2015).

I.1.3 - Lamin Assembly

Lamins polymerize into higher order insoluble structures *in vitro* observably in concentrations as little as 5µg/mL (Glass and Gerace, 1990). Lamins are capable of polymerising spontaneously *in vitro* to form short filaments, starting with elongation by head-to-tail

assembly. When this occurs, they initially form 3.5-nm-thick proto-filaments, as implied by cryo-ET studies (Turgay *et al*., 2017), and will later associate laterally to form paracrystals (Aebi *et al*., 1986). Models of lamin assembly have been recently much enhanced by the increased efficacy of partial crystallisation (Ahn *et al*., 2019), allowing enhanced modelling of molecular interactions following divide-and-conquer approach first put forward by Strelkov *et al*., in 2001. Partial crystallisation-based modelling of lamins is supplements studies showing comparison of lamin behaviour with assembly models established in cytoplasmic IFs such as vimentin (Moir *et al*., 1991; Heitlinger *et al*., 1992; Foisner and Gerace 1993; Herrmann *et al*., 2004; Ben-Harush *et al*., 2009; Taimen *et al*., 2009). Direct head-to-tail association is unique to lamins, contrasting with the overlapping, half-staggered, anti-parallel side-by-side association of dimers observed for cytoplasmic IF proteins. Sedimentation equilibrium methods show that *in vitro*, lamin dimers can associate into tetramers in a concentration-dependent manner, and the protofilaments thicken. The amino-terminal head domain is important for the formation of head-to-tail polymers *in vitro* and full filaments *in vivo*. When *in vitro* and membranes are absent most lamins form paracrystalline arrays with a distinctive axial repeat pattern, which can in some circumstances also be observed *in vivo*, such as in circumstances of overexpression. Scanning Electron Microscopy, due to recent advances in the imaging techniques of scanning tunnelling microscopy using field emission techniques, has advanced to stage in which this method can be deployed on the insides of the nuclear membrane. Here, *in vivo* assembly, both of endogenous and exogenous lamins can be examined (Goldberg *et al*., 2008) showing significant differences in A-type and B-type lamin assembly *in vivo* (Min *et al*., 1996).

I.1.4 - Laminopathies and IF Interactions

Mutations in Lamin A cause 17 distinct diseases and include forms of cardiomyopathy, muscular dystrophy, lipodystrophy and a premature aging disease called progeria via the progerin mutant protein (Dittmer and Misteli, 2011), comprising at least 400 distinct mutations (Kang *et al*., 2018). Lamin B mutations in contrast have been linked to only two genetic diseases, a rarity linked to how Lamin B mutations are almost always embryonic (Liu *et al*., 2000) or shortly afterwards (Vergnes *et al*., 2004) lethal. Many are located in the α-helical central rod domain required for lamin polymerization and assembly. Cells with mutations here, show lobulated nuclei, a separation of lamins A and B, abnormally clustered centromeres, mislocalised telomeres and heterochromatin (Taimen *et al*., 2009). Lamin A mutations have

been directly connected to chromatin misregulation by studies of cardiomyocytes and mouse embryonic fibroblasts (Nikolova *et al*., 2004; Sullivan *et al*., 1999; Worman, 2012). Altered levels of lamins are also indicative of various cancers, as well as the stage of tumour development and can be used in analysing cancer biopsy (Zhou *et al*., 2014). A-type lamins are also phosphorylated outside of mitosis, with up to 20 sites linked to lamin dynamics and location (Torvaldson *et al*., 2015). Mutation-induced deficiencies are a common problem in cytoplasmic IFs as well (Binkley *et al*., 2002), and as with lamins, particularly within the conserved LNDR and TYRKLLEGE motifs first characterised in keratin-14 (Steinert *et al*., 1983), and CP49 (Sawada *et al*., 1995). This investigation hypothesises that mutations in cytotardin, both in terms of tail deletion and substitution mutation in these regions could have similarly significant effects and which would also be visible *in vitro*.

Chaperone proteins are also critical to the cryptobiotic properties of tardigrades. Heat Shock Proteins (HSPs) have a long history of expression in all corners of the tree of life, from insects (Li *et al.*, 2009) to grapes (Ji *et al*., 2019) even down to the scale of small HSPs in the marine viruses *Synechococcus* and *Prochlorococcus* (Maaroufi and Tanguay, 2013). Novel members of the Hsp family have been observed, as have elevated levels of recognised Heat Shock Proteins like Hsp70, in tardigrades exposed to extreme environmental stresses such as high heat environments. Some cytoskeletal IF proteins can be solubilised with HSPs: in eye lenses they can prevent assembly of vimentin and GFAP. *R. varieornatus* has a large number of 20kDa Heat Shock Proteins, which present an excellent opportunity to study ways in which the novel IFs of tardigrades interact with the rest of the proteome (FitzGerald *et al*., 1991; Nicholl and Quinlan, 1994; Willsie and Clegg, 2002; Basha *et al*., 2003; Reuner *et al*., 2010; Boothby, 2018).

I.2 - Tardigrades

Tardigrades, named in 1777 by Lazzaro Spallanzani from the Latin for “slow steppers” are also known colloquially as water bears or moss piglets, having first observed and given the latter nickname by Johann A.E Goeze in 1773. Organisms of this bilaterian phylum, ranging from approximately 0.05-1.2 millimetres in body length, are known for their extremophile tendencies including such as survival of freezing, desiccation, osmotic stress (Welnicz *et al*., 2011), high pressure, temperature (Doyère, 1842, Westh and Ramløv, 1991), radiation

(Horikawa *et al*., 2008) and even vacuum conditions (Greven, 2018, Jagadeesh *et al*., 2018). The phylum *Tardigrada*, traditionally placed within *Ecdysozoa*, has two major clades: *Eutardigrada* and the more diverse *Heterotardigrada* (Kamilari *et al*., 2019), and are found in various habitats around the world including fresh water, marine and limno-terrestrial domains, such as the moss from which they are nicknamed (Nelson, 2002). Their extraordinary stress-tolerance is a consequence of their ability to transform into a reversible ametabolic state within extreme environments, a process known as cryptobiosis, or a "tun" state, describing the compact, desiccated state specific to tardigrades. Unlike during diapause, the state of minimalised metabolic activity often observed in arthropods (Tauber *et al*., 1986; Chapman, 1998), some mammalian embryos (Fenelon *et al*., 2017) and the Daf signalling-triggered "Dauer" state found in *Caenorhabditis elegans* (Lamitina and Strange, 2005), during the tun state tardigrades are completely inactive and retain as little as 2-3% of their body water (Crowe, 1972; Welnicz *et al*., 2011). As water is fundamental to all living organisms anhydrobiosis induced by desiccation is one of the most common and well-studied forms of cryptobiosis. Anhydrobiosis can be achieved by many extremotolerant tardigrade species and other metazoans such as rotifers and nematodes. This phenomenon was first discovered in the 17th century due to the studies of Antonie van Leeuwenhoek (Wright, 2001). In experiments he revived inactive rotifers by introducing them to water, thus opening up the possibility that some form of survival without water is possible for specialised organisms (Boothby, 2019). For most organisms, desiccation results in severe and fatal cellular and organ damage. The ability of tardigrades to survive extreme conditions has led to their increasing use as a model organism for astrobiologists (Goldstein, 2018, Jagadeesh *et al*., 2018).

Tardigrades possess novel intermediate filament proteins unlike those explored in *Chordata*, instead expressing two lamins and a third, unexplored lamin-like protein localised in the cytoplasm (Hering *et al*., 2016). Origins of the latter lie in divergence, in form and function, for example following duplication mutations, of nuclear IF proteins. Given that IFs form some of the most resilient cellular structures in vertebrates, have strain hardening properties and are commonly linked to stress responses, they form an important avenue of research into any organism which commonly encounters environmental stress. Tardigrades are capable of surviving intense external pressure from sources such as deep underwater environments, as well as the internal pressures inherent to desiccation during anhydrobiosis, so the study of tardigrade IFs is highly pertinent to the overall properties of the organism. Cytotardin is the name given to the novel protein discovered in 2016 with characteristically lamin-like

morphology has been observed in the cytoplasm of tardigrades. It was specifically located forming structural bands reinforcing the cell membrane (Hering *et al*., 2016), indicating the common IF function of a stress fibre (Denais *et al*., 2016; Ahn *et al*., 2019). First observed in *H. dujardini*, cytotardin appears as a belt around the cell, and occurs exclusively in ectodermal tissues such as the epidermis and gut (Hering *et al*., 2016).

I.3 – *R. varieornatus*

The tardigrade species *R. varieornatus* is one of the most stress-resistant tardigrade Species, capable of entering the tun state much more rapidly than more commonly studies tardigrade species such as *H. dujardini* (Hering *et al*., 2016) so comparative genomics between tardigrade species is of great scientific interest (Hashimoto *et al*., 2016) in order to reveal potential mechanisms underlying their tolerance. *R. varieornatus* can tolerate even rapid desiccation, requiring as little as an hour to transition completely to the tun state, whereas *H. dujardini* can require as much as 24 hours to prepare for complete desiccation (Neves *et al*., 2020). While the visual changes caused by the tun state are well documented, many of the underlying metabolic mechanisms remain poorly explored. Transcriptional profiling of this species revealed only minor differences in gene expression during dehydration indicating that non-transcriptional genetic differences may be responsible for the disparity in tardigrade survivability. As well as possessing constitutively high levels of the unique tardigrade chaperone proteins Cytoplasmic Abundant Heat Soluble (CAHS) and Secretory Abundant Heat Soluble (SAHS), *R. varieornatus* also possesses a cytotardin significantly different from that of *H. dujardini*, as well as an A-type "lamin 1" and a B-type "lamin 2" (Hashimoto *et al*., 2016; Yoshida *et al*., 2017). All of these proteins have been linked to tardigrade-specific paths of evolution from more mainstream proteins such as lamins in the case of cytotardin, and FABPs in the case of SAHS (Yamaguchi *et al*., 2012; Fukuda *et al*., 2017). *R. varieornatus*'s lack of dependence on transcriptional regulation for surviving desiccation may be the reason their ability to enter the tun state is much less time-sensitive compared to *H. dujardini* and *P. richtersi* (Hashimoto *et al*., 2016). As cytotardin occurs exclusively in ectodermal tissue, this is one of many stress bearing structures found in tardigrades. The muscle attachments in tardigrade limbs themselves superficially resemble basal lamina-reinforced 'double hemidesmosome' structures (Listgarten, 1974; Gross and Mayer, 2019). Interestingly, such structures have also been described from the cycliophoran symbion *pandora* (Gerace *et al*.,

1978). It is important to note that desmosomes and hemidesmosomes are typically associated with cytoplasmic IFs, which are almost entirely missing in panarthropods (Hutchison *et al*., 1994; Gullmets *et al*., 2017). This fits with growing evidence that tardigrades may not fit in this group, including both Hox gene composition (Hashimoto *et al*., 2016) and wider shotgun-sequencing based models (Laumer *et al*., 2019).

Genome sequencing extremotolerant tardigrade species shows an expansion of multiple stress-related genes, including six more superoxide dismutases than in most other phyla, often additional DNA repair and a novel intermediate filament (IF) protein, the presence, and evolution of which are strongly associated with stress tolerance. With the recent gene sequencing of the tardigrade species *R. varieornatus* and *H. dujardini*, tardigrade research is becoming an increasingly promising area for the discovery and study of novel proteins, including those not directly related to extremophile behaviour, such as a new cytochrome B5 (Pekny and Lane, 2007; Hashimoto *et al*., 2016; Fukuda *et al.*, 2020). Tardigrades are also notable for their lack reliance in many species on common desiccation survival agents like trehalose (Elbein *et al*., 2003), used commonly to create "bioglass" self-preservation in desiccated organisms (Hengherr *et al*., 2008). Varying from none to at most 2.9% body mass, (generally less than 1%) this cannot be the sum of the anhydrobiotic factors and thus the presence of these novel intermediate filament proteins in tardigrades leads to immediate questions of the potential impacts their variation, and degree of variation, in each individual species may have upon tardigrade survivability (Westh and Ramløv, 1991; Hengherr *et al.*, 2008; Jönsson and Persson, 2010).

I.4 – *T. pacificus*

Omnastrophes solanii pacificus, also known as *Ommastrephes pacificus* (Steenstrup, 1880), *Ommastrephes sloani pacificus* (Sasaki, 1929), *Todarodes sloanei pacificus* (Steenstrup, 1880) or simply *Todarodes pacificus*, is the squid species whose eye proteins are also investigated here. Colloquially called the Japanese flying squid, Japanese common squid or Pacific flying squid (Thermo Scientific, 2013), is a squid of the family *Ommastrephidae*. This animal lives in the northern Pacific Ocean, from the entire coast of China up to Russia, across the Bering Strait east towards the southern coast of Alaska. The Japanese squid can live in water from 5 to 27 °C and tend to inhabit surface waters of 100 m but can go as deep as 500m (Seafood

Watch. 2016). As organisms that produce advanced structural proteins, especially for use in their advanced optical and nervous systems, squid have become an area of interest in IF research (Tomarev and Zinovieva, 1990). *T. pacificus* possesses a novel IF with the same 42 a.a. extension in the coil 1B region, as with cytotardin. The protein was found in the eye lens (Tomarev *et al*., 1993), which in cephalopods as in spiders forms from neighbouring tissue, contiguous to the retina. As with the tardigrade cytoplasmic IF, this lens protein displays a high degree of divergence from its vertebrate lens counterparts, which are produced by cells from the sensory pre-placodal ectoderm (Koenig and Gross, 2020). Since the cellular concentration of actin appears lower in the lens of squids than in other animals such as cattle, this gives rise to the theory that IF proteins are the major constituents of the squid lens cytoskeleton (Siezen, 1982). Novel eye lens IFs are highly important to eye development, for example the chicken beaded filament CP49, orthologous to Bsfp2. This protein, like cytotardin and the eye lens IF also carries an extension to coil 1b, albeit a longer one at 49 a.a. than that commonly associated with invertebrate cytoplasmic IFs (Sawada *et al*., 1995). Eyes, like cytoplasmic IFs, are a feature that has evolved repeatedly and independently in different phyla of metazoans, (Koenig and Gross, 2020) and are required to produce stable, long lasting lenses which in the event of unfitness incurs strong selective pressure. This project investigates if these lamin-like features the lens IF shares with cytotardin result in similar behaviour.

I.5 – Aims and Objectives

Cytotardin, as a highly lamin-like IF protein could represent an alternate “missing link” in IF protein evolution, with giving indications as to the possibilities of paths taken, or not taken by other cytoplasmic IF evolution events. Differing structural performance in similar environments may provide still more examples to help characterise the proteins. Thus the characterisation of cytotardin provides an insightful window not just into the mechanisms of cellular location peculiar to the protein itself, but as an opportunity to explore existing theory with regards to the evolution of IF proteins as a whole.

The speed, strength and structural complexity of *R. varieornatus* IF structures may give clues to the roles played, and the molecular evolutionary roles made, by novel tardigrade IFs. *In vitro* dynamics of filamentous proteins may be useful in illustrating the catalytic properties of IF associated proteins such as chaperones, which are important to extremophiles, but also in

human-relevant processes such as aging. Additional questions presented are the effect of cytotardin on the physical properties of its solvents, and to what degree it can replicate the gel forming off viscosity augmenting abilities of other, better characterised IFs. It is also of interest to discern whether structural commonalities with the *T. pacificus* lens IF translate to similar *in vitro* behaviour.

This study aims to explore the structure, behaviour and research potential of *R. varieornatus* IFs (hypothesised as orthologs to cytotardin, lamin-2 and lamin-1 respectively from Hering *et al*., 2016). These three have each highly different end terminal domains, the molecular effects of which may be indicative of the features needed by IFs to form and be restricted to formation in multi-filament bodies. Whilst the theory of recent cytoplasmic adaptations of duplicated lamin proteins leading to intermediate filament diversification is well supported in the literature, the biomolecular mechanisms for them have not been so well characterised. BLAST shows cytotardin is significantly shorter than the lamins in non-rod domain areas, which presents a wealth of potential sites where differentiating factors may be found, as well as the specifics of how cytotardin mutated to stay in the cytoplasm. The Hering *et al*. study in 2016 raises extensive questions as to the *in vitro* assembly properties of *R. varieornatus* IFs, and whilst their filament characteristics were demonstrated by light microscopy, molecular biological characterisation by TEM is yet to be performed. Neither has there been any attempt to analyse the biophysical and molecular properties of *R. varieornatus* IFs, and we aim to change this.

Part II – Materials and Methods

The IF genes, in pET23 plasmids, were cloned in DH5α bacteria, then transferred to BL21 bacteria for expression which as induced with IPTG on the T7 promoter within lac operon. pET23 were used with ampicillin resistance and the replication origin first explored in pBR322 (Zaner *et al.*, 1982).

II.1 Major Materials List

- BL21 (for example pLysSE "One Shot", the more precise "Origami" B or, as used in this study: pLysS "Rosetta") competent cells with DE3 lysogen containing T7 polymerase attached to the lac operon
- Luria Bertani (LB) media: Lennox, including plates: 10g tryptone, 5g Bacto yeast extract, 5g NaCl/L)
- Antibiotics (1000x stocks: carbenicillin 50mg/ml, chloramphenicol 34mg/ml),
- IPTG 1M stock solution
- TEN buffer (50mM Tris-HCl pH 8.0, 1mM EDTA, 100mM NaCl, 10mM $MgCl_2$).
- A+N Buffer (50mM Tris-HCl pH 6.8; 1mM EDTA 1% (w/v) SDS
- 5X Laemmli Sample buffer (100mM Tris-HCl, 5mM EDTA, 5% (w/v) SDS, 10mM DTT, 50% (v/v) glycerol plus bromophenol blue to colour (Laemmli, 1970)
- High Salt Buffer (1.5 M KCl, 10mM Tris-HCl, 5mM EDTA, 1% Triton X-100)
- 10X SDS PAGE Running Buffer (3% Tris-HCl pH 8.8, 14.4% glycine, 1% SDS, w/v)
- Medicell Membranes Ltd. DTV12000.01.15 visking tubing – Size 1 Inf Diameter 8/32" 6.3 mm: 15M. MWCO - 12-14000 Daltons

II.2 Bioinformatics Analysis

DeepCoil, ExPASy, Uniprot and JPred 4 have also proved important in making molecular models of the target protein. DeepCoil and DeepCoil 2 estimates probabilities of coiled coil formation (Zimmerman *et al*., 2018; Ludwiczak *et al*., 2019; Gabler *et al*., 2020) combined with JPred 4 α-helix and beta sheet predictions were used to produce consensus maps of each protein (Lupas *et al*., 1991; Drozdetskiy *et al*., 2015; MacGowan *et al*. 2019). Hidden Markov

Model-based coiled coil prediction was also used (Delorenzi and Speed, 2002). These models were cross-referenced with existing Uniprot models. Models were fed a.a. sequences in FASTA format. Links are available here for DeepCoil:
https://toolkit.tuebingen.mpg.de/tools/
JPred4:
http://www.compbio.dundee.ac.uk/jpred/index.html

II.2.1 Nuclear Sequence Prediction.

For determining nuclear location sequences, the 100 sequence predictors-based ensemble, NucPred was used. The program aggregates the positive and negative evaluations of whether the protein spends some proportion of its life in the nucleus, and returns the fraction that responds positively along with probabilistic analysis based on the programs giving said identity (Bramier *et al*., 2007).
The individual predictors are evolved using an evolutionary machine learning approach, AKA genetic programming on a set of known proteins. The predictors use regular expression pattern matching to make the yes/no decision and the regular expressions are themselves evolved using the open source PerlGP system available here:

http://bioinf.cs.ucl.ac.uk/psipred/&uuid=39c915bc-f9b3-11ea-8d55-00163e100d53
http://bioinf.cs.ucl.ac.uk/psipred/&uuid=387e3036-f9b1-11ea-b80f-00163e100d53

PredictNLS was used to determine Nuclear Location Sequence location (Murat Cokol, Rajesh Nair and Burkhard Rost) and the source code is available here:
https://rostlab.org/owiki/index.php/Packages

II.3 Making Competent Cells

The DH5α cells were cultured in LB-Lennox media, then harvested and repeatedly washed in ice cold (referring to as near as possible to 0°C without initiation of freezing) sterile 0.1M $CaCl_2$. When adding 0.5 ml of the overnight culture into 50 ml of LB in a 200-ml flask, the broth is prewarmed to 37 °C and put on an adhesive coated 60+rpm shaker until OD_{600} of 0.6 is reached, which will be approximately four hours later. The culture is then chilled on ice and

transferred to a sterile centrifuge tube and pelleted by centrifugation at 13,300 rpm for 5 minutes at 4 °C using a Micro Star 17R centrifuge. Cells are then resuspended in 20 ml of ice-cold, sterile 0.1M $CaCl_2$ and incubated on ice for 20 minutes. After at least another round of resuspension, they are collected in the same manner as before, mixed to 20% (w/v) glycerol (also ice cold) and flash frozen using liquid nitrogen, then transferred to -80°C storage. Aliquots of 100-200 µl at a time of competent cells were then used for each set of transformation preparations.

Procedure went as according to the methods detailed in (Dagert and Ehrlich, 1979) when modified for broad range performance at the expense of super-efficient transformation by Chang *et al*., 2017 and Shiraishi, n.d., ret. 2020. This was useful was this study used B-strain BL21 which has significant metabolic differences compared to the K-12 strain (Marisch *et al*., 2013) used by Dagert and Ehrlich.

II.4 PCR, Ligation & Transformation

Sequence	**3' restriction site**	**5' restriction site**	**Buffer**
Cytotardin	NdeI	BamHI	NEB3.1
Cytotardin Tail-less "CTD"	NdeI	Sal1	Tango Orange
CytotardinLNTRΔ31C Head Section	NdeI	XhoI	CutSmart
CytotardinLNTRΔ31C Tail Section	XhoI	BamHI	CutSmart
T. pacificus Eye Lens IF L10112.1	NdeI	BamHI	NEB3.1

Table 1: Restriction Enzymes used in POI Engineering and Expression

Point mutations and deletions were engineered by PCR cloning of the wild type cytotardin plasmid using as primers bespoke oligonucleotides ordered from Integrated DNA

Technologies. After digestion of the PCR product ends and cleaning with a Sigma Gel Cleanup Kit as according to the manufacturer's instructions, they were inserted into pET23 plasmids with T4 DNA ligase, using a Golden Gate ligation for LNTC cytotardin. The eye lens IF sequences were subcloned from pcDNA3.1 and the cytotardin was subcloned from pGEM-T Easy plasmids supplied by Prof. Roy Quinlan. The resultant plasmids were cloned using DH5α *E. coli* with 50µL of *E. coli* to 1µL of miniprep plasmid DNA. After plasmid mini-preparations using Sigma Miniprep Kits according to manufacturer's instructions and checked for 260/280 ratio to confirm purity (Wilfinger *et al*., 1997), digests were performed to confirm presence of restriction sites, the absence of the wrong restriction sites, and the correct size of insert. This was performed using restriction enzymes and buffers detailed in Table 1, and run on 1% agarose gel alongside Thermo Fisher GeneRuler 100 bp Plus DNA Ladder (Thermo Fisher, 2021).

Sanger sequencing to confirm the DNA electrophoresis results was performed by DBS Genomics at the Durham University Biosciences Department. Big Dye Terminator v3.1 was used to prepare samples for an Applied Biosystems (ABI) 3730 DNA Analyser. Plasmids showing the incorrect sequence were then re-digested using Sigma Gel Extraction Kits to produce more pET23 plasmid material for the next ligation.

Once the plasmid sequence was confirmed to match that of its IF template, a sample of the it was harvested from were sample is combined with sterile glycerol at a ratio of 0.2ml Glycerol to 0.8ml overnight culture and flash-frozen with liquid nitrogen for -80^{0}C storage. The plasmid is then used to transfect competent BL21 Rosetta cells by heat shock. The agar plates on which they transformants were spread were prepared by melting sterile agar (standard LB Lennox mix + 1.5% agar, 0.05% (w/v) glucose and carbenicillin at 50µg/ml).

II.5 Expression

Three colonies were harvested per plasmid, and used to inoculate 2ml of LB with carbenicillin (and depending on the vector chloramphenicol as well) and 0.05% w/v glucose to suppress transfected protein expression for short amounts of time without inhibiting induction (Marisch *et al.*, 2013). After confirmation of expression by IPTG induction, an uninduced culture is frozen down in liquid nitrogen as previously described. Induction then occurred with 0.5mM

IPTG and rotary shakers on 500ml culture for protein production and purification when the OD600nm reaches 0.6. The resultant stocks that can be reduced to 50ml by centrifugation and resuspension with 1L bottles at 8000rpm, 15 minutes at 4^{o}C and a JLA-8.1000 rotor.

II.6 Purification

Purification of cytotardin occurred in two stages. Firstly, the isolation of inclusion bodies, then chromatography.

II.6.1 Inclusion Body Preparation

Following protocols outlined in Perng *et al*., 2004, the sample was suspended in TEN buffer with added sigma protease inhibitor (0.5 ml to a 25 ml tube), and transferred to homogeniser with added lysozyme at 0.25 mg/ml to facilitate bacterial lysis. After Dounce homogenisation, Benzonase nuclease was added 10µl/25ml extract to a final concentration of 10 units/ml) to digest the *E. coli* chromatin and reduce viscosity. Pefabloc, an irreversible serine protease inhibitor was added to the inclusion body preparations at 4µM to prevent degradation of target protein (Gold and Fahrney, 1964; Powers *et al*., 2002). The inclusion body preparation then proceeded as according to Quinlan *et al*., 1989, resuspending the pellet repeatedly in the High Salt Buffer in the materials list followed by TEN/TE buffer, then re-pelleting using a Beckman-Avanti J20 I centrifuge at 4^{0}C with a JA20 rotor at 16,000 rpm. The final pellet was dissolved in 20mM Tris-HCl, with 8M Urea and 2mM EDTA and solid components were removed by a Beckman-Coulter Optima ultracentrifuge at 55,000rpm.

II.6.2 Chromatography

Over the course of an hour a MERCK Hitachi L-6210, L-4000, L-4250, D-6000, L-6000, L-6200A complex was used to flush out a TMAE ion exchange column with an increasing concentration from 0M to 1M NaCl at pH 8.8 from 20mM Tris-HCl, with 8M Urea and 2mM EDTA. The cleaning cycle used followed a cycle of pH10, 0.5M NaOH solution, 18.2 MΩ.cm deionised water, then a mixed 1M NaCl and 0.02% w/v Na-azide solution; all for 10 minutes each after which the system is flushed with low pressure ddH2O.

When impurities remained in the fractions, the HPLC purification was repeated with the substitution of 1M NaCl for 1M Guanidinium hydrochloride, which required a less rapid gradient of increase to fractionate and purify the protein more effectively. All Urea and salts were filtered through 0.2 micron nitrocellulose membranes with a VMR vacuum pump after dissolution.

Reverse-phase HPLC was also used to bind protein stocks to a Bio-Rad Hi-Pore RP-304 column for purification and separation, during the attempted TIPS-EBX modification. Under the HPLC conditions, where cytotardin and Lamin A elute at 40% acetonitrile to 0.1% trifluoroacetic acid solution, a fraction of the Lamin A still presents itself as a dimer due to disulphide crosslinking.

II.6.3 BCA Assay

Spectrophotometry using a BioTek ELx800 at 570nm confirmed all protein concentrations mentioned in this thesis. Samples were each tested twice using Cu+/Bicinchoninic Acid-based solution (Smith *et al*., 1985) against several sets of predetermined BSA measures with 562nm absorbance being the optimum wavelength for the materials. The tests were performed with a Thermo Scientific Pierce BCA kit using BSA standards provided therein.

II.7 IF Assembly *in vitro*

IFs were stored solubilised in 8M Urea (Herrmann *et al*., 2004) and dialysed into target solutions using dialysis tubing. Concentrations of 0.2 and 0.1 mg/ml were used for most assemblies of IFs, based off the HeLa cells vimentin concentration average, which is 0.15mg/ml (Luby-Phelps, 2000). This is however significantly lower than the concentrations observed *in situ* for the assembly of proteins like keratin, which can be expressed at as high as up to 40mg/ml in dedicated epithelial proteins such as keratinocytes (Feng *et al*., 2013). All solutions not containing divalent cations had 1mM EDTA added to chelate trace metal ions and deactivate metalloproteases (Thompson *et al*., 2012), and those with cysteine-containing proteins had 1mM DTT added to reduce cysteine residues to prevent covalent interactions. To bind one-per-molecule cysteine residues as molecular markers (Aryal *et al*., 2006; Majzik *et al*., 2010; Caprile *et al*., 2012), 5nm diameter gold beads were added in a saturated colloid at a

1:20 ratio to the dialysis bag 30 minutes before, and to the container after (for 10 minutes) the sample was isolated for negative stain in preparation for electron microscopy.

Dialysis tubing was prepared by boiling repeatedly in deionised water with EDTA and transferred to a suitable vessel containing 20% ethanol at 4^0C. When filled with dialysis substrate, the tubes were placed in solution and stirred with a magnetic bar above a 1KA C-Mag MS7 stirrer.

II.8 SDS-PAGE

For the analytical gels in this study, 11% and 12% SDS-PAGE gels used with 4.5% stacking gel and run at 25mA. Staining was done with Coomassie Blue R250, with the destain solution 150% diluted with water so as to reduce mechanical impact on the gel from dehydration.
Sedimentation assays were conducted after dialysis using Medicell Membranes Ltd. DTV12000.01.15 visking tubing and a 30% sucrose cushion at 1:1 volume with the sample. Sucrose cushions are commonly used to separate out low-density material such as viral membranes (Boroujeni *et al.*, 2018) and exosomes, lipid-protein complexes between 30 and 150nm in diameter (Pol *et al.*, 2012; Gupta *et al.*, 2018). The percentage of protein drawn down into the pellet serves as a way of quantifying the amount of protein aggregated into structures above the size dictated by the centrifugation force and time. When the supernatant had to be concentrated for SDS-PAGE, the Wessel & Flügge method was used (Wessel and Flügge, 1984).
Immunoblotting was performed using the Bio-Rad semi-dry blotting method according to the manufacturer's specifications. The lysates used as negative controls for the Western blots were MDA-MB-231 is a human breast epithelial cancer cell line established using samples taken from a 51-year-old caucasian female with a mammary adenocarcinoma (Cailleau *et al.*, 1978). Gel and Western blot imaging were performed using the Thermo Fisher iBright 1500 using proprietary BrightEyes software.

II.9 Electron Microscopy

Electron microscopy samples were negatively stained following the methods laid out in Smith and Seegan, 1984 and Perng *et al.*, 1999, following off concepts developed by Valentine *et al*., 1968. Samples were caught between mica and 5nm carbon sheets, then immersed to 2% uranyl acetate solution and bound to 3.05mm copper grids. Specimens were observed using a Hitachi 7600 transmission electron microscope.

II.10 Viscometric Procedures

Initial experimentation used cytotardin solution in 2mM pH 8.8 Tris-HCl buffer. Glass microscope slides were coated in dichloromethylsilane as per established methods for cleaning and coating (Hua *et al*., 2014). Ten drops of 0.2mg/ml protein solution were placed on the slides and left to adjust for 15 minutes before imaging with the iBright. Continuous shear viscosity was tested using an AR2000 microrheometer using 0.5ml volumes, all measurements repeated twice, at 25 degrees centigrade. Further experimentation was done using a Netszch Kinexus Pro+ using 50µl volumes at 25 degrees centigrade. For all but the first of the large volumes, a vapour trap was used in order to minimise the effects of evaporation on the fluid body. Dioleoylphosphatidylcholine or DOPC, as well as mineral oil and a vapour trap was also used for this purpose and to examine interactions between cytotardin, phase barriers and lipid membranes.

II.11 Chemical Modification of Cytotardin

II.11.1 TIPS-EBX Modification of Cytotardin

The protein and TIPS-EBX were dissolved in MeCN/water (3:1, 250 mL) with TFA (2%; it could be omitted at the expense of the yield) producing a clear solution. Then [AuCl(SMe_2)] (52.3 mg, 117 mmol) was added and the reaction was stirred overnight at room temperature. Next day, solid NaI was added to the yellow solution followed by a few drops of 1M sodium ascorbate. The former being added to dissolve protein-Au-TIPS-ethynyl complexes, and the latter were added to reduce any iodine formed. MeCN was removed in vacuo, causing the

cytotardin to precipitate in entirety. The ratios of these ingredients followed those used in Hansen *et al*., 2016.

The suspension was centrifuged for 5 min at 13,300 rpm on a Micro Star 17R centrifuge producing a gold precipitate and clear supernatant, which was redissolved in 6M guanidine hydrochloride with 50mM Tris-HCl 7.0, and purified by reverse phase HPLC, after several repeated centrifugations at 13,300 rpm to sediment any remaining large particles that might disrupt the chromatography. The pure fractions were pooled and lyophilized to produce the desired TIPS-ethynyl protein.

II.11.2 Cu-Phenanthroline catalysed Crosslinking of Cytotardin

The crosslinker used was copper bound to 1, 10 Phenanthroline, which catalyses the air oxidation of sulfhydryl groups (Kobashi, 1968). Stock solutions (1.8 and 3.6 mM) were prepared just before use (due to the several hour long half-life of phenanthroline in solution) by mixing copper sulphate with the phenanthroline at a mole to mole ratio of 1:2. Copper can also form a complex with Tris-HCl, even when EDTA and 1, 10-phenanthroline are present, and catalyse oxidation of sulfhydryl groups (Takahashi *et al*., 1981). Crosslinking was terminated by addition of iodoacetamide or DTT (final concentrations, 50 mM). Stock solutions were diluted 1:50 with target solution (Quinlan and Franke, 1982, 1983).

Part III: Main Data & Results

III.1 Bioinformatic Analysis

Lamins are Type V IF proteins, which are characterized by a long (i.e., 352 a.a. compared to 310 a.a. of vertebrate cytoplasmic IF proteins) central α-helical coiled-coil rod domain with a long coil 1b that they share with invertebrate cytoplasmic IFs (Lin and Worman, 1993; Zimek *et al*., 2002), and a complex carboxy-terminal tail domain harbouring a nuclear localization signal (NLS) and a globular Immunoglobin-like fold (Dhe-Paganon *et al*., 2002, Krimm *et al*., 2002, Strelkov *et al*., 2004). These features from IF evolution represent targets to look for in the sequence analysis of *R. varieornatus* IFs.

The relatively low similarity between the cytotardin with the A-type lamin 2, and even more so with the B-type lamin 1, whilst still sharing the hallmark features of a Type V IF suggests that the cytoplasmic IF of tardigrades is not a recent evolution. Especially since *R. varieornatus* and *H. dujardini* IFs are highly divergent in sequence, with only 74.3% sequence identity between cytotardins from that of fellow *Hypsibiinae* subfamily member *H. dujardini* (Fig. 2.2), compared to 100%, 97.4% and 98% sequence identity between human vimentin and that of *Gorilla gorilla (gorilla), Mus musculus* and *Sus scrofa* respectively. This does not necessarily translate to divergence of structure and the two cytotardins still share higher sequence identity with each other than any other proteins (Fig 2.2, 2.1). The two species are closely related, although discerning the relationship between *H. dujardini* and *R. varieornatus* within the subfamily level has proved difficult (Pilato *et al*., 2011; Tumanov *et al*., 2020).

III.1.1: Overview

Cytotardin in *Ramazzottius varieornatus* is 484 a.a. long protein we would expect to feature the 40 a.a.-long coil 1a, 140 a.a. coils 1b and 2, a characteristic of Type V IFs, although shared with cytoplasmic IFs in invertebrates (Lin and Worman, 1993). These coils appear to begin with coil 1a at the 24th a.a. and end on the 59th. Coil 1b is predicted to begin on the 70th residue, and ends on the 205th, while coil 2 runs from 230th to 370th (Fig. 2.1). There is nonetheless clear disruption in these coils relative to the structures of their fellow type V IFs in this species as DeepCoil analysis shows relatively reduced likelihood of coiled coil

A

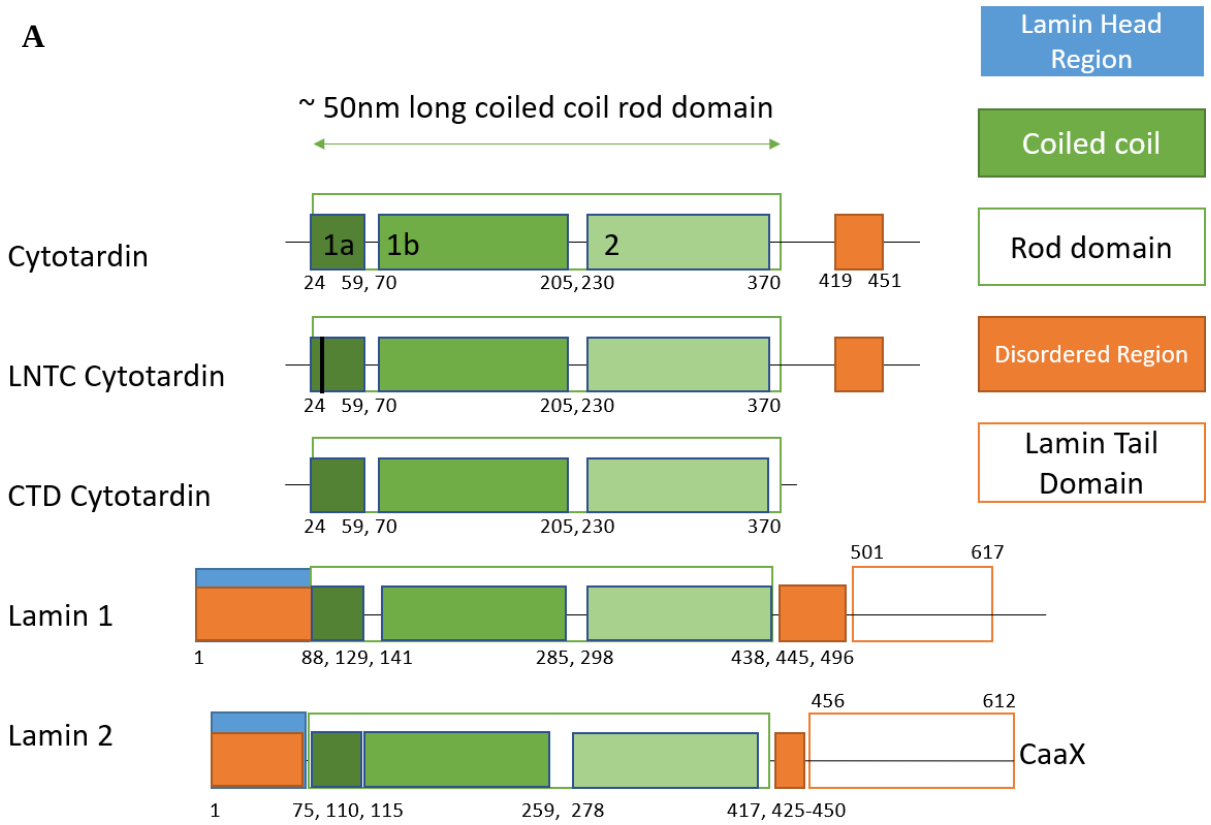

B

R. varieornatus	Cytotardin	"Lamin A (Lamin2 homolog)	" Lamin B (Lamin1 homolog)
Molecular Weight	56201.94 Da	69747.71 Da	72680.36 Da
Isoelectric Point(pl)	5.83	5.75	5.82
Charge at pH5	13.47	19.37	17.49
Charge at pH7	-6.68	-13.76	-7.64
Charge at pH9	-12.02	-20.62	-14.53

C

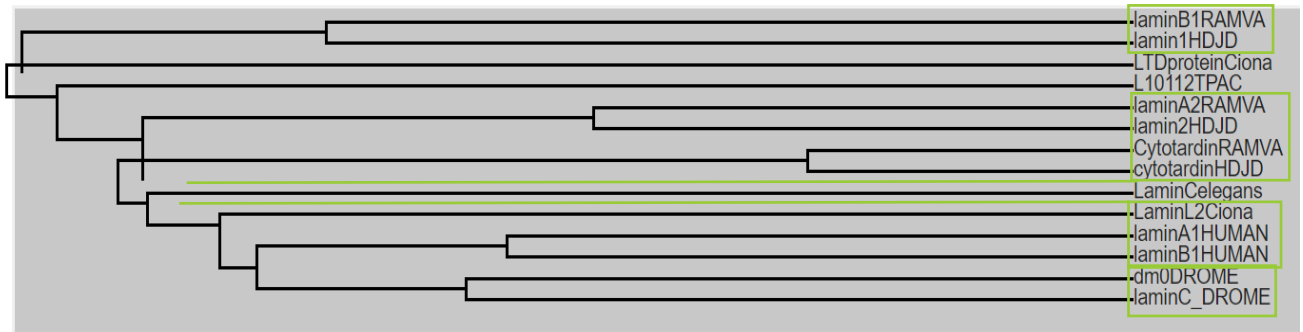

Fig. 2.1: Modelling and Comparison of POI

(A) Structural diagram of the IFs in this study. **(B)** Table comparing predicted physical properties of the *R. varieornatus* IF proteins, with the aid of Benchling's in-built chemistry predictor (https://www.benchling.com/). Uniprot phylogenetic **(C)** sequence analysis of IF proteins across *Chordata*, Euarthropoda, Nematoda, and Tardigrades.

formation in the rod region. It has a large motif not present at what would be position 398 its counterpart in fellow tardigrade *H. dujardini*. The tail region of *R. varieornatus* cytotardin is vestigial in comparison to even its *H. dujardini* counterpart, let alone the more beta-sheet prone tail of its lamin ancestor.

Lamin 2 in *R. varieornatus* is a 612 residue long protein. Of the three cytotardin IF proteins, it bears the highest sequence homology to the lamin 2 of *H. dujardini*, and is an A-type lamin. Whilst it contains almost all the hallmark features of a lamin, the sequence homology and CaaX box to constitute an A-type lamin at that. It has an acidic isoelectric point as does its B-type counterpart. The CaaX box is a motif that has been shown in other A-type lamins to be essential for binding enzymes used to prenylate and carboxyl methylate the lamin, ensuring effective nuclear membrane binding (Kitten and Nigg, 1991).

III.1.2 Sequence analysis of *T. pacificus* Lens IF

L10112.1 is a novel cytoplasmic IF protein found in the lens of the squid *T. pacificus* which also possess lamin-like morphology with a 42 a.a. extension on coil 1b, like that of cytotardin, in line with current hypothesis about the lamin-like features of invertebrate IFs. The two species also exist at similar temperature ranges, from 5-15 degrees Celsius, and both can survive the high pressures of deep ocean. As an invertebrate IF it also represents a novel evolution of cytoplasmic IFs. Longer than cytotardin but shorter than the lamins at 614 a.a. long, it is one of the three IFs found in *T. pacificus*, the other two being a lamin and a neurofilament (Tomarev *et al*., 1993). As with the tardigrade proteins, L10112.1 is not without comparisons to nematodes, as it is analysed by Uniprot to have the highest E-value based sequence identity with the nematode *Diploscapter pachys*. L10112.1 is primarily comparable to cytotardin in how it is also a lamin-length coiled-coil cytoplasmic IF, with the same 42 a.a. coil 1B extension, which evolved independently. This is strongly indicated by both the evolutionary history of their associated species and the relative sequence identity of L10112.1, which is comparably different to that of cytotardin when compared against most of the over two dozen IFs compared (Table 2, 3). Like cytotardin and the *R. varieornatus* lamins, it is predicted to have an acidic isoelectric point, and show sequence homology with the LNDR and TYRKLLEGE motifs in similar locations. This, as well as some similar environmental pressures shaping the evolution of the protein leads to the question of whether there is similar behaviour *in vitro* in terms of

assembly patterns of aggregation rates, as well as whether this would occur under similar buffer conditions.

A

Entry	Protein names	Identity
A0A1D1VDN8	**IF rod domain-containing protein** (Ramazzottius varieornatus)	100.0%
A0A125S9M6	**Cytotardin** (Hypsibius dujardini)	74.7%
A0A5N5Q4N1	Uncharacterized protein (Pangasianodon hypophthalmus)	30.9%
A0A5F5PL78	Lamin A/C (Equus caballus)	33.0%
F6ZY40	Lamin A/C (Equus caballus)	33.0%

B

Entry	Protein names	Identity
A0A1D1VDN8	**IF rod domain-containing protein** (Ramazzottius varieornatus)	100.0%
A0A125S9M6	**Cytotardin** (Hypsibius dujardini)	74.7%
A0A667X966	Uncharacterized protein (Myripristis murdjan)	33.7%
A0A667X978	Uncharacterized protein (Myripristis murdjan)	33.5%
A0A667WV58	Uncharacterized protein (Myripristis murdjan)	33.5%

C

Entry	Protein names	Identity
A0A4W5L7D6	Uncharacterized protein (Hucho hucho)	32.3%
A0A452IL52	Lamin A/C (Gopherus agassizii)	32.3%
A0A452IKQ3	Lamin A/C (Gopherus agassizii)	32.3%
A0A667WYC3	Uncharacterized protein (Myripristis murdjan)	33.3%
A0A4W5L8W9	Uncharacterized protein (Hucho hucho)	31.7%

D

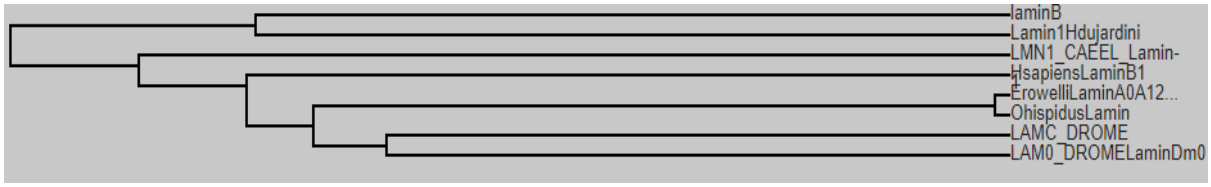

E

Sequence Identity *R. varieornatus*	RAMVA Cytt	RAMVA Lamin 2	RAMVA Lamin 1	HDJD Cytt	HDJD Lamin 2	HDJD Lamin 1
cytotardin	100	21.85	15.252	74.349	21.127	16.792
Lamin 2	21.85	100	23.83	21.609	60.386	20.768
Lamin 1	15.252	23.83	100	17.353	22.694	40.211

Fig. 2.2: POI Sequence Identity

RAMVA Cytotardin sequence submitted into Uniprot sequence comparison and compared against the whole database of sequences by three metrics. Combined Uniprot Score **(A)**, Raw Sequence Identity **(B)** and sequence similarity probability, or "E value" **(C)** Uniprot phylogenetic analysis **(D)** of lamin-1. Comparative genomics **(E)** of the tardigrades *Hypsibius dujardini* and *Ramazzottius varieornatus*.

III.1.3: Comparison and Predicted Properties of Cytotardin

It is hypothesised in Hering *et al*., 2016 that the B-type lamin 1 is the closest ancestor of cytotardin in *H. dujardini*, while this conclusion is not apparent in *R. varieornatus*. The next most similar protein to *R. varieornatus* cytotardin, after its *H. dujardini* counterpart, are from vertebrates (Fig. 2.2). Those of which that are identified are all A-lamins (Fig. 2.2). Cytotardin bears greater sequence identity with the A-type lamin 2 than to the B-type lamin 1 (Fig. 2.2, 2.1), with a 21.85% vs 15.25% sequence identity in each of them respectively shared with cytotardin. That said, this phenomenon only occurs in the tardigrades, whereas when compared to other lamins, regardless of whether A-type, B-type or not yet differentiated by the literature, cytotardin shares an approximately 20% shared identity with other lamins but a closer to 15% identity with other cytoplasmic IFs. Consequently lamins, not cytoplasmic IFs may be the better models for cytotardin assembly, and this study aims to explore this.

Cytotardin R31C or "LNTC" is a mutant featuring an Arginine to Cysteine mutation, similar to that found in many keratin-related skin disorders (Coulombe *et al*., 1991; Wood *et al*., 2003), as the changes in the boundary regions of the central rod domain are among the most damaging mutations to keratin function (Irvine and Mclean, 1999). The LNDR site, analogous to the LNTR site on cytotardin, is extremely well conserved (Fig. 2.3B being an example), with the Mycetozoan amoeba *D. discoideum* being the most closely related organism to express IF-like proteins without the canonical LNxR sequence (Krüger *et al*., 2012), instead using isoleucine instead of leucine and histidine instead of asparagine. Here the amphipathic arginine residue, R is replaced by a more hydrophobic but still somewhat polar cysteine residue (Iyer and Mahalakshmi, 2019), which also has a much more acidic isoelectric point. This will likely disrupt the structure of the heptad repeat surrounding the beginning of coil 1A, as well as the conserved LNDR motif, leading to difficulty self-assembling.

Cytotardin CTD, standing for C - Terminal Deleted is a mutant cytotardin variant created to examine the effects of a completely truncated tail domain on cytotardin assembly. The mutation comes from a stop codon placed at position 1174 in the DNA sequence, or after the 390th a.a.. The break is placed shortly after the end of the coiled coil region and completely removes the tail, including almost entirely removing the predicted beta sheet forming regions essential for Ig-like Lamin Tail Domain regions to develop (Ruan *et al*., 2012). Together the proteins

introduced, along with the aforementioned mutants, in section III.1.1 represent the proteins of interest (POI) in this study.

A

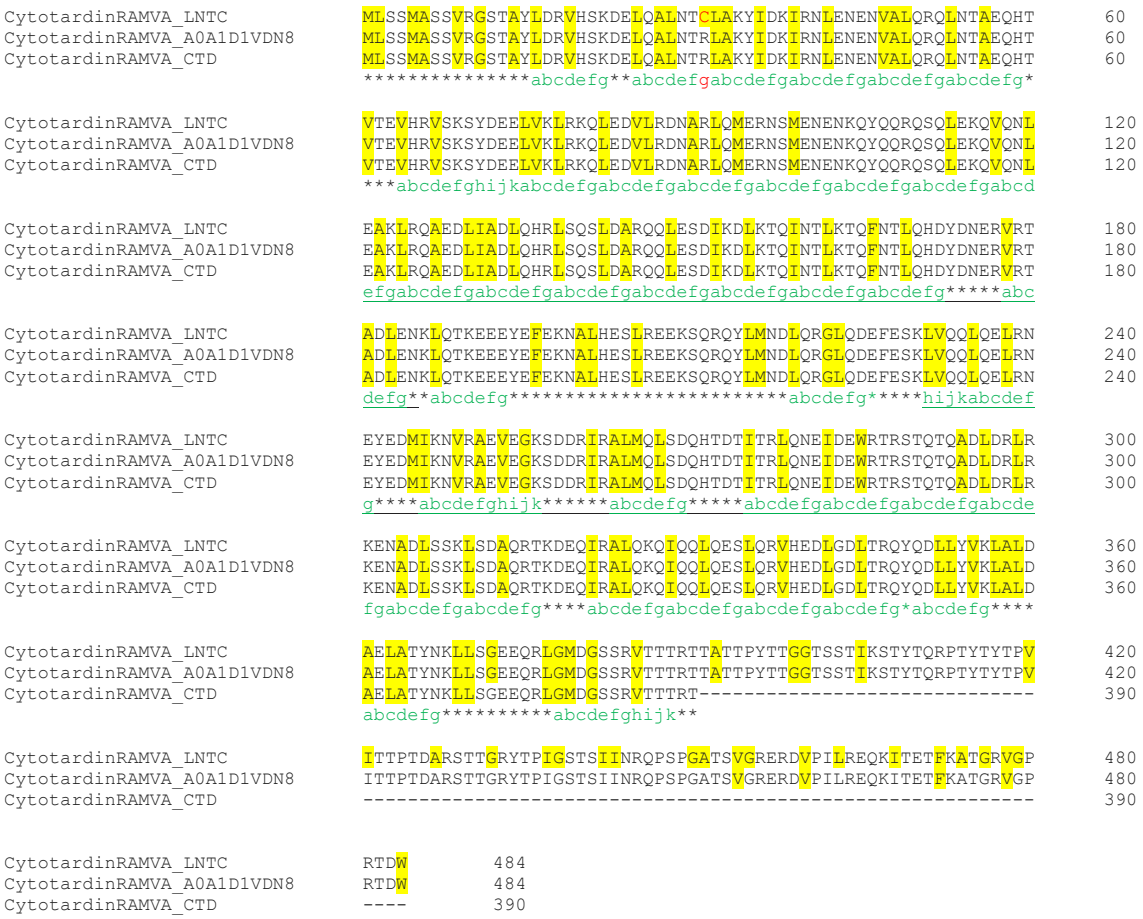

B

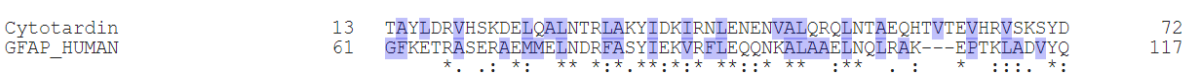

Fig. 2.3: Potential α-helix Positions in Cytotardin and Mutants Thereof

(A) Whole sequence comparison with rod region underlined. Hydrophobic residues highlighted in yellow, including both heptad (Parry *et al*., 1977) repeat domains abcdefg and potential extensions creating hendecad (Parry, 2006) repeat domains a,b,c,d,e,f,g,h,i,j,k. Heptad positions annotated manually, and remaining data extrapolated from JPred4 (Drozdetskiy *et al*., 2015) **(B)** Alignment of the LNTR region in cytotardin with the LNDR region in GFAP.

III.1.4 Head Regions

Strelkov *et al*., 2004 links regions within coil 1a to the head to tail assembly step, also known as the A_{CN} interaction (Eldirany *et al*., 2021) first reported by Quinlan *et al*., 1989, postulating that that the head-to-tail linkage of two lamin dimers involves strong electrostatic attractions of distinct clusters of negative charge located on the opposite ends of the rod domain with arginine clusters in the head domain and the first segment of the tail domain. Given the conservation of arginine residues in the head, 1a and tail regions, this raises the question of whether head to tail assembly modes may be found in cytotardin.

Heitlinger *et al*., 1992 links the loss of head region in chicken lamin B to loss of head to tail assembly capacity. Since cytotardin is significantly reduced in the size of its head region compared to lamins, this raises the implication that the head to tail, or A_{CN} assembly mode may not be available to it. The TRITRLQ motif is shown to promote head to tail binding stage in mouse lamins, but cytotardin does not appear to possess an equivalent sequence (Kazuhiro *et al*., 2007). However Kreplak *et al*., 2004 links hydrophilic RRATR and RITR regions in the lamin head domain to the distinct head to tail assembly process of lamins and cytotardin possesses an alignable sequence of this kind in the first α-helix leading into the coil 1a region.

III.1.5: Coil 1a

The coil 1a region of cytotardin begins at least 22 residues in, as predicted by DeepCoil, though DeepCoil 2 (Zimmermann *et al*., 2018; Ludwiczak *et al*., 2019; Gabler *et al*., 2020) makes a more conservative estimate of 27 residues in as the start site. Uniprot's own predictor predicts the coil 1a region beginning as residue 20. However, there is a potential α-helix unit starting at residue 15 as predicted by JPred. The lamin 1 also has a potential α-helix shortly before the main 1a region. As seen in Fig. 2.3, this prediction does have a basis in an unambiguous HPPHCPC α-helix beginning at residue 15, whereby H is a hydrophobic residue, P is a polar residue and C is another charged residue. This region may serve some functions for the head domain however, as lamin assembly models in Kreplak *et al*., 2004 link it to the head to tail assembly pathway associated with lamins as this initial α-helix carries a pocket of positively

IF	Head	1a	1b	2	Tail
RAMVA Cytotardin	20	35	135	140	114
RAMVA Lamin 1	94	40	140	140	116
RAMVA Lamin 2	75	40	140	140	156
HDJD Cytotardin	18	40	143	139	81
HDJD Lamin 1	85	40	143	139	207
HDJD Lamin 2	76	41	140	140	188
E. rowelli Lamin	43	34	132	137	122
C. elegans Lamin	44	34	133	140	184
DROME Dm0	55	37	138	143	213
DROME Lamin C	47	39	138	146	218
TPAC Eye IF L10112.1	76	42	142	139	179
Ciona intestinalis Lamin	23	44	145	139	86
Human Lamin B1	33	35	134	143	200
Human Lamin A	33	37	138	141	281
Human Vimentin	94	32	92	139	59
D. discoideum Lamin NE81	130	40	140	140	124

Table 2: IF Rod Domain Proportions Comparison

Comparison by number of residues of the major regions and proportions of IF proteins in tardigrades, invertebrates and vertebrates. Protein analysis from Uniprot (white) or the authors analytics (shaded, see Methodology). *D. discoideum* lamin NE81 is explored in Krüger *et al*., 2012, Batsios *et al*., 2019

charged residues linked with the head to tail interaction in lamin head regions. All estimates, however, are unanimous in locating the end of coil 1a within residues 56-59. DeepCoil predicted residue 56 as the endpoint, while JPred 4 projected α-helix ending at position 58. Uniprot predicts the end of coil 1a at residue 59, which is where the α-helix depicted in Fig. 2.3 ends, again with an unambiguous HPPHCPC sequence.

The linkage of cytotardin to the molecular basis of head to tail lamin-style assembly is further supported by how cytotardin possesses conserved negatively charged LENE regions near the beginning of coil 1a, which are of the kind predicted by Kreplak *et al*., 2004 to bind positive pockets within the beginning of tail regions to complete the A_{CN} interaction. The LExE pattern is conserved in many lamins, as well as both *R. varieornatus* and *H. dujardini* cytotardin, but not those of tardigrades, where both lamins from both species possess two glutamine residues consecutively.

III.1.6: Coil 1b

Coil 1b shows regions linked with the A_{11} interaction, these may have implications for the assembly of cytotardin at the lateral alignment level of structural organisation. Coil 1b is estimated in cytotardin to start at residue 70 by JPred 4's estimations, as do DeepCoil2's, while the original DeepCoil program returns residue 64. The most obvious α-helix candidates sit at positions 64 and 74, albeit not with perfect charged residue components to their sequences. There then exists the implication, that going by Ahn *et al*., 2019's use of hendecad repeats in the L1 linker region, residues 70-74 may form a hendecad repeat region extension to the beginning of coil 1b.

The end of coil 1b is estimated to end at residue 213 by JPred 4's estimations, 255 by DeepCoil and 210 by DeepCoil 2. Uniprot's own sequence analysis is also not explicitly clear about which point coil 1b ends at, with the coil ending at 207 and then a second coil running from 228 to 259, appearing to coincide with DeepCoil's estimation. However since Uniprot already assigns the second coil a length of 140 a.a., it agrees best with existing models that the first coil endpoint, 207 a.a. be the implied endpoint for coil 1b. This is supported by Fig. 2.3, where the seven a.a. region beyond residue 205 is lacking in the hydrophobic residues required for α-helix formation.

IF	Post CC Length	Recognised LTD region	NLS	NucPred Score	CaaX Box
RAMVA Cytotardin	100	No	NO	0.56	NO
RAMVA Lamin 2	156	No	KRRL	0.92	CVIM
RAMVA Lamin 1	116	No	KRRDL	0.76	NO
HDJD Cytotardin	81	No	Incidental - RKR	0.87	NO
HDJD Lamin 1	207	115	NO	0.93	CVIM
HDJD Lamin 2	188	120	KKRK	0.91	NO
E rowelli Lamin	122	No	KRKR	0.93	CAIM
C elegans Lamin	184	116	KRRR	0.75	CSIM
DROME Dm0	213	127	KRKR	0.95	CAIM
DROME Lamin C	218	No	KRRR	0.89	NO
TPAC L10112.1 Eye IF	143	No	NO	0.65	NO
Ciona intestinalis Lamin	86	No	KRRSRRK RKR	0.96	CSIM
Human Lamin B1	200	117	GKRKR	0.86	CAIM
Human Lamin A	281	118	KKRK	0.93	CSIM
Human Vimentin	59	No	NO	0.58	NO
D discoideum Lamin NE81	201	123	RKRKR	0.96	CLIM

Table 3: IF Tail Region Features Comparison

Comparison of the major regions and proportions of IF proteins in tardigrades, invertebrates and vertebrates, analytics as detailed in Materials and Methods.

III.1.7: Coil 2

Cytotardin shares the conserved LLxxEE pattern at the end of coil 2. This region has been linked to head to tail assembly and the A_{22} binding by Ahn *et al*., 2019, and this motif could potentially serve as a negatively charged region required for head to tail interaction as according to the models proposed by Kreplak *et al*., in 2004. Uniprot estimates this coiled coil region comes in two parts, the first part beginning at residue 228 and the second part ending at residue 348. JPred 4 estimates that this region extends to residue 370, with the combined fit of heptad repeats matched to the HPPHCPC pattern leading to the conclusion that a 230-370 total length for the domain is most likely.

III.1.8: Tail

The tail region of *R. varieornatus* cytotardin when compared to that of *H. dujardini* has a 17 residue long divergent region, followed by a 14 residue long deleted region beginning at the end of coil 2 at residue 384 in *H. dujardini*, corresponding to residue 383 in *R. varieornatus*. The C- terminal deleted mutant variant of cytotardin was produced so as to both study the effects on filamentation, which can be quite significant, of lacking the tail region (Kaufmann *et al.*, 1985; Heitlinger *et al*., 1992). This truncation also to allows measurements to detect whether the loss of the tail domain leads to altered banding patterns in paracrystal, thus giving clues to the proportions of the cytotardin molecule. Prolines, amino acids strongly incompatible with α-helix formation, are entirely absent in all but the tail of cytotardin (Conway and Parry, 1988). The tail of cytotardin also possesses conserved arginine residues of the kind linked in Strelkov *et al*., 2004 to the head to tail assembly mode, albeit fewer of them than its lamin counterparts. As per the models postulated in Kreplak *et al*., 2004, these positively charged arginine residues, conserved in the tail region attract to the conserved negatively charged region in the LENE sequence in the coil 1a region and enable head to tail assembly. This was shown in experiments on GFAP and vimentin by Quinlan *et al*., in 1989, where the A_{CN} interaction enabling residues are shown to present on the root of the tail. As such, only complete deletion of the tail region prevented assembly, while desmin remained assembly competent after losing only the second half of its tail. The fact that the proteins used in that experiment, desmin and GFAP are both also cytoplasmic IF proteins with even shorter tails than cytotardin means this is potentially a useful model for tail region interactions, though not so much coiled coil interactions as they possess a different length

coil 1b. Given this sequence and the position of all these charged residues is near identically conserved in the *H. dujardini* cytotardin, this and the previous sections similar identification of critical regions in every component conserved in cytotardin, presents a compelling argument for the use of the A_{CN} assembly mode and thus lamin-type assembly in cytotardin. The lamin-1 has its NLS at residue 486, the A-type lamin at 443, with KRRDL and KRRL sequences more similar to human lamins than those of *E. rowelli* or *C. elegans*, though it shares the essential KRR part of the motif with *C. elegans* and thus may be considered more similar in the nature of its NLS. Cytotardin in *R. varieornatus*, unlike in *H dujardini* with several vestigial RKR regions, does not have anything resembling an NLS. NucPred gave cytotardin a score of 0.56, Lamin 2 0.92 and Lamin 1 0.76. In comparison the respective scores for *H. dujardini* cytotardin, Lamin 2 and Lamin 1 were 0.87, 0.93 and 0.91, implying a high degree of adaptation to cytoplasmic IF function between the two tardigrade species. However, given that immunofluorescence labelling in Hering *et al*., 2016 shows *H. dujardini* cytotardin to be localised outside the cytoplasm and the fact that the RKR sites in *H. dujardini* cytotardin did not align with those in the paralogous lamins implies the NucPred score of *H. dujardini* cytotardin is inaccurately high. In order to verify the modelling data so far discussed, *in vitro* experimentation is required.

As shown in Table. 0.2, both cytotardins lack any CaaX box, and *R. varieornatus cytotardin* lacks residues 389-402 found in *H. dujardini* cytotardin, reflected both in total peptide length and size of sequences similar to immunoglobulin-like tail domains (Krimm *et al*., 2002), implying greater divergence from their respective lamin ancestor. Notably, the 14 a.a. deletion region does not likely - by JPred 4 prediction of prospective beta sheet regions essential for the creation of anything approaching an Immunoglobin-like lamin tail - constitute part of a Lamin Tail Domain (LTD) proper, may indeed be a linker region as backed up by Uniprot structural predictions citing the region as a disordered one. This is further supported by how the deleted region is glycine-rich, a motif connected by Almagor *et al*., 2013 to high peptide flexibility. Whilst the *R. varieornatus* cytotardin does in fact have significant differences in its tail domain and less in the way of beta sheets required for a LTD, having 6, its *H. dujardini* counterpart 7 beta sheet domains compared to 14 detected in JPred analysis of human Lamin B1. *R. varieornatus*'s own lamins 1 and 2 do both have 14 of these beta sheet domains also. The reduced size and number of *R. varieornatus* cytotardin's beta sheet domains may instead come from the various mutations, including an insertion at residue 461. Despite cytotardin's divergence from its lamin ancestors, it has still conserved some lamin-like elements of its

morphology such as the proportions of the rod region and potential self-binding sites that will be discussed later in this section.

III.2: Cytotardin

III.2.1: Expression and Purification of Cytotardin

Our first goal was to establish whether the proteins of interest (POI) could be acquired in quantity for testing. To produce the Cytotardin (abbreviated "CYTT" when necessary) and the other POIs, bioproduction by expression in *E. coli* was required due to the low biomass of tardigrades as harvest of material from whole organisms such as in Quinlan *et al*., 1984, or Herrmann *et al*., 2004 was impractical. Instead, transgenic expression in bacteria was attempted. A plasmid carrying the required sequence were cloned in DH5α and the plasmids were screened first by digests with the restriction enzymes used to engineer them (Table 1), and then the presence in the plasmids of the cytotardin DNA sequence was confirmed by Sanger sequencing. The plasmids were then subcloned into BL21 *E. coli*, and overexpression was induced with IPTG (Fig. 3.1), all as detailed in Materials and Methods Parts 4 and 5, while induction with IPTG was monitored by SDS-PAGE as described in Part 8.

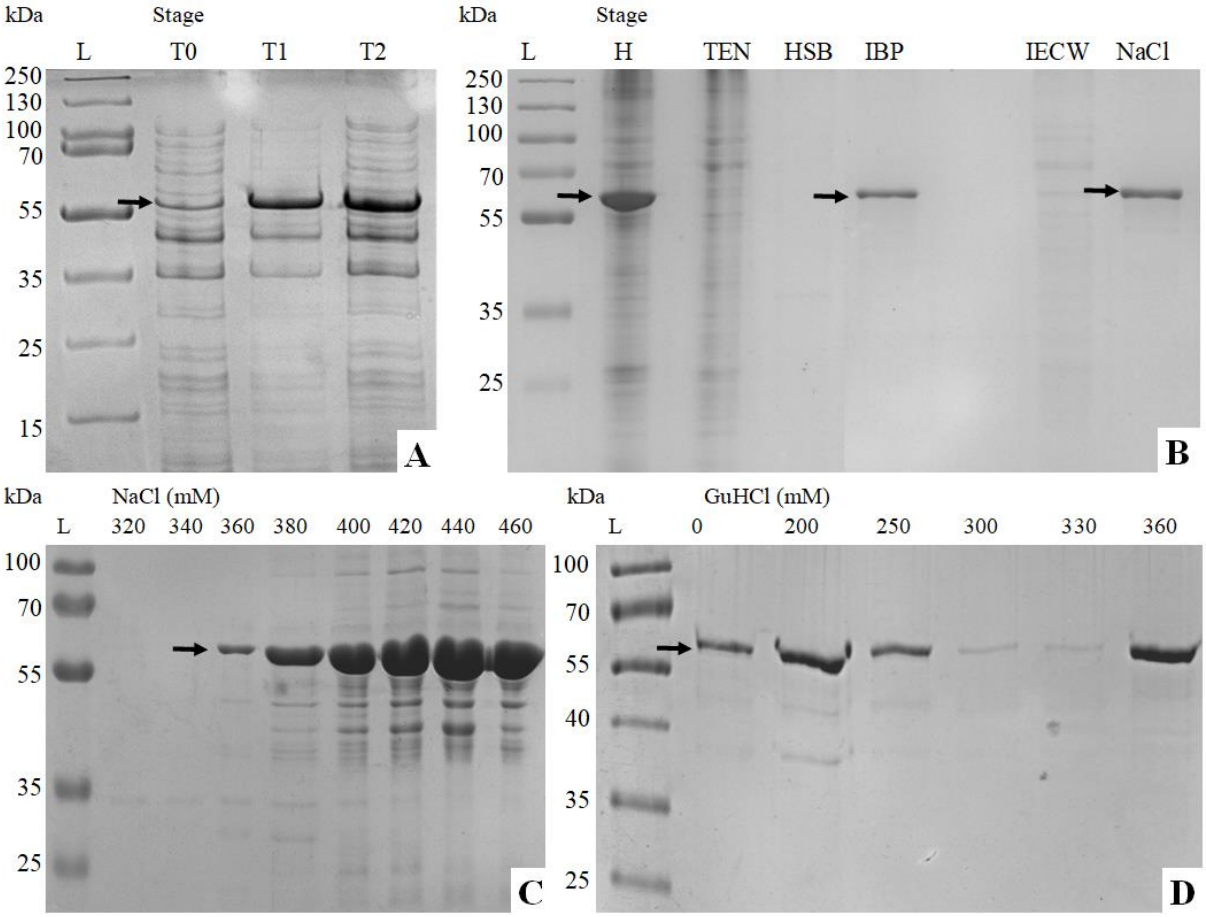

***Fig. 3.1*:** Induction and Purification of Cytotardin in *E. coli*

(A) Cytotardin induction at 0h, 1h and 2h, on 6h grown 20ml culture **(B)** Summary of purification steps, lanes from left to right: molecular ladder "L", washed and homogenised BL21 *E. coli* "H", impurities washed off in TEN buffer ("TEN"), non-cytotardin material washed off with High Salt Buffer ("HSB"), the resultant inclusion body preparation ("IBP"), impurities removed by IEC ("IECW"), cytotardin purified using NaCl based IEC ("NaCl"), and that purified using GuHCl based IEC ("GuHCl"). **(C)** SDS-PAGE gel of IEC fractions from TMAE column with calculated NaCl concentration shown horizontally across the top. **(D)** GuHCl mediated IEC marked the with the calculated concentration of GuHCl on the horizontal annotation. Lanes "L" are MWt markers indicated in kDa on the left, concentrations marked in mM on top.

Cytotardin, and the other POI formed insoluble inclusion bodies, the sedimentation of which, was used as a way to purify the material by washing off more soluble bacterial proteins, with the remaining impurities being removed via Ion Exchange Chromatography (IEC). Here the cytotardin was dissolved in 8M urea buffered by 20mM Tris-HCl pH8.8 and bound to a TMAE column. Initially NaCl was used to elute the bound cytotardin in a gradient from 0 to 1M NaCl. Due to the presence of lower molecular weight material in the cytotardin-containing fractions, attempts were made to elute with guanidine hydrochloride, which yielded better results, as evidenced in (Fig. 3.1). Here, cytotardin was eluted from the column at a NaCl concentration of 0.36M and over, whereas when exposed to the same concentration of guanidine hydrochloride it was eluted from the column more purely.

III.2.2: *In Vitro* Assembly of Cytotardin

To study the *in vitro* assembly properties of cytotardin, Tris-HCl buffer was used to control solution pH and ionic strength, though cytotardin has shown capacity to form aggregates and networks in NaH_2PO_4, Triethylammonium bicarbonate (TEAB) and 2-(N-morpholino)-ethane sulphonic acid (MES) buffered solutions as well. When dialysed out of the 8M into lower molar urea solution, the cytotardin forms disordered aggregates (Fig. 3.2), as a preliminary stage before more complex *in vitro* assembly before moving on to reticulated structures. The first assembly method attempted was assuming an *in vitro* assembly speed comparable to well-studied vertebrate IFs such as vimentin and desmin (Karabinos *et al.*, 2003). Here cytotardin would be first dialysed out of the 8M urea solution, into 2M urea solution and then into 0M urea, 2mM Tris-HCl 8.8 for 30 minutes at which point disordered networks form. When negatively stained the cytotardin will display reticulated structures as a preliminary stage before more complex *in vitro* assembly, and it behaves similarly during an additional 30 minutes in 2mM Tris-HCl 8.0 or 7.4. Following this, dialysis into 2mM Tris-HCl pH 7.4 for

30 to 60 minutes leads to the formation of reticulated networks of filament-like structures averaging 5-10nm in width begin to form, evocative of those characterised by cryo-electron tomography in Turgay *et al.*, 2017. These show visible bulges along ~25nm intervals, as marked by arrows in Fig. 3.3 B and C. Fig. 3.3C shows cytotardin assembling from compacted, just as it can from uncompacted cytotardin material.

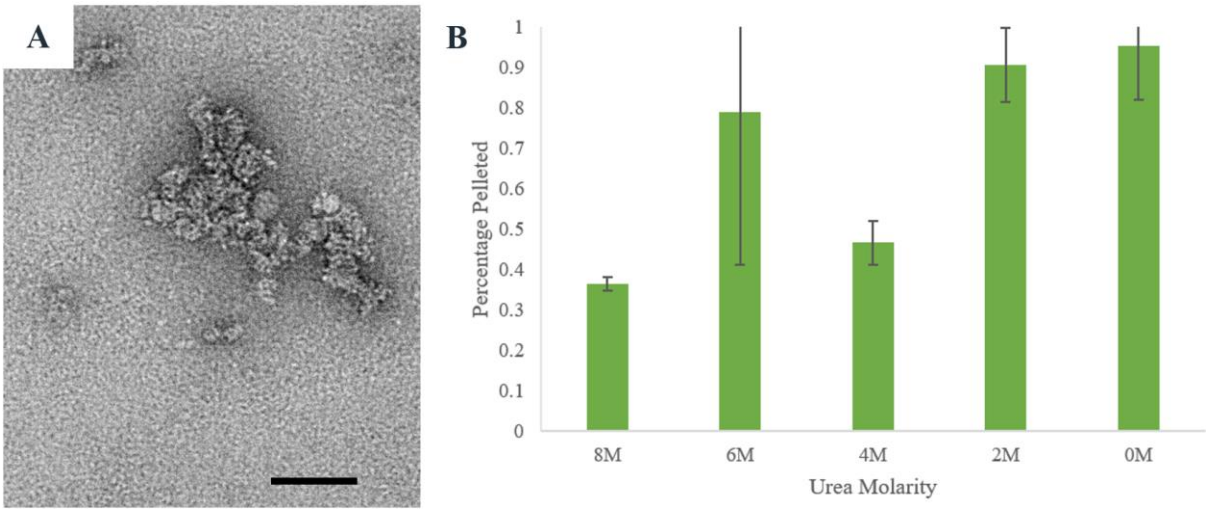

Fig. 3.2: Cytotardin restricted to low length aggregates in 4M Urea and above
Cytotardin under electron microscopy imaged at 6M Urea **(A)**; quantified with exploratory sedimentation assay at 77,100g for 1h **(B)**. Scale Bars 100nm, error bars are standard error.

Then, after another hour of dialysis in 15mM Tris-HCl pH 7.4, fibre-like structures appear, often with non-compacted material (Fig. 3.3B) or smaller filament structures (Fig. 3.3C) visibly connected to the fibre. The final stage of this in vitro assembly occurs when the ionic strength of the concentration is increased to 15mM Tris-HCl, leading to extensive assembly and aggregation of the structures. This type of structure can also be seen by rapid, heavily stirred dialysis directly to a pH of 7.4 at a lower ionic strength concentration such as 2mM. Similar reticulated structures are visible, though the reticulated networks appear more stable and persistent in the solution, showing head to tail tetrameric/protofilament-like structures with an average width of 7.4nm ±2nm, fitting loosely with the observed widths of *C. elegans* lamins in (Tenga and Medalia, 2020). IF thickness can vary by a ratio of up to three times along a filament, as in vimentin (Herrmann *et al.*, 1996).

To measure the efficiency of cytotardin assembly, sedimentation assays were performed, in which cytotardin left to assemble for a given time was centrifuged so that the supernatant and

pellet could be compared to see which contained what proportion of the original protein (Fig. 3.3D-E). For the first sedimentation assay solutions of cytotardin were dialysed from 8M to 2M Urea, into a sequence of buffers as set out by Fig. 3.3. In the case of this cytotardin *in vitro*

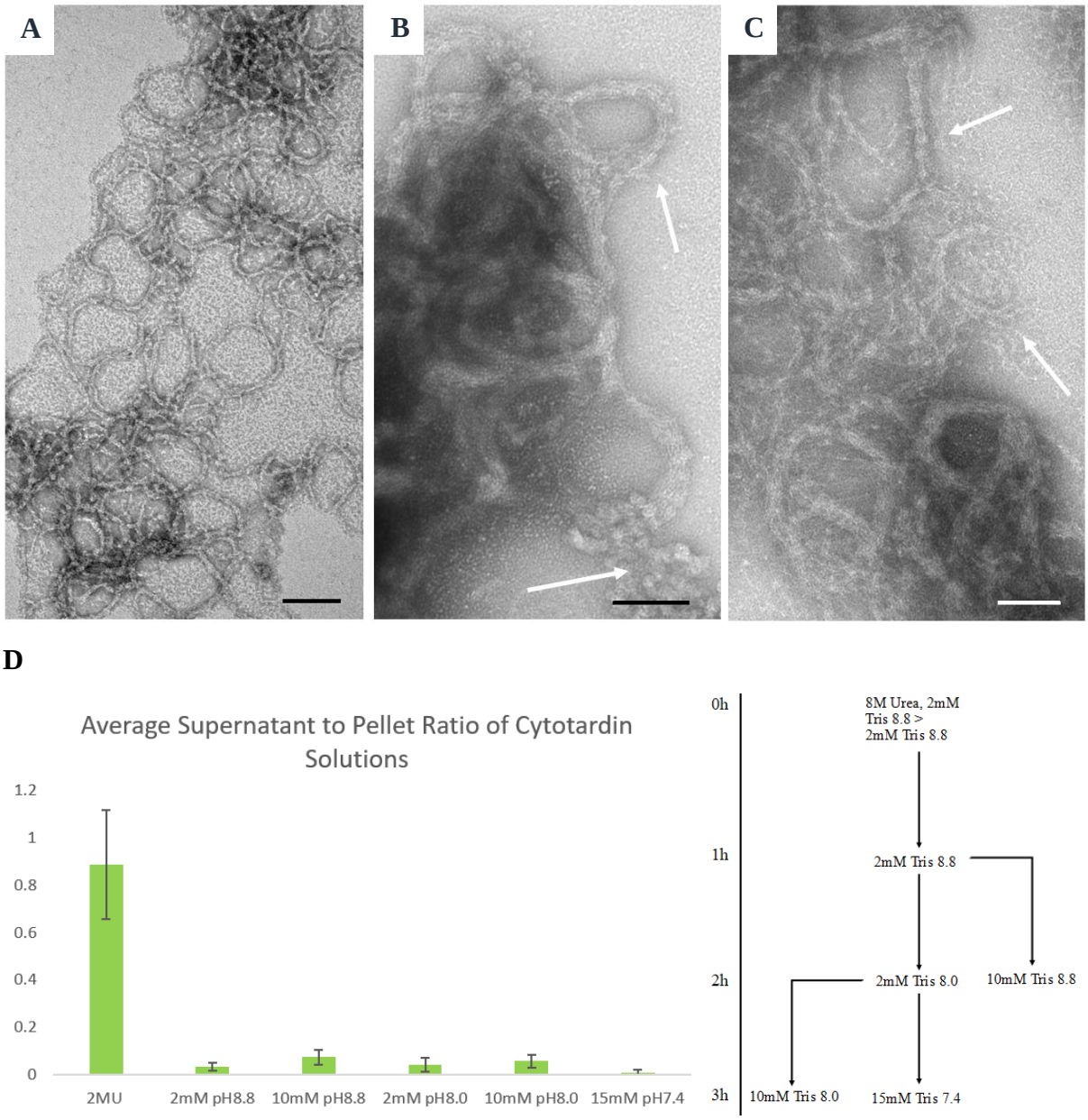

Fig. 3.3: Cytotardin Assembly *in vitro*

EM of negatively stained cytotardin after 30m in 2mM Tris-HCl 7.4 **(A)**. Cytotardin after dialysis for 30 minutes in 2mM Tris-HCl pH 8.8 and 2mM Tris-HCl pH 8.0 each, now dialysed for 1h in 15mM Tris-HCl pH 7.4 **(B, C)**, transition from forms found in **(A)** marked with arrows. **(D)** Data shown from analysis of pelleting of cytotardin at RCFs of 2.14 x 10^5, 1.37 x 10^5, and 7.71 x 10^4 g for 30 minutes with a TLS-55 rotor. Alongside, a chart to the with dialysis time labelled on the left. Scale bars are 100nm, error bars are standard error.

assembly procedure, pelleting of cytotardin occurred at RCFs of 2.14 x 10^5, 1.37 x 10^5, and 7.71 x 10^4 g for 30 minutes with a TLS-55 rotor. The k factors of the centrifugations were 60.5, 94.5, and 168 respectively, leading to the sedimentation of bodies over 121S, 189S and 336S respectively. That the overwhelming majority of cytotardin is found in the pellet, in these structures provides a biophysical demonstration of the efficiency with which it assembles.

III.2.3: Cytotardin can form Paracrystals

Divalent cations, such as the used in Heitlinger *et al*., 1992 and Karabinos *et al*., 2003 have been shown to induce paracrystal formation in lamins, whilst monovalent cation presence is both useful for paracrystal and filament growth (Aebi *et al*., 1986). This presented the hypothesis of whether cytotardin would act similarly.

Cytotardin forms paracrystalline bodies after 1 hour's exposure at a 2mM Tris-HCl pH of 8.8 to 20mM $MgSO_4$ (Fig. 3.4A). These bodies are flexible enough to regularly form splits and loops, and are often found with pre-compaction stage material visible alongside. Cytotardin paracrystals develop further after overnight exposure to the $MgSO_4$ solution, producing a triple banded system (Fig 1.4B), as fitting with the predictions in the IF assembly model posited in Ahn *et al*., 2019 and the X ray crystallographic studies of vimentin fragments in Guzenko *et al*., 2017. This also suggests that the paracrystal subunits are dynamic. Various stages of the paracrystallisation process are available in paracrystals formed by cytotardin after exposure to $CaCl_2$. After long term exposure to the $CaCl_2$ solution, the cytotardin displays similar paracrystalline properties and banding patterns to the truncated B1 lamins featured in (Heitlinger *et al*., 1992). Protofilament sized bundles are observed laterally associating (Fig. 3.4D), clustering together at certain sections (Fig. 3.4E) and finally forming large paracrystals (Fig. 3.4F). The banding pattern in the $CaCl_2$ buffer bears some resemblance to models of lamin assembly and paracrystallisation earlier described in the literature, such as Min *et al*., 1996 and Ben-Harush *et al*., 2009. Though there is significant variation in individual bands across small widths of the paracrystal, the banding pattern in initial $MgSO_4$ cytotardin paracrystals averages at 24nm.

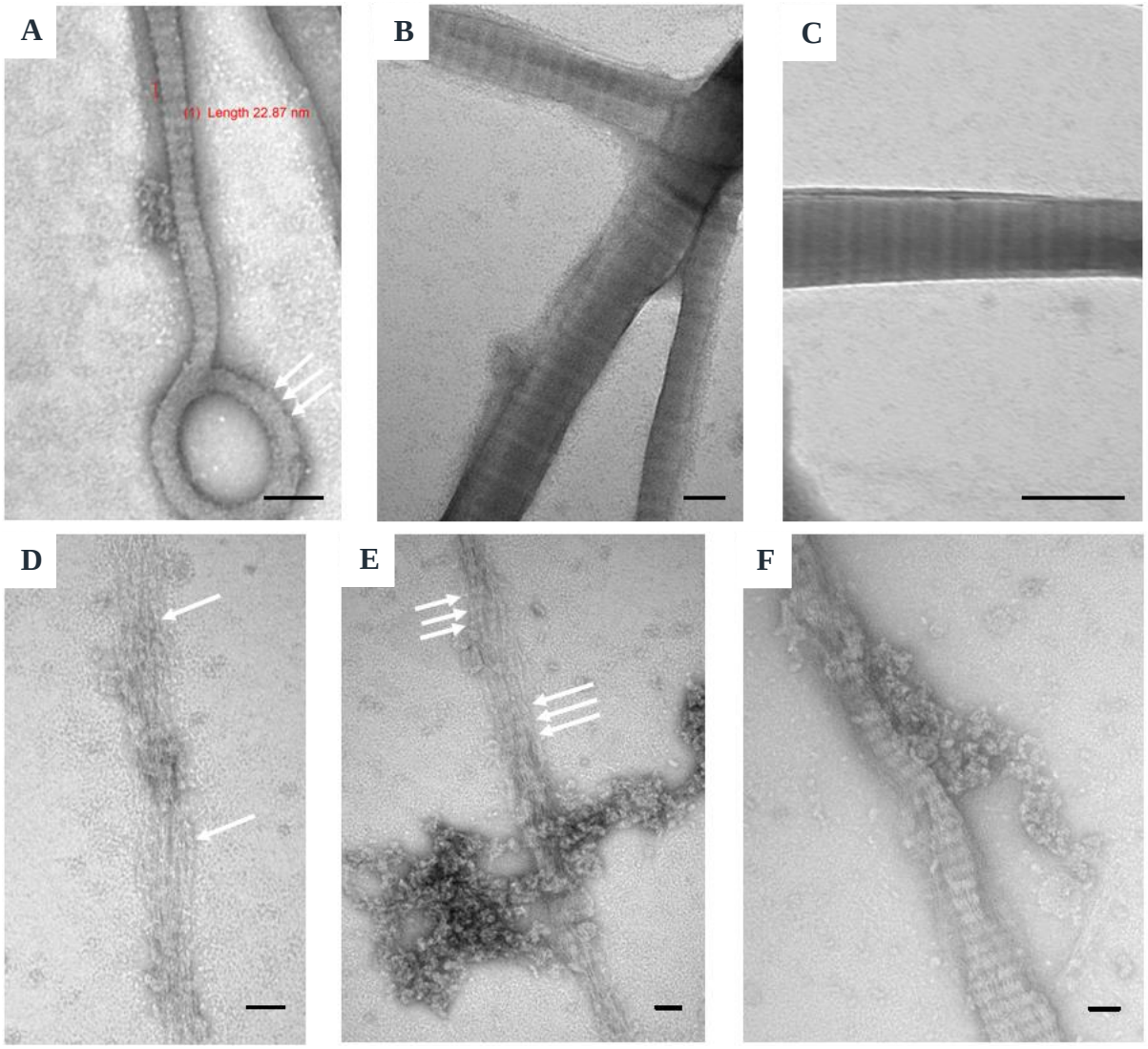

Fig. 3.4: Cytotardin forms Paracrystals across a Range of Divalent Cations

(A) Cytotardin after 1h dialysis into 2mM Tris-HCl pH of 8.8 to 20mM $MgSO_4$. Segmentation in loop marked with arrows. Cytotardin after 20h dialysis into 2mM Tris-HCl pH of 8.8 to 20mM $MgSO_4$ **(B)**, with close up and measurements **(C)**. Triple banding pattern marked with arrows. **(D-F)** Montage of paracrystal formation by cytotardin after exposure to 2mM Tris-HCl 8.8, 20mM $CaCl_2$. Scale bars 100nm.

III.2.4: Cytotardin can form Paracrystals without Divalent Cations

Given the assembly efficiency of cytotardin, attempts were made at inducing *in vitro* assembly by single step dialysis into 15mM Tris-HCl 7.4, equivalent pH to a well oxygenated cell, and 15mM Tris-HCl 7.6, just above the limit of cellular pH in non-extremophiles. A less forceful sedimentation assay was attempted, using an RCF of 2400g, for 10 minutes (minimum $3.17x10^5$S bodies), in which over 90% of the material sedimented in all samples taken, the first being after 10 minutes of dialysis. In order to show a rate of aggregation for the material, the

sedimentation assay was repeated using both a lower centrifugation time of five minutes and a lower cytotardin concentration – the latter showing differing sedimentation rates as would be expected (Fig. 3.5D). Cytotardin displayed the capacity to rapidly assemble with over 90% of the resultant bodies having minimum Svedberg coefficients of $6.04x10^5$S (Fig. 3.5D) at pH 7.4 within 15 minutes of initiating dialysis out of 8M urea. The paracrystals produced are capable of interconnecting both with each other and with the pre-compaction reticulum (indicated by arrows, Fig. 3.5C) to produce large networks tens of micrometres across.

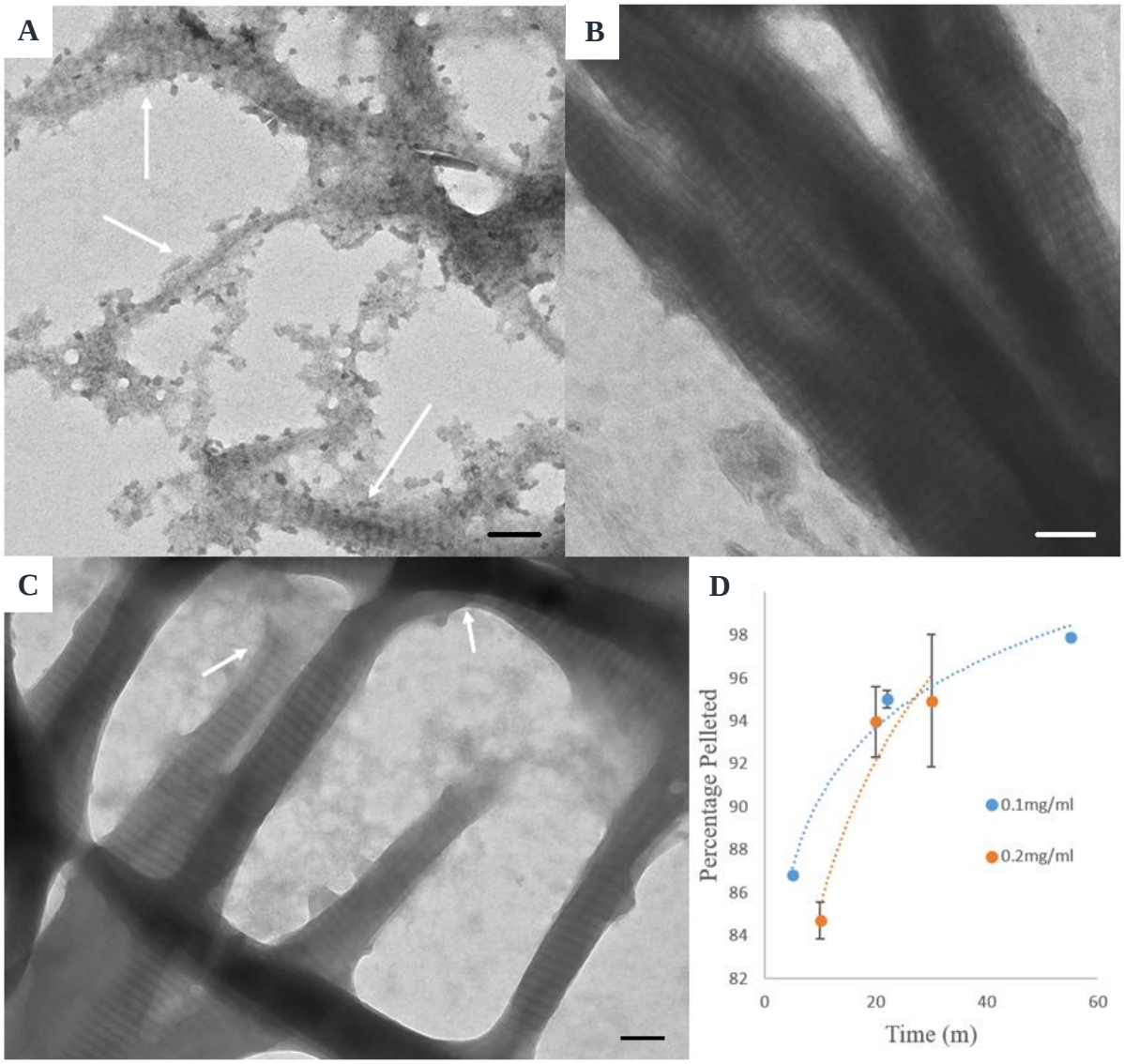

Fig. 3.5: Cytotardin can form Paracrystals without Divalent Cations

Structures produced by cytotardin after dialysis directly into 15mM Tris-HCl 7.4 buffer, after 15 minutes **(A)**, after 1h **(B)**. Structures produced by cytotardin after 1h dialysis into the 15mM Tris-HCl 7.6 buffer **(C)**. Sedimentation of cytotardin 2400g for 5 minutes, over time during dialysis directly into 15mM Tris-HCl pH 7.4 solution **(D)**. All buffers had 1mM EDTA. Scale bars 100nm, Error bars are standard error.

III.2.5: Cytotardin Paracrystallisation can occur Across Diverse Ionic Conditions

The paracrystals created at 2mM Tris-HCl pH 8.0 averaged 25nm in banding pattern, as did those formed at 2mM Tris-HCl pH 8.8 (Fig 3.6). Cytotardin was then tested for paracrystallisation capacity in other buffer conditions. To test whether cytotardin could form paracrystals at both weaker and less alkaline cellular pH than 15mM Tris-HCl pH 7.4, cytotardin was dialysed at 0.5mM Tris-HCl pH7.1, forming 25nm banding pattern paracrystals. To test whether cytotardin could form paracrystals at cellular pH with a cellular molarity of monovalent cations (Milo *et al*., 2010), modelled here with 100mM NaCl, the cytotardin not just formed paracrystals with a 25nm ± 0.9nm banding pattern (Fig. 3.6A), but

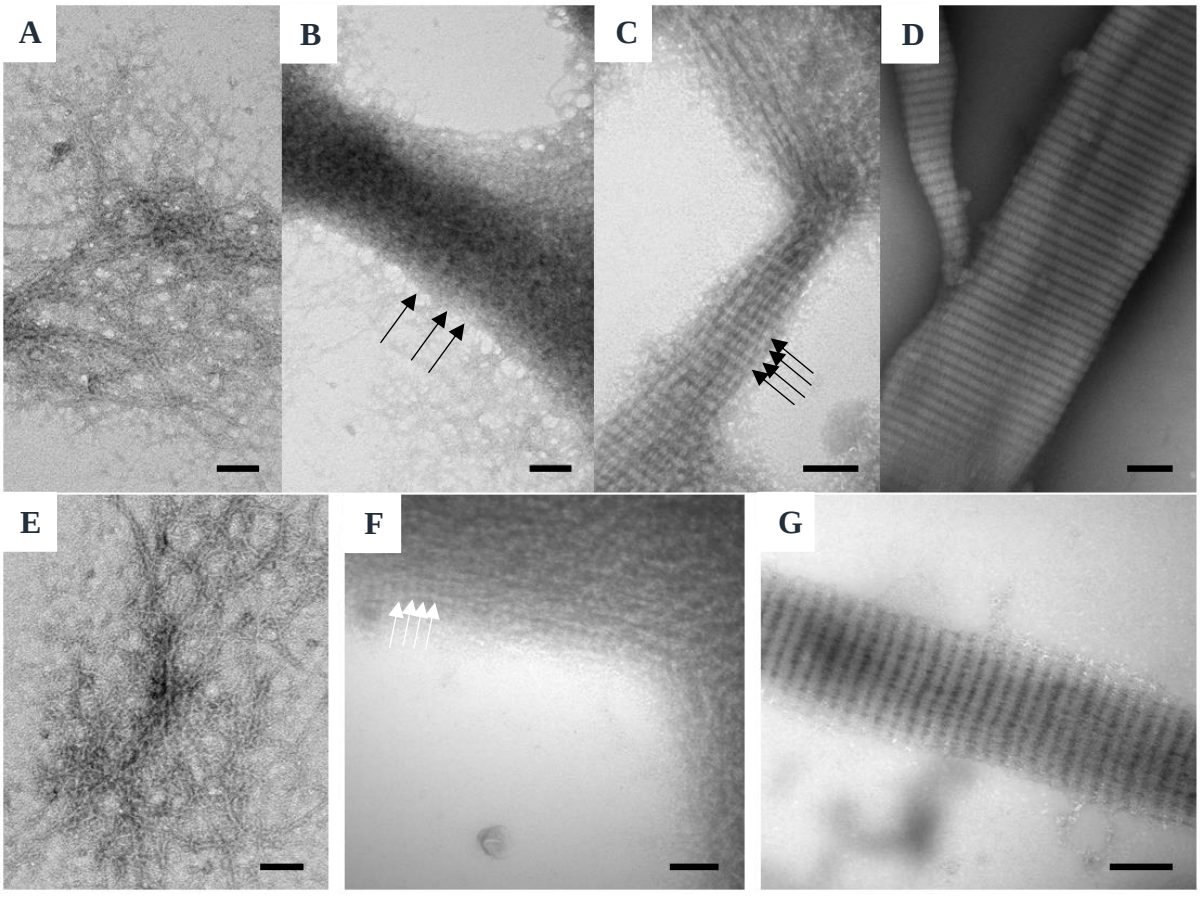

Fig. 3.6: Cytotardin can form Paracrystals at High pH without Divalent Cations

Paracrystallisation stages in cytotardin at pH 8.0 in Tris-HCl Buffer. Images taken 15 minutes after dialysis into 2mM Tris-HCl 8.0 **(A, B)** Samples taken 45 minutes after dialysis in 2mM Tris-HCl pH 8.0 **(C)** Samples taken 1h after dialysis in 0.5mM Tris-HCl pH 8.0 **(D)**. Paracrystallisation stages in cytotardin at pH 8.8 in 2mM Tris-HCl Buffer, taken 15 minutes in **(E)**, taken 45 minutes in **(F)**, taken 1h in at 10mM Tris-HCl 8.8 **(G)**. Scale bars 100nm.

the resultant bodies were heavily interlinked on a scale covering many tens of µm. In order to test whether cytotardin could form paracrystals under the influence of divalent cations whilst also potentially affected by other ionic solutes, cytotardin was dialysed into a combined 20mM NaCl, 20mM $MgSO_4$, 20mM Tris-HCl 8.8 solution, which was negatively stained showing extensive *in vitro* assembly, but current estimates on banding pattern length reach 24.3nm ± 0.6nm. This was accompanied by sedimentation assay to pellet all structures produced over $6.04x10^5$S.

To test if cytotardin could be observed forming complex structures in the absence of any ions whatsoever, cytotardin was negatively stained following dialysis into 18.2 MΩ.cm deionised water and subject to the same strength sedimentation assay as that in the 20mM Tris-HCl, 20mM NaCl, 20mM $MgSO_4$ buffer. While paracrystals were found, and similar rates of aggregation were found in the sedimentation assay to those in the aforementioned high ionic strength buffer, the paracrystals in the dH_2O (Fig. 3.7E) showed far greater morphological similarity with those of the 0M NaCl Tris-HCl pH 7.1 buffer (Fig. 3.7A) than with those grown in NaCl-containing solutions (rest of Fig. 3.7). This, and the implications from the lower width that imply faster paracrystal formation (Javadi *et al*., 2019) than for the NaCl-free paracrystals leads to the conclusion that monovalent cation concentration helps promote cytotardin paracrystal assembly. Judging by the significant reduction in large cytotardin bodies after 10 minutes dialysis in the dH_2O not seen elsewhere, it would support the possibility illustrated in the micrographs that cytotardin paracrystals have a far greater flexibility and stability (Fig 1.6).

As a result of these experiments, it was concluded that cytotardin possessed an unparalleled ability to self-assemble into paracrystals both without the requirement for cations in the solution, and at an extreme range of pH and ionic strength.

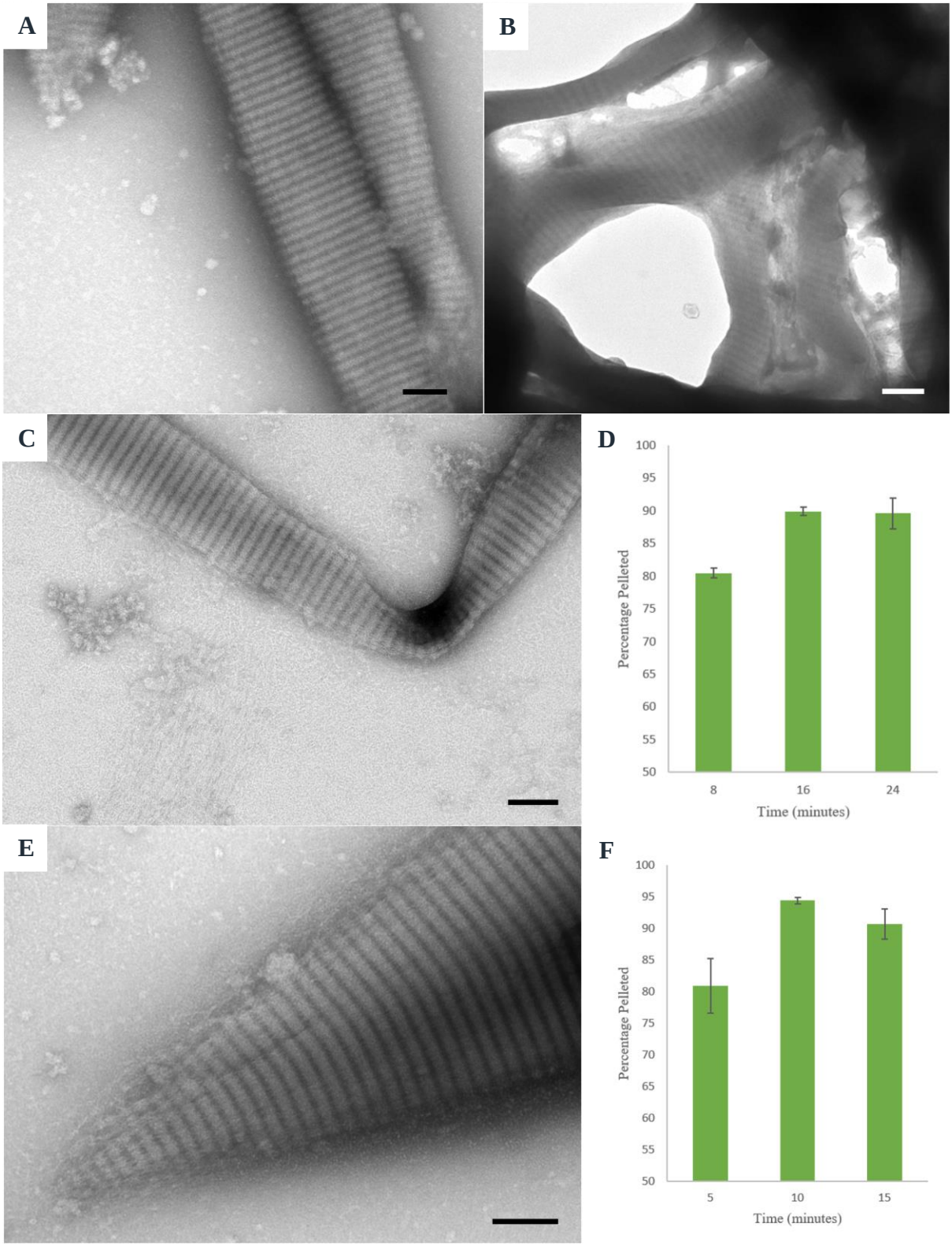

Fig. 3.7: Cytotardin can form Paracrystals regardless of ion levels

Cytotardin dialysed into 0.5mM Tris-HCl 7.1, 0M NaCl after 1h **(A)** and 15mM Tris-HCl 7.0, 0.1M NaCl after 30m **(B)**. Cytotardin dialysed into Tris-HCl 8.8, NaCl, $MgSO_4$; all 20mM **(C)** and pellet ratio vs time in minutes from sedimentation assay thereof conducted at 2400g for 5 minutes **(D).** Cytotardin dialysed into deionised water **(E)** and sedimentation assay thereof conducted at 2400g for 5 minutes **(F)**. Scale bars 100nm, error bars are standard error.

III.2.6 Cytotardin can increase Solution Viscosity and form Gels

Solutions of assembled IFs cannot just increase the viscosity of a solution, but induce gel formation. This is physically defined as a solution with a higher elastic than viscous modulus. IF based gels exhibit strain stiffening; that is, they stiffen under strain, avoiding the large deformations which could damage or disrupt the network (Kornreich *et al.*, 2015). This of course does not occur when the onset of strain is too rapid for the gel to withstand, as in this case the network simply ruptures.

In order to test the mechanical capacity of cytotardin solutions, the first experiments performed were simple continuous shear rate tables (Fig. 3.8A) performed on cytotardin solutions at 0.2mg/ml compared well to equivalent concentrations of BSA included as a control, peaking at viscosities measured at 4cP and predicted to be lower (Monkos, 1996) and to water at 0.89cP. Whilst some data has been excluded due to the predominant influence of the measurement device's internal friction, some of which, specifically the sample's viscosity and internal strain at over 1000Hz, were re-included as they raise the question of interactions between the cytotardin networks and the internal currents that affect the kinematic component of the viscosity, in rapid-flow situations. The oscillatory viscometric sample data also raises questions over whether the silicone oil or DOPC used to prevent evaporation may have had any effect on measurements sue to interaction of cytotardin with the water-fluid interface (Traub *et al.*, 1986) or the materials having mixed with the fluid body. As the impact of cytotardin at these concentrations failed to increase viscosity sufficiently to achieve gel formation, 1mg/ml solutions were then tried (Figure 1B), which were then shown by time sweeps to persistently exceed 1000cP, or 10^{-0} Pa.s. The 2mM pH 8.8 cytotardin solutions were weaker as the previous data suggested, weakening under the strain from an order of 10^{1} to 10^{0} Pa.s. The cytotardin in 15mM Tris-HCl pH 7.1 is most viscous, with the 0.1M NaCl buffer samples persisting at 10^{1} Pa.s and the 0M NaCl sample peaking at 10^{2} Pa.s. In order to ascertain the ability of these cytotardin solutions to act as a gel, frequency sweeps were conducted in order to compare the viscous and elastic moduli, in which all both samples "Sample 6", "Sample 7" and "Sample 9", and their respective repeats, all showed significantly higher elastic than viscous moduli (Fig. 3.8C). A longer, time sweep rheological examination was also performed and again confirmed the same result, with the error rate for viscous moduli calculated to be 0.004Pa.

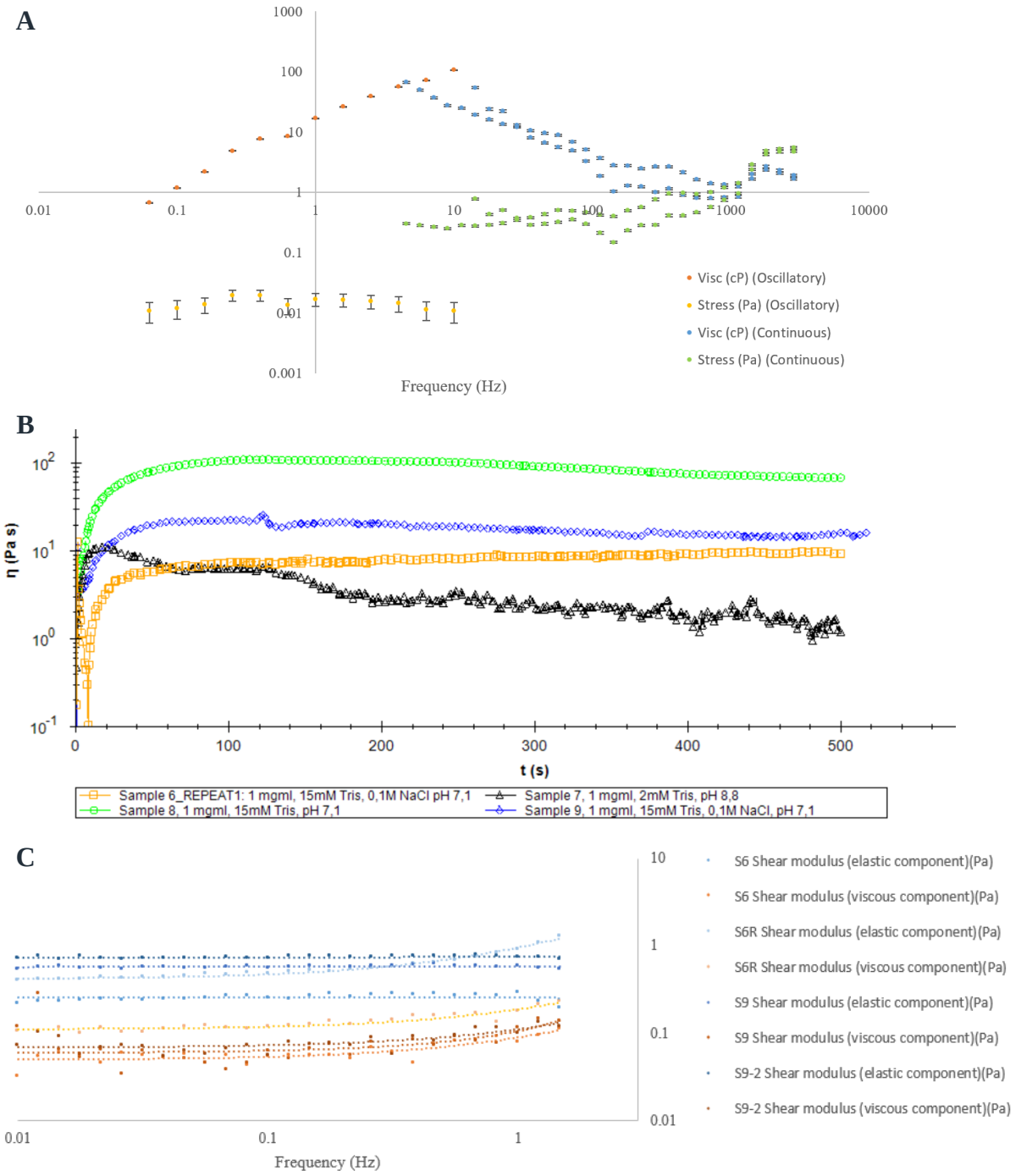

***Fig. 3.8*:** Viscosity and Shear Moduli for Cytotardin Solutions

(A) Comparative viscometry of 0.2mg/ml cytotardin solutions in 2mM Tris-HCl pH 8.8: A variety of 0.2mg/ml cytotardin solutions. **(B)** Viscometry via 0.5Hz Time Sweep of 1mg/ml cytotardin solutions. For the reader, viscosity η 1 cP = 10^{-3} Pa.s. **(C)** Comparative viscometry and analysis of 1mg/ml cytotardin solution via Frequency Sweep. Elastic Moduli in blue, Viscous Moduli in red/orange. Error bars are negligeable unless shown otherwise on all measurements, the viscosity values shown in A(i) are error barred by standard deviation.

III.3: Cytotardin Mutants

III.3.1: C-Terminal-Deleted (CTD) mutant cytotardin

Once the CTD-cytotardin plasmid was produced as described in Materials and Methods, it was screened by restriction endonuclease (NdeI-Sal1, plus NdeI-BamHI as a control) digest, followed by Sanger sequencing. The CTD mutant was engineered by placing a stop codon at position 1171 in the cytotardin DNA sequence, producing a 390 a.a. molecule all but completely lacking in a tail region.

III.3.2: Expression and Purification of CTD mutant Cytotardin

Inclusion Body Preparation (IBP) went as described in Materials and Methods, and similarly to section III.1.1 with minor differences (Fig 4.1). TE buffer was used instead to TEN buffer for the final step so the NaCl from the TEN buffers previously used for the final suspension and centrifugation cycle of the IBP did not interfere with binding to the TMAE column, where the CTD cytotardin eluted between 0.2 and 0.23M guanidine hydrochloride. Pure fractions were stored for further use and samples were added to a montage of the purification process (Fig. 4.1B).

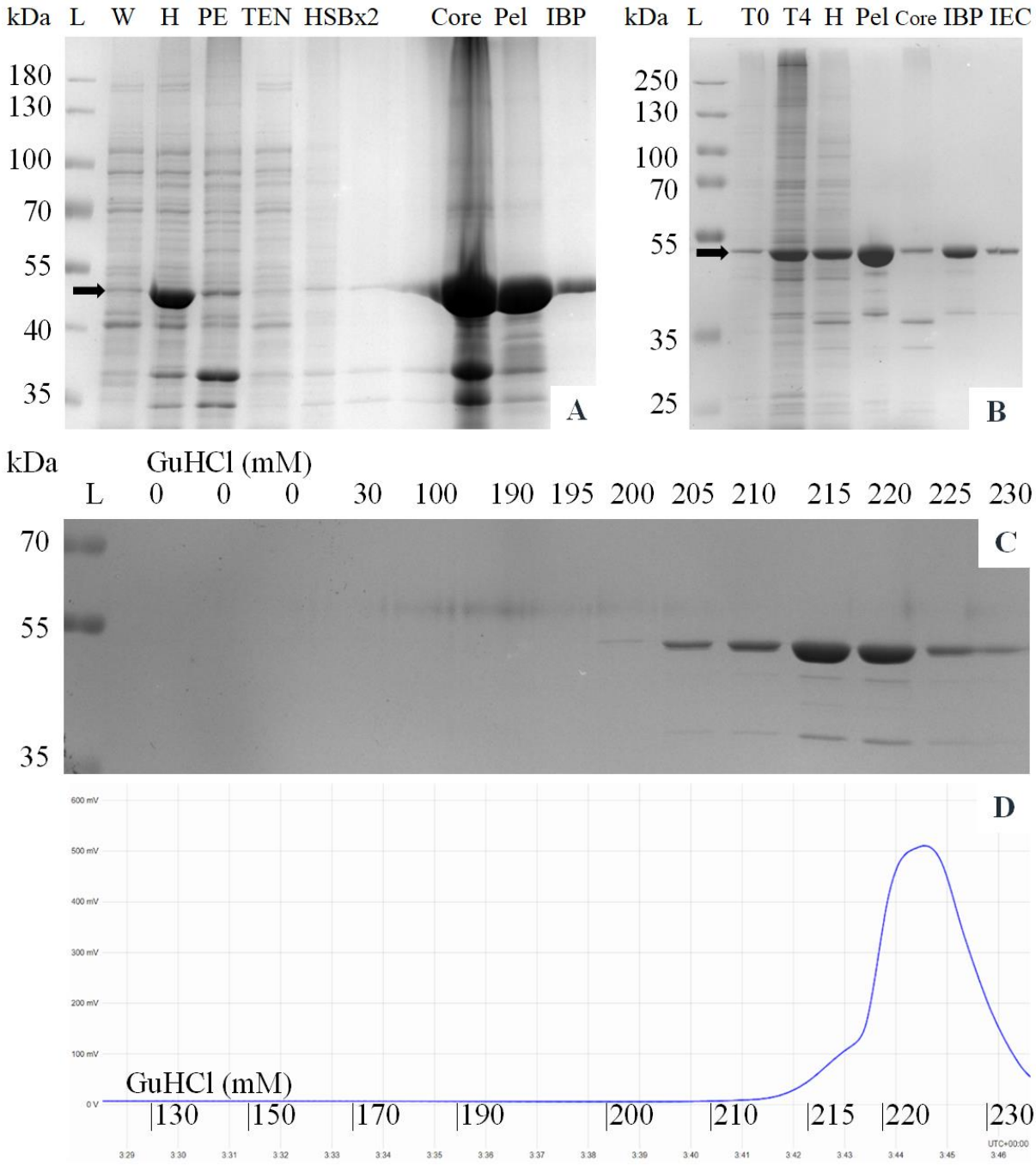

Fig. 4.1: Expression and Purification of CTD Cytotardin

(A) Inclusion Body Preparation: lane "W" with material washed off the BL21 pre-lysis, bacterial homogenate "H", distinct lighter material "PE" mechanically removed off the edge of the pellet during centrifugation, material washed off with "TEN" buffer, both high salt buffer washes "HSB", the pellet core "Core", the main pellet body "Pel" and the finished IBP "IBP" **(B)** Summary of purification: uninduced BL21 "T0", induced BL21 "T4", homogenate thereof "H", the final pellet from which the inclusion body prep was extracted ("Pel"), the darker pellet core ("Core"), the finished IBP ("IBP"), fraction purified via IEC ("IEC"). **(C)** Fractions from IEC of the IBP, fractions labelled by molarity of GuHCl at which they eluted. **(D)** Chromatogram of CTD IEC. Lanes "L" carry the MWt markers, annotated to the left in kDa, GuHCl concentration marked in mM.

III.3.3 *In Vitro* Assembly of CTD mutant Cytotardin

CTD cytotardin, like its wild type counterpart, tends to aggregate rapidly when not solubilised in 8M Urea solutions, albeit not as rapidly and densely as the wild type (Fig. 4.2). Initial experiments followed the procedures successful for wild type cytotardin in Fig. 3.3. Self-associating less efficiently than the wild type, CTD formed uneven reticula at most pH, only producing reticulated filaments of similar uniformity at pH 8-7.4. Similar experiments in 0.5mM Tris-HCl were also tried, and the filaments showed reduced reticulation above pH 7.1.

The initial sedimentation assays conducted, shown in Fig. 4.2, at 77,100g to bring down anything above 336S, showed the 8.2% sedimentation for CTD mutant within the first hour, 13.5% after two hours and 14.5% after four. Additional exploration implied approximately 12.1% of this was in bodies over 672S, which combined with the significantly reduced rate of aggregation over the last two hours of the main experiment supports the hypothesis that aggregation was limited rather than just delayed. Additional sedimentation assays were performed on CTD cytotardin in 15mM Tris-HCl pH 7.6 at 2400g for 10 minutes and the rate of at which the cytotardin bodies reach a minimum of $3.17x10^5$S, this experiment being performed for both wild type and CTD mutant cytotardin (Fig. 4.2). The CTD mutant displayed considerably lesser capacity to assemble into comparably dense networks to the wild type (averaging 6.4% sedimentation over the first 30 minutes compared to 90.4% in cytotardin,

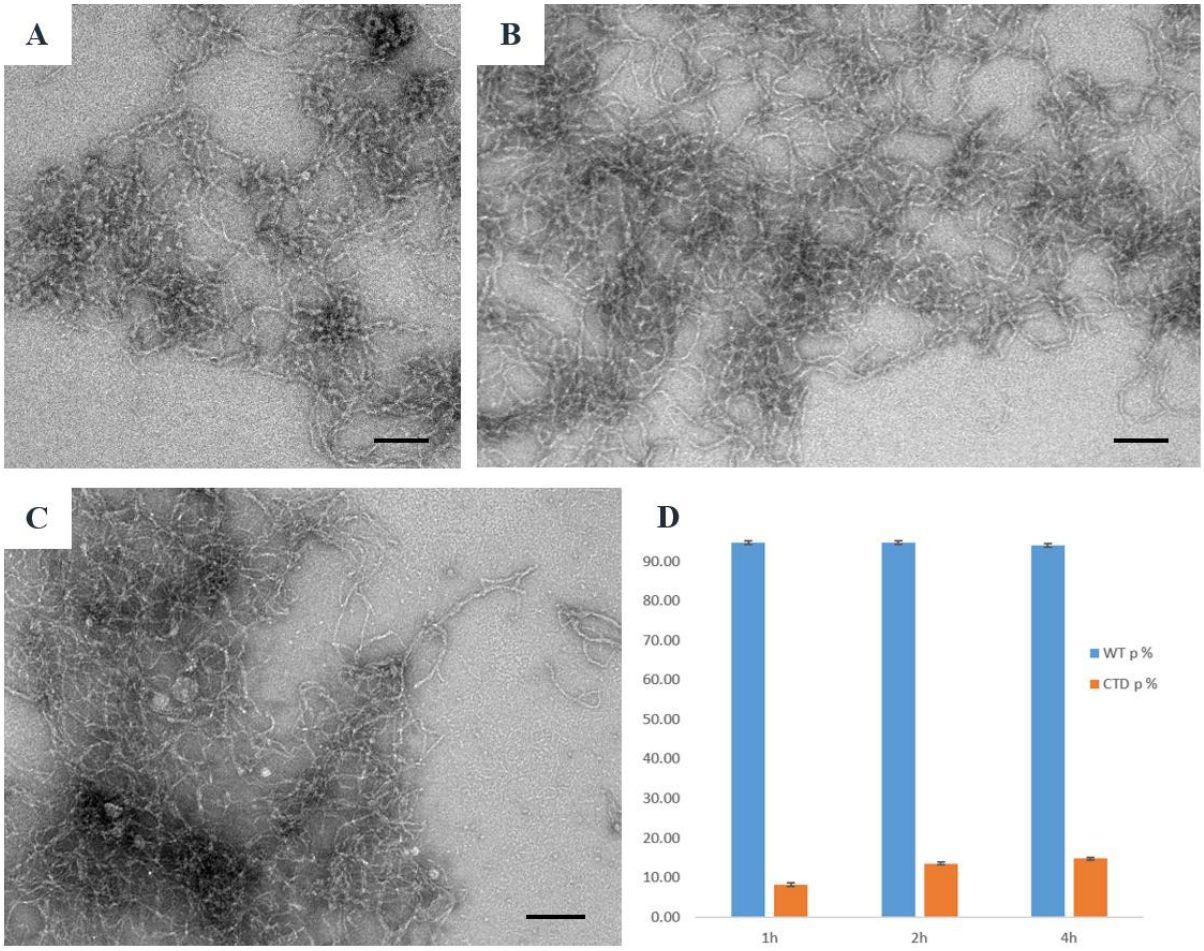

Fig. 4.2: *In vitro* Assembly of CTD Mutant Cytotardin

(A) CTD-cytotardin in 2mM Tris-HCl pH 8.8. **(B)** CTD-cytotardin in 2mM Tris-HCl pH 8.0 **(C)** At 15mM Tris-HCl, pH7.4 these reticulated networks. **(D)** Sedimentation Assay at 77100g for 30 minutes of wild type cytotardin and CTD mutant, showing percentage of the protein assembled into centrifugable bodies upon dialysis into 15mM Tris-HCl pH 7.6. All buffers with 1mM EDTA. Scale bars are 100nm, error bars are standard error.

during 2400g-10 minute centrifugation), and took over an hour to form structures visible with the naked eye compared to its wild type counterpart which could do so in as little as 15 minutes. More powerful sedimentation, for 30 minutes at 137,000g - and thus constructs over 189S in size - managed to sediment approximately 50% of the CTD-cytotardin after the first hour of assembly, though from four to eight hours only 40% of the CTD cytotardin was sedimented. As such these experiments indicated that the CTD mutation not just inhibits the ability of cytotardin to form large constructs, but the long term stability of reticulum it produces.

III.3.4: Paracrystal formation is inhibited in CTD-cytotardin

Paracrystal formation was not completely achieved when exposing CTD cytotardin to Ca_{2+} ions, shown here with 0.2mg/ml CTD-cytotardin in 20mM $CaCl_2$, buffered by 2mM Tris-HCl,

beginning to assemble into paracrystals after 1h (Fig. 4.3A). However, this paracrystalline pattern disappears as the filaments develop and by at least 20h they completely lose the banding pattern (Fig. 4.3B), rather than develop it as the wild type does under long term exposure to divalent cations (Fig. 3.4).

Though divalent cations are usually associated with the development of paracrystalline structures (Heitlinger *et al*., 1992; Karabinos *et al*., 2003), here 2mM Tris-HCl pH 8.8, 20mM $MgSO_4$ solution induces the formation of 10nm filament sized structures (Fig. 4.3C). After 4 hours, this process has further progressed, forming extensive but less ordered filament reticula capable of covering tens of µm across. At 0.2mg/ml, little above the concentration of vimentin in a Hela cell (Luby-Phelps, 2000), this filament protein is capable of creating reticulated networks of IF-width filaments despite lacking all but the first 20 residues of its tail domain.

This impaired ability to form paracrystalline bodies with a consistent banding pattern between filaments in the presence of divalent cations confirms established literature surrounding the importance of the tail domain in the response of IFs to divalent cations (Lin *et al*., 2010 Aufderhorst-Roberts and Koenderink, 2019; Brennich *et al*., 2014). A range of CTD cytotardin solutions were negatively stained, including the low ionic strength solutions tried on wild type cytotardin, and whilst the wild type was able to form paracrystals across a range of pH 7.1-8.8 Tris-HCl solutions at as little as 0.5mM Tris-HCl, the CTD mutant was unable to form sustainable paracrystals in any of them.

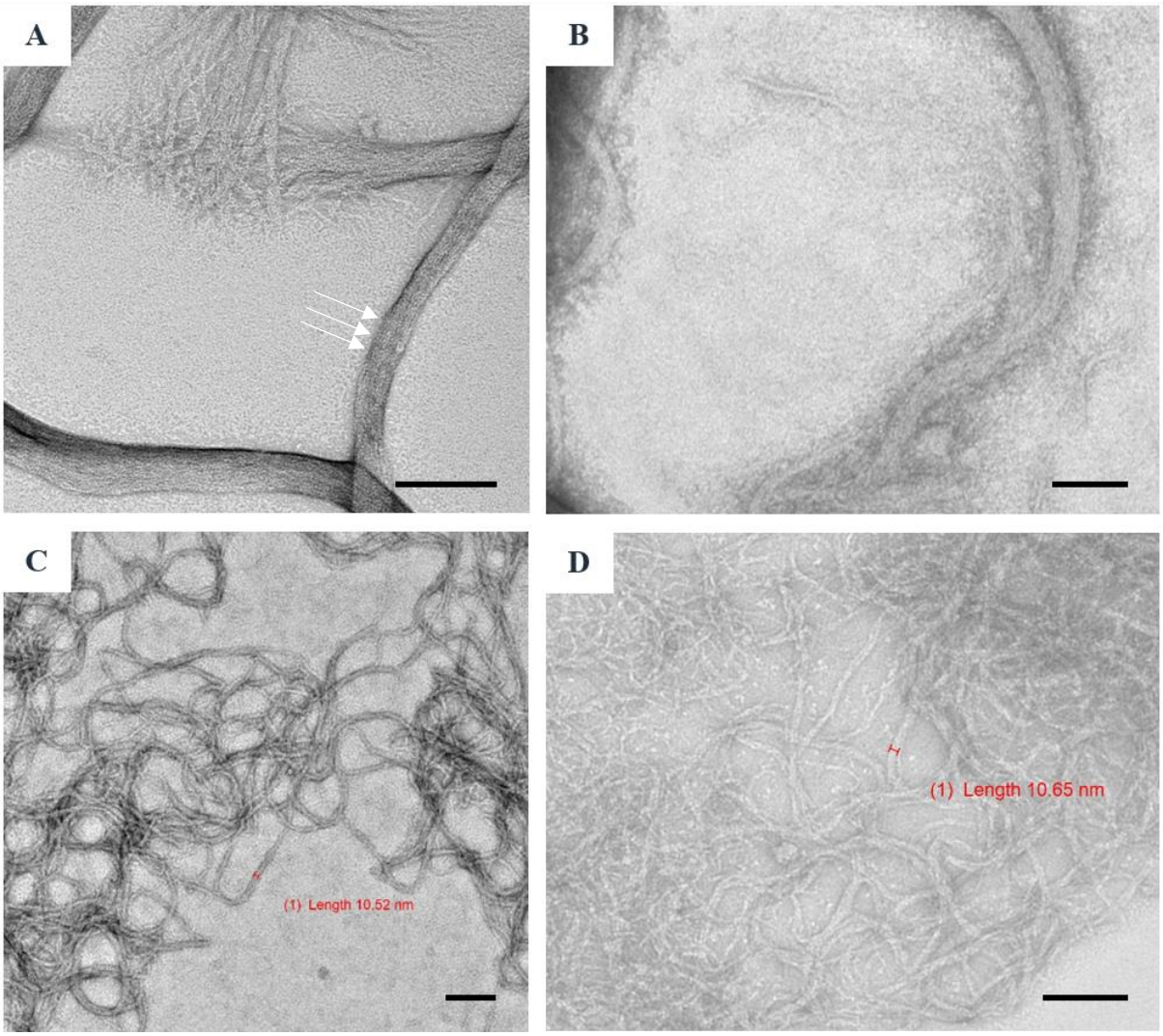

Fig. 4.3: Response of CTD Mutant Cytotardin to Divalent Cations

TEM of negatively stained sample of 0.2mg/ml CTD-cytotardin in 20mM $CaCl_2$, buffered by 2mM Tris-HCl pH 8.8 after 1h **(A)**, after 20h **(B)**. CTD-cytotardin in 2mM Tris-HCl pH 8.8, 20mM $MgSO_4$ solution after 1h **(C)**, after 4h **(D)**, in 2mM Tris-HCl pH 8.8, 20mM $MgSO_4$ solution. Scale bars 100nm.

III.3.5: Cytotardin R31C mutant cytotardin “LNTC”

Arginine to cysteine mutations in the LNDR motif of coil 1A are linked to multiple genetic conditions such as the first causative genetic factor documented for Epidermolysis Bullosa Simplex in keratin-14. To investigate whether cytotardin functions similarly enough to this well-characterised protein for such a mutation to be disruptive, as well as to support chemical modification and cross-linking (Ahn *et al*., 2019) capabilities, this arginine-to-cysteine cytotardin mutant was created. Once the LNTC-cytotardin plasmid was produced by Golden Gate ligation as described in Materials and Methods, it was screened by restriction endonuclease (XhoI-a site shared by both insert and vector, plus NdeI-BamHI as a control) digest, whereby LNTC-carrying vector would cut in both digests, wild-type just with NdeI-BamHI. Followed by Sanger sequencing confirming CGG Arginine codon to a TGC Cysteine codon and XhoI site presence. In order to optimise induction, cultures were tested for the time taken to enter a stationary phase of growth, and exhaust their glucose supply leading to “leaky” expression of the T7 RNA polymerase within the lacUV5 promoter leading to spontaneous expression of the target protein without the addition of IPTG (Fig. 4.4A; Oh *et al*., 2009; Zhang *et al*., 2015). As premature expression can be deleterious to bacterial growth, especially as these proteins are highly insoluble and form inclusion bodies, the overexpression study here also factored in the propensity for the BL21 cultures to exhibit this phenomenon, and to recover from it once regrown in a glucose-replenished medium.

III.3.6: Expression and Purification of LNTC mutant Cytotardin

Inclusion Body Preparation went as described in Materials and Methods, and section III.1.1, minor differences detailed in Fig. 2.5. LNTC cytotardin was further purified with IEC using guanidine hydrochloride, demarcated above each lane on Fig. 2.5B by their calculated guanidine hydrochloride molarity (Fig. 2.5). The higher weight bands originating from disulphide cross-linking were eliminated by the increase of DTT concentration, as first demonstrated by Smithies, 1965, to 10-12mM (Fig. 2.5E).

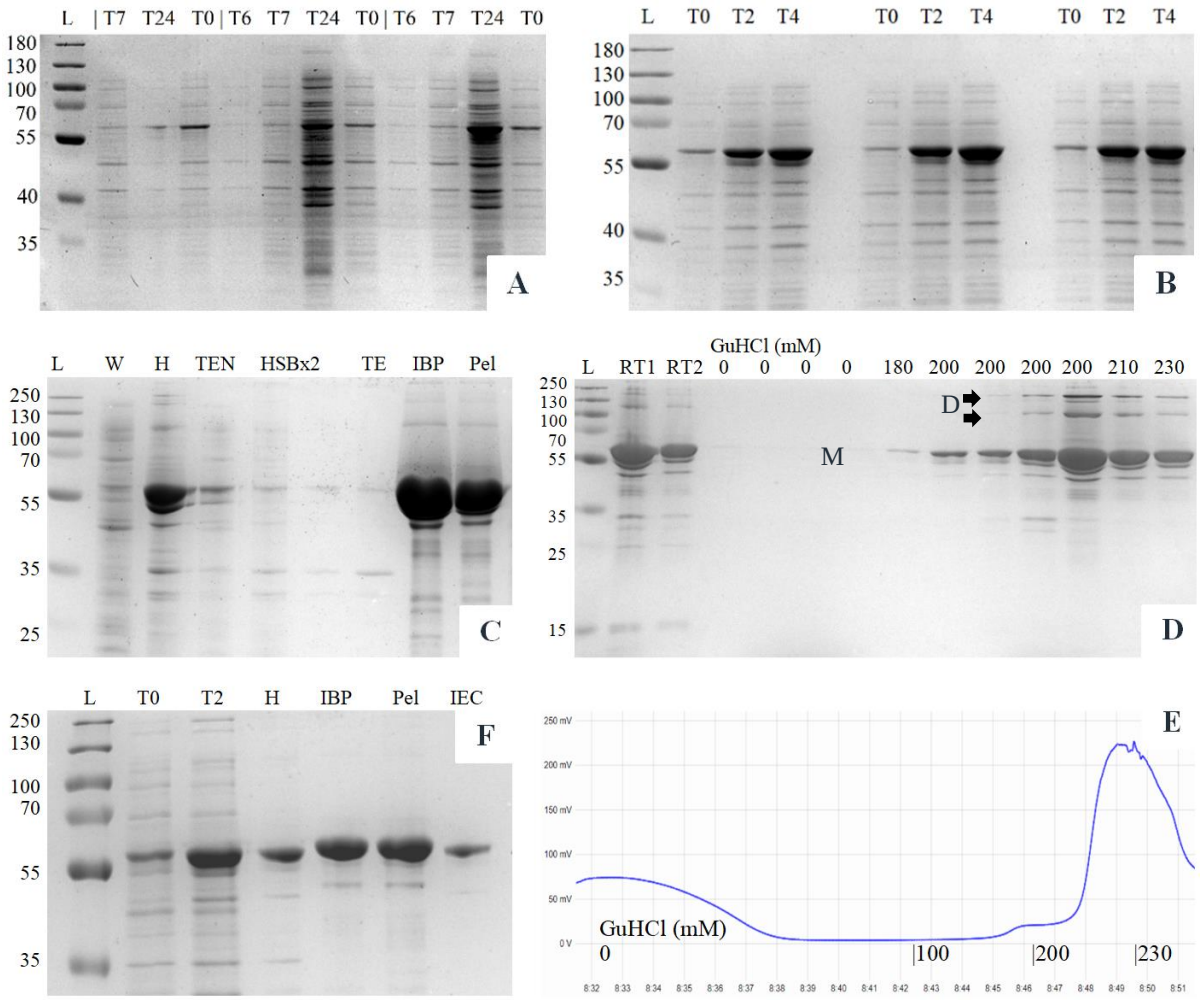

Fig. 4.4: Engineering of LNTC Cytotardin

(A) SDS-PAGE of BL21 cultivation and glucose depletion in stationary growth phase, where "Tx" marks the number of hours since media replenishment and induction after regrowth in fresh media **(B)** at "T0", where "Tx" marks number of hours since induction. Lanes marked "L" carry the MWt markers, annotated in kDa to the left. **(C)** IBP used to purify the LNTC cytotardin upon induction, with. IEC of LNTC with a rising GuHCl gradient, demarcated above each lane by their GuHCl molarity **(D)**, the absorption peak at 280nm wavelength is shown in chromatogram **(E)**. Summary of purification **(F)**, with lanes from left to right: pre-induced BL21 "T0", induced BL21 "T2", homogenate thereof "H", the finished IBP "IBP", the pellet from which it was extracted "Pel", and IEC purified fraction "IEC". Lanes marked "L" carry the MWt markers, annotated in kDa to the left.

III.3.7: *In Vitro* Assembly of LNTC cytotardin

Assembly of LNTC mutant cytotardin after 1 hour in in 2mM Tris-HCl pH 8.8 buffer (Fig. 4.5) led to an irregular reticulated network characteristic to that already observed in cytotardin in this buffer. At a pH of 8.0 under 2mM Tris-HCl solution, the LNTC mutant behaved the same, and kept to this pattern even at increased ionic strength from 20mM Tris-HCl solution and

50mM NaCl was added. Though this latter solution produced ordered assembly in cytotardin and has been used to equilibrate lamins before paracrystallisation (Karabinos *et al*., 2003), this did not produce ordered assembly in the mutant. Assembly of LNTC mutant cytotardin in following an additional hour 15mM Tris-HCl pH 7.4 buffer, with EDTA and DTT. This structure also occurs when LNTC cytotardin is dialysed directly into this solution. However unlike in the wild type, it is only in these conditions that paracrystallisation has occurred. Sedimentation assays (Fig. 4.5C) showed that whilst there was qualitative restriction on the ability of LNTC cytotardin to produce ordered structures such as paracrystals or filaments, for example how the LNTC mutant has not been observed to do so at pH 7.6-7 (Fig. 4.5D), unlike in wild type cytotardin, and the resultant changes did not produce an order of magnitude change in sedimentation of the LNTC mutant. At 2400g for 10 minutes, after dialysis in 15mM Tris-HCl pH 7.6, the LNTC mutant cytotardin is revealed to create at least $3.17x10^5$S bodies at a not entirely dissimilar rate. Aggregation occurs at a slower rate for LNTC cytotardin than for the wild type cytotardin, and appears not to be as uniform as implied by the larger error of the mean. Unlike with the wild type, LNTC cytotardin does not seem to produce paracrystals in as wide a variety of conditions. This implies some impairment in the ability of this mutant variety to laterally associate. Given the relatedness of the LNTC mutation to some of those known to cause Epidermolysis Bullosa Simplex, this gives the strong implication that the effects of the LNTC mutation are disruptive, rather than a full knockout, as indicated by the smaller pH range for assembly.

As was suspected due to the already disproportionate "random" crosslinking during purification in the LNTC mutant (Section III.2.6), experiments were run in order to confirm the affinity between LNTC sites in the assembly of their eponymous cytotardin mutant. What can be also noted is the presence of dimerization bands marked "D" in Fig 2.5 at much greater intensity than in the much more cysteine rich *T. pacificus* IF proteins, indicating by proximity that the LNTC site is indeed a binding site for the assembly of the protein. The multiple bands can be speculated as due to the potential for either antiparallel or parallel disulphide bond formation having different effects on the way the combined peptide travels through the SDS-gel. Since deliberate disulphide crosslinking via catalysts has been used as a molecular tool in other IFs (Rodgers *et al.,* 1996), it was attempted in LNTC cytotardin as detailed in Materials and Methods, as well as Fig. 4.5. Cysteine residues can also be bound by nanoscopic bodies of gold, as detailed in Methods II.7, with this providing insight into the molecular orientation and position of LNTC cytotardin when forming large scale structures (Fig. 4.5F).

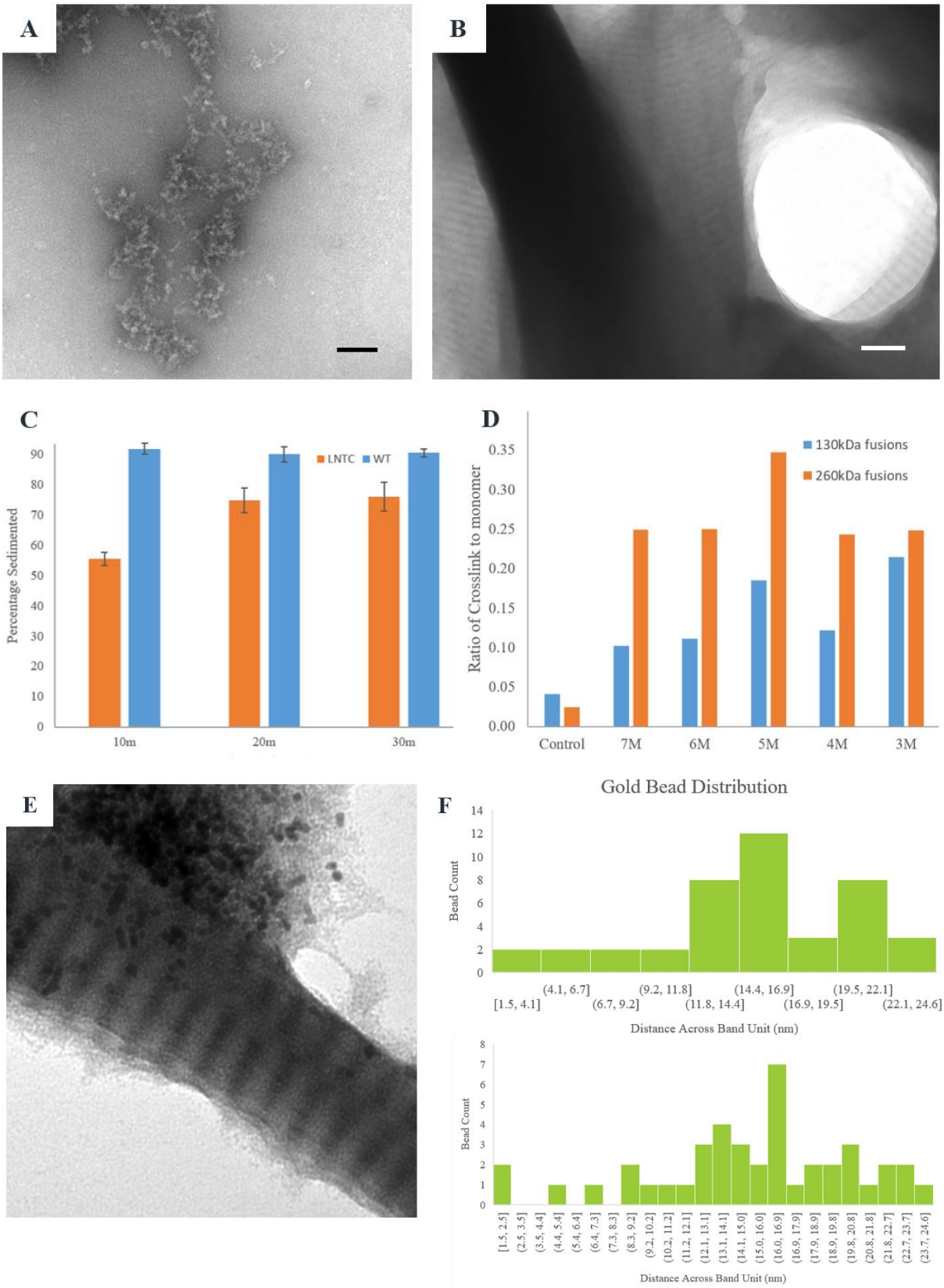

Fig. 4.5: Capacity of LNTC Mutant to Assemble is Limited

(A) TEM of negative stain of LNTC mutant cytotardin after 1h in in 2mM Tris-HCl pH 8.8 buffer, showing a characteristic reticulated, disordered network. **(B)** Assembly of LNTC mutant cytotardin in following an additional 1h 15mM Tris-HCl pH 7.4 buffer. All buffers contain 1mM EDTA and DTT. **(C)** Sedimentation Assay

of LNTC cytotardin dialysis in 15mM Tris-HCl pH 7.7, as compared to the wild type. Sedimentation occurred at 2400g for 10 minutes. **(D)** Ratio of Cu-P disulphide-crosslinked LNTC cytotardin to mono-molecular LNTC cytotardin digitally analysed. Samples ordered by molarity of urea in solution. **(E)** LNTC paracrystal marked with gold beads, positions analysed in histogram from the beginning of the dark band as position 0 (extending to 7.8nm across) to the end of the light band of the 24.9±0.4nm (standard error) banding pattern **(F)**. This indicated the 31st amino acid of LNTC cytotardin is squarely in the middle (16.0-9nm) of the pale band (7.8-24.9nm), similarly to Ahn *et al*., 2019's lamin model. Scale bars are 100nm, error bars are standard error.

III.4: *R. varieornatus* Lamin-2 & *T. pacificus* Lens IF

III.4.1: *R. varieornatus* Lamin 2 is capable of forming reticulum *in vitro*

The *R. varieornatus* paralog to the protein identified as lamin-2 by Hering *et al.*, 2016 has displayed assembly characteristics so far consistent with other Lamin paralogs. It also tends to form CaaX box-to-CaaX box cysteine cross-links that can be removed with DTT. Lamin 2 at 2mM Tris-HCl pH 8.8 (Fig. 5.1A) produces the same uneven reticulum as found in other IFs in this buffer (Fig. 4.5A). This behaviour continued when the samples were transferred to 2mM

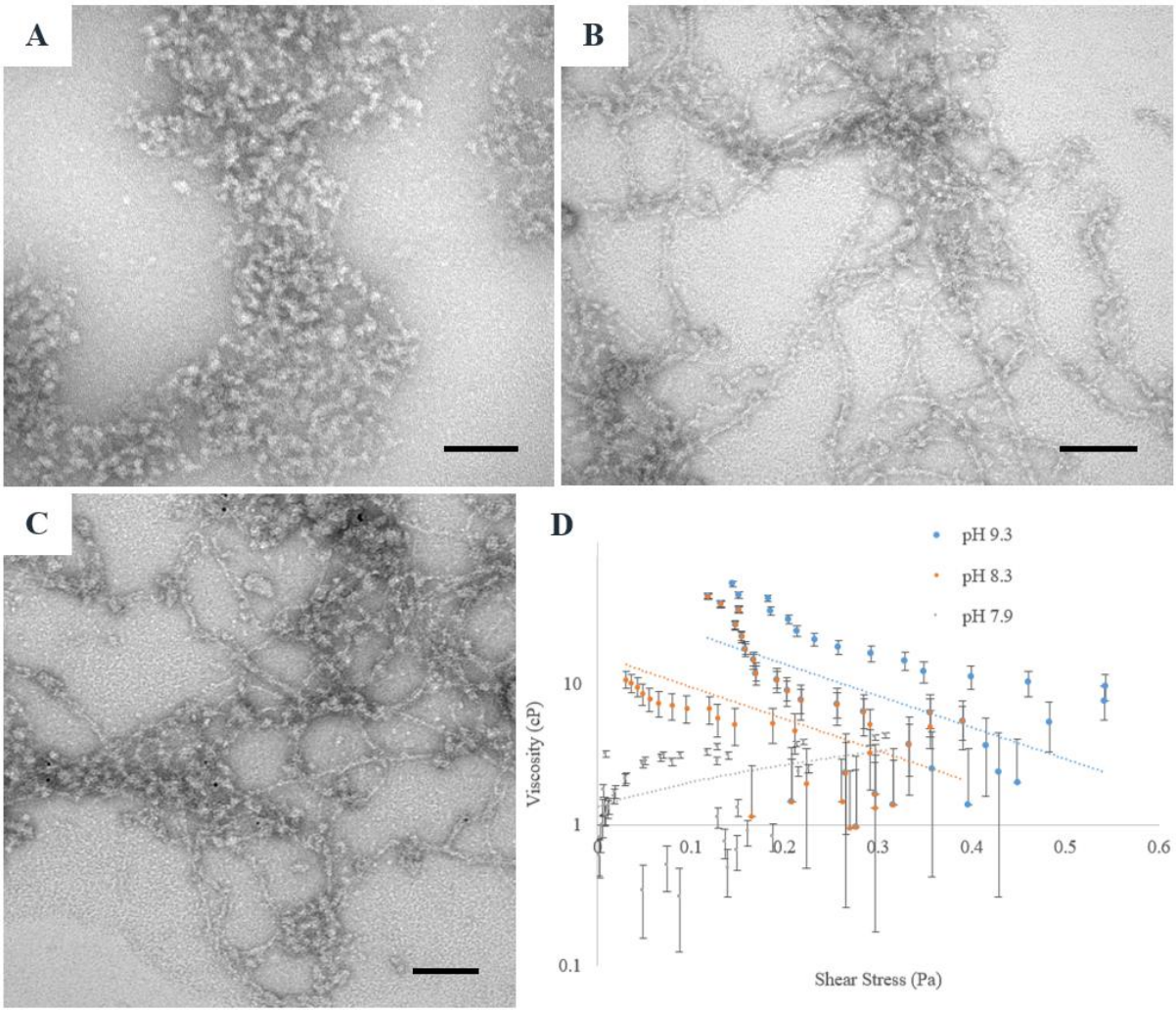

Fig. 5.1: Assembly of *R. varieornatus* Lamin 2

Lamin 2 at 2mM Tris-HCl pH 8.8 **(A),** Lamin 2 at 2mM Tris-HCl pH 7.6 **(B)**, Lamin 2 at 15mM Tris-HCl pH 7.4 **(C)**. Bulk viscometry of 250µl Lamin A at 0.5mg/ml using an AR2000 viscometer **(D)**. All solutions with 1mM EDTA, DTT. Scale bars are 100nm, error bars are standard error.

Tris-HCl pH 8.0. When lamin 2 is dialysed into 2mM Tris-HCl pH 7.6, here one observes see what average at 10.0nm ±1.8nm width filament-like structures (Fig. 5.1C). At higher ionic strength on this pH, the morphology resembles more the characteristics of Fig. 4.5A with less even filament width, implying that this isn't the best condition for lamin-2 assembly. At 15mM Tris-HCl pH 7.4, it shows filament-like reticulated structures as well (Fig. 5.1). The Lamin 2 protein used here was produced recombinantly and purified by ion exchange chromatography by Gemma Gordon.

Viscometry of the lamin 2 using continuous shear rate measurements of 0.5mg/ml solutions was conducted with the AR2000 microrheometer when available. Here the solution displayed low but significant viscosity across a range of pH corresponding to that of the high pH disordered reticulum, and at lowest pH tested, the viscosity increased temporarily with increasing strain and time, before breaking under the continuous shear rate test.

III.4.2: *R. varieornatus* Lamin 2 can form Paracrystals

The *R. varieornatus* A-lamin forms paracrystals after a variety of assembly processes across a wide pH range. Whereas cytotardin can form paracrystals after one-step dialysis into high pH solutions of divalent cations, the lamin 2 requires an equilibration step, tested using paracrystallisation methods from a range of different species' lamins. Eventually, approaches based on the paracrystallisation of a range of Chordate IFs were successful in causing paracrystal formation. Lamin 2 after 1 hour's exposure to 15mM Tris-HCl pH 7.4 (Fig. 5.1), is shown, followed by an additional 2 hour exposure to 25mM Tris-HCl pH 9, 20mM $CaCl_2$ (Fig. 5.2). At this point paracrystals assemble and form extensive networks, and display dimensions that can vary significantly relative to the position in reaction to stress placed upon them , implying some kind of internal mobility to the paracrystal. This protocol "a" was developed by Karabinos *et al*., 2003 for *C. elegans* lamin. The sedimentation assay that accompanied these experiments showed significantly increased aggregation upon the introduction of the protein to the divalent cation buffer. The sedimentation assay differed slightly in that the first buffer had a pH of 7.6 but otherwise had identical conditions. The A-type lamin of *R. varieornatus* can also form paracrystals after extended equilibration. After 20 hours exposure to 15mM Tris-HCl pH 7.4, followed by 5 hours at 25mM Tris-HCl pH 9, 20mM $CaCl_2$ paracrystal development occurs in sufficient quantity to cover tens of µm. This protocol "b" was developed by Karabinos *et al*., 2003 for the domestic chicken *Gallus gallus domesticus* lamin B2. In both cases the A-

lamin required significantly less time than either protocol described, as in comparison the with the *C. elegans* protocol "a" requiring three hours and the chicken lamin protocol "b" requiring 25 hours, *R. varieornatus* has required only 1 hour in the equilibration buffer at 15mM Tris-HCl pH 7.4 and as little as 30 minutes in the pH 9, 20mM $CaCl_2$ buffer. Here one observes that the lamin when left unchecked can form structures sizing easily in excess of the tardigrade's

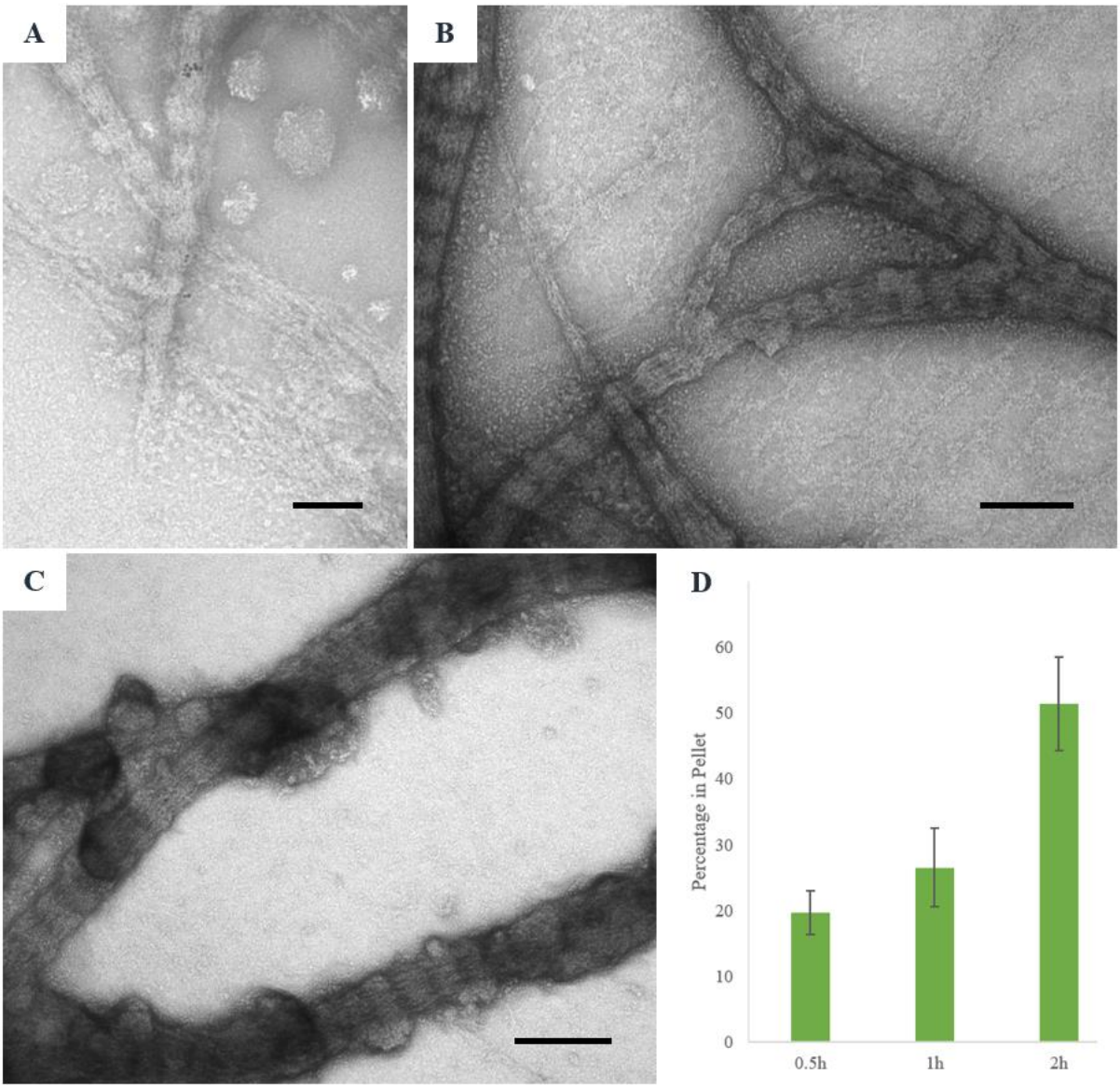

Fig. 5.2: High pH paracrystal formation in Lamin 2

Lamin A after 1h exposure to 15mM Tris-HCl pH 7.4, followed by 2h exposure to 25mM Tris-HCl pH 9, 20mM $CaCl_2$ ends **(A)**, and main body **(B)** of paracrystals, following protocol "a". 20h exposure to 15mM Tris-HCl pH 7.4, followed by 5h at 25mM Tris-HCl pH 9, 20mM $CaCl_2$ **(C)**. Sedimentation assay analysis **(D)** of the protein when pelleted at 2400g for 10 minutes, following protocol "a". Scale bars are 100nm, error bars are standard error.

biological requirements for a lamin, despite the high pH. This, tied with the implications of lamin 2 being the closest relative of cytotardin (Fig. 2.1-2), would provide some explanation for the capacity of a highly lamin-like protein to become a rapidly assembling IF whilst still keeping lamin like characteristics. Similar behaviour in how the lamin 1 of *R. varieornatus* responds the divalent cations was not observed by TEM of negative stain, however given the established limits of the negative stain procedure this is a subject that needs further exploration. Methods used to assemble *in vitro* the lamin of *Ciona*, a tunicate whose lamin bears morphological resemblance to cytotardin, were also successful on the lamin 2 of *R. varieornatus*. These experiments also demonstrated that the addition of NaCl to lamin 2 solution induced small filament assembly as in the *Ciona* lamin the buffer was designed for (Fig. 5.3).

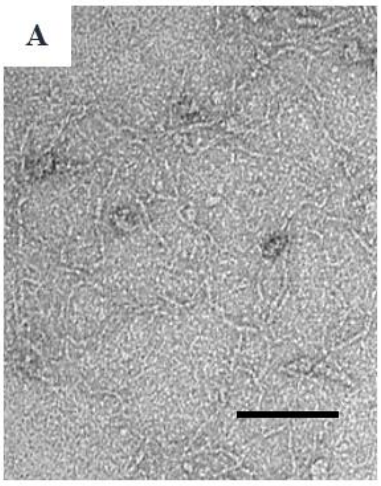

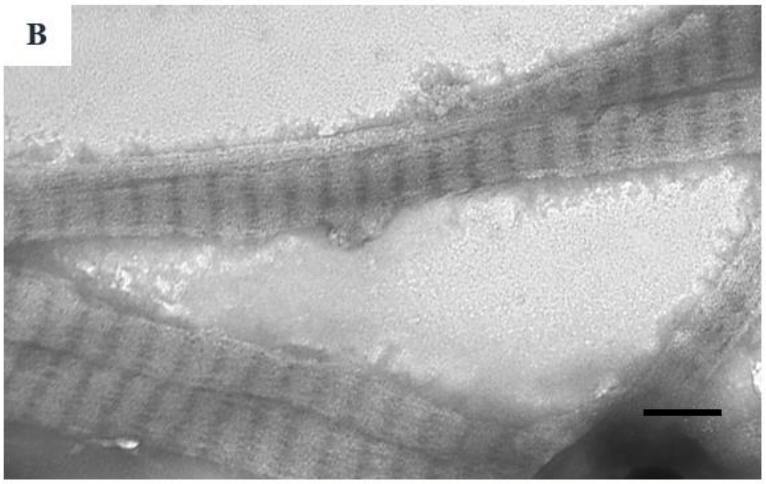

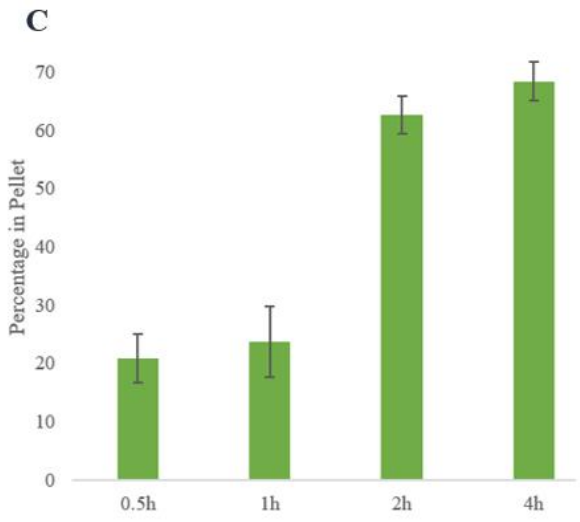

D

IF Sample	Width (nm)	Error (nm)
CYTT: 20mM: MgSO4, NaCl, Tris 8.8 1h	24.3	0.6
CYTT: ": MgSO4 1h	23.9	0.5
CYTT: ": MgSO4 20h	50.7	0.4
CYTT: ": CaCl2 1h	26.3	0.8
CYTT: 15mM Tris 7.6	24.2	0.4
CYTT: 0.5mM Tris 7.1	25.2	0.3
LNTC: 15mM Tris 7.4	24.9	0.4
CTD: 2mM Tris8.8 20mM CaCl2 2.5h	18.0	0.5
LMNA: Karabinos CaCl2-a	48	3
LMNA: Karabinos CaCl2-b	32	2
LMNA: Karabinos CaCl2-c	50	4

Fig. 5.3: Lamin 2 Paracrystals and Comparison Thereof

Lamin 2 after 1h exposure to 2mM Tris-HCl pH 8.0, 50mM NaCl **(A)**, followed by 2h exposure to 20mM Tris-HCl pH 7.2, 20mM $CaCl_2$ **(B)**. These paracrystals display dimensions that can vary significantly relative to the position and stress placed upon them. **(C)** Sedimentation assay analysis of the protein when pelleted at 2400g for 10 minutes. **(D)** Table of banding pattern lengths in aforementioned paracrystals, in comparison with those of cytotardin. Scale bars are 100nm, error bars and column are standard error.

Sedimentation assay was also attempted using protocols in (Heitlinger *et al*., 1992), where both *R. varieornatus* lamins were first put into a high pH buffer designed to produce head to tail, or even protofilament assembly state, as occurred in the chicken lamins it was designed for. Both were dialysed at 0.5mg/ml through 4M and 2M urea for an hour each, before transferring to a high pH buffer for one hour (25mM Tris-HCl, 150mM NaCl; 1mM EDTA, DTT, pH 8.5). After transfer to MES buffer (25mM MES, 150mM NaCl; 1mM EDTA, DTT, pH 6.5), for one hour, samples were sedimented to produce the assays in Fig. 5.4. Here, both lamins of *R. varieornatus* showed the ability to self-assemble, in 2 hours, large scale ($3.17x10^5$S) bodies.

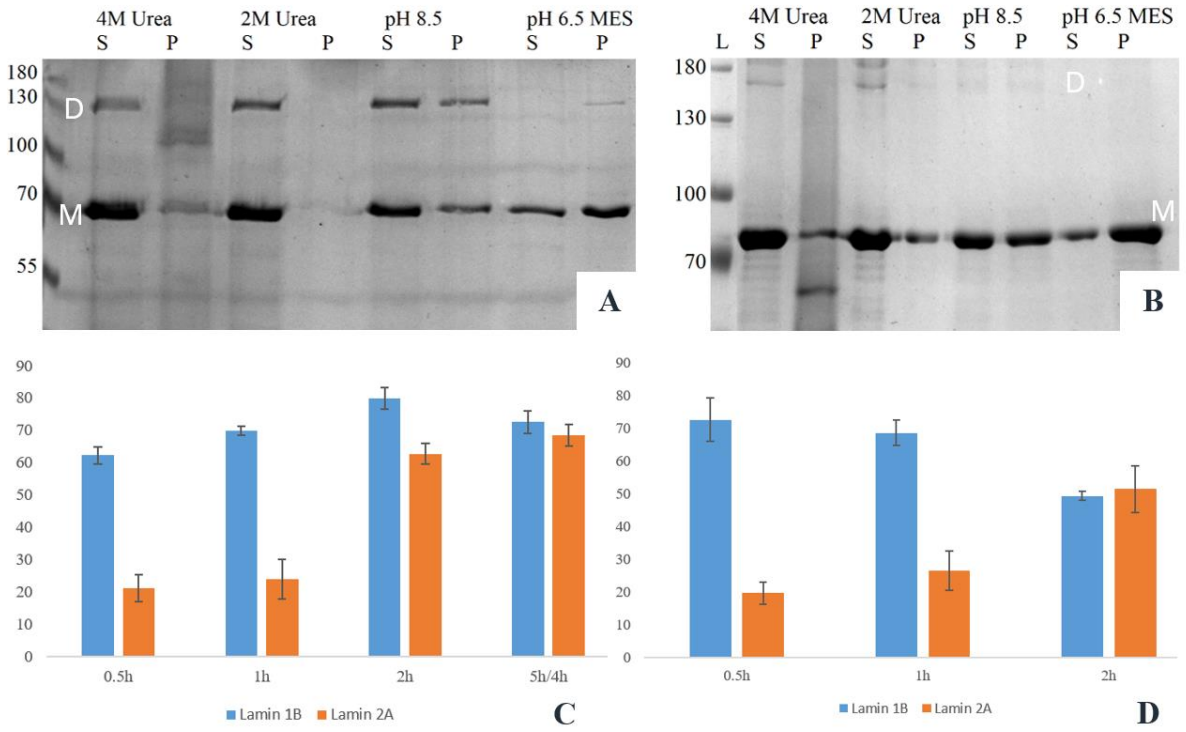

Fig. 5.4: Assembly of *R. varieornatus* lamins

Sedimentation assay at 30krpm for 1h on a TL-55 rotor, for Lamins 2 **(A)** and 1 **(B)**. Monomeric main band marked M, disulphide-linked dimers marked D. Sedimentation assays of lamin 1 and 2 at 2400g for 10m, on samples dialysed according to the protocols in Fig. 3.2 **(C)**, 3.3 **(D)**. comparing proportion of protein pelleted. Error bars are standard error.

III.4.3: Expression and Purification of *T. pacificus* Lens IF

The novel lens IF protein L10112.1 has a similar extended coil 1B in the rod domain to that of cytotardin. Compared to the tardigrade IFs, it has both some differences in the coil domain, and a significantly longer tail domain, so may assemble differently (Tomarev *et al*., 1993).

T pacificus lens IF DNA subcloned into pET23 from pGEM-T Easy samples as described in Materials and Methods, screened by plasmid digest and submitted for Sanger sequencing before subcloning and induction (Fig. 5.5).

Purification of L10112.1 began with IBPs (Fig3.5A) as described for (Fig. 4.1, 4.5), although the L10112.1 protein appeared even less soluble than the rest of the BL21 cellular material, and the resultant inclusion bodies aggregated much more tightly than the cytotardin, creating a highly rigid "bran flake" material (Fig. 5.6C). Ion Exchange Chromatography was conducted on the inclusion body preparations of L10112, which eluted from TMAE column at guanidine hydrochloride concentration of 0.21M. The L10112 samples were then treated with 10mM DTT to remove the disulphide- created aggregated before weighing on SDS PAGE (Fig. 5.6 B, D).

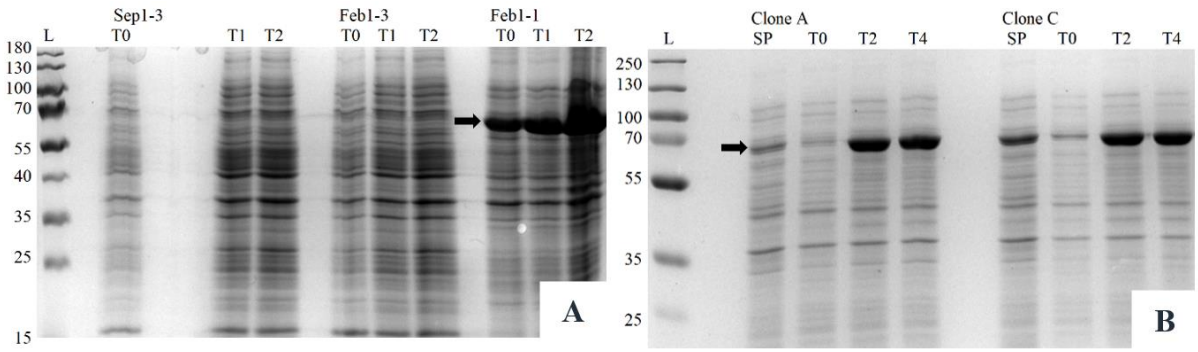

Fig. 5.5: Induction of L10112.1 and selection for reliable expression

BL21 *E. coli* induction of transformed BL21 cultures from each plasmid sample at "Tx" where x is the time in hours after addition of IPTG **(A)**, subsequent expression of clones from the successful culture **(B)**, first sample taken at stationary phase ("SP"); cultures were regrown in fresh media, induced at "T0" with samples taken then, two and four hours later . Lanes marked "L" carry the MWt markers, annotated in kDa.

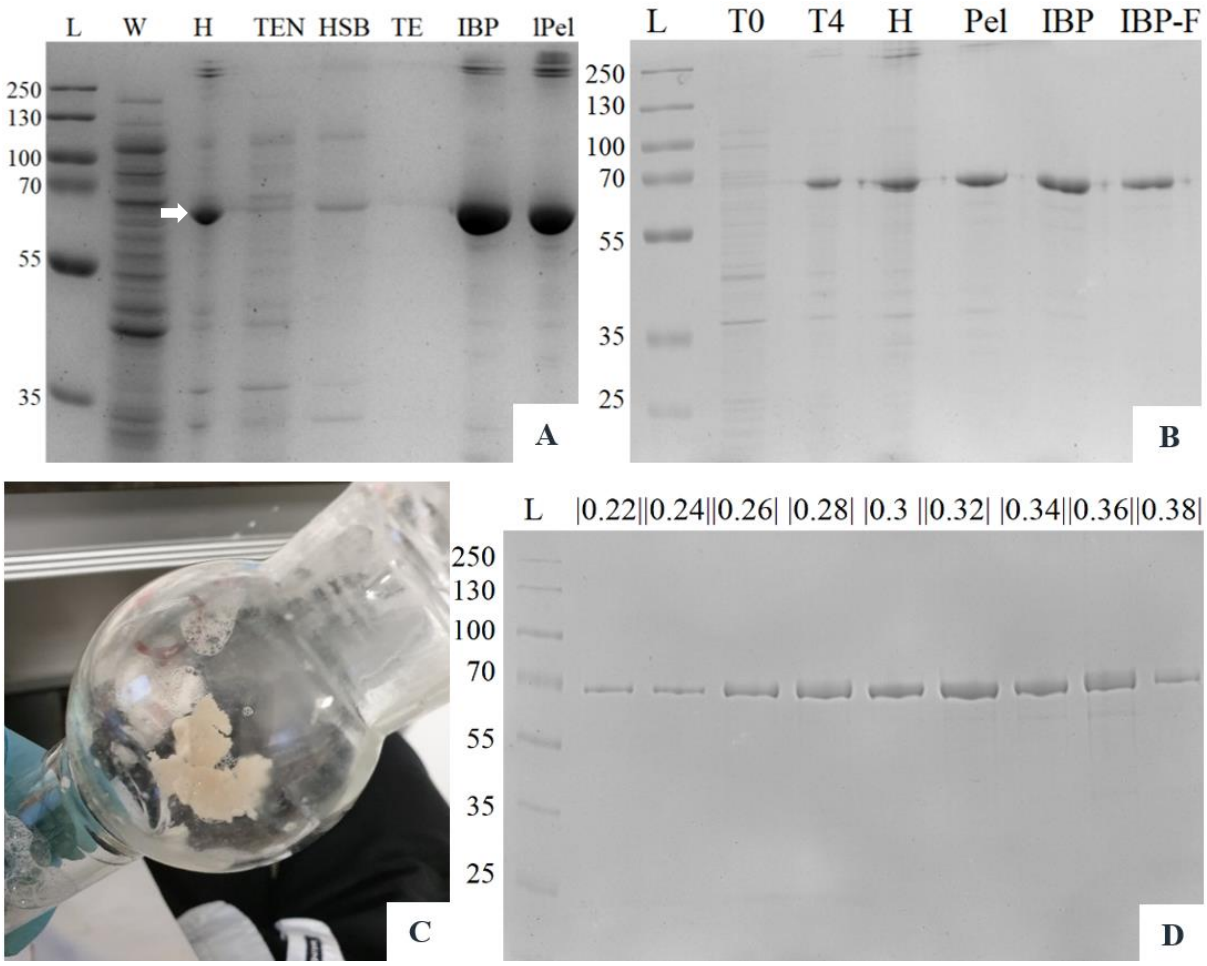

Fig. 5.6: Purification of L10112.1

(A) IBP with lane labels meaning as in previous figures; initial bacterial wash detritus "W", bacterial homogenate "H", TEN buffer wash detritus "TEN", High Salt buffer wash detritus "HSB", final was detritus "TE", finished IBP "IBP", remaining pellet "lPel". Summary Gel **(B)**: lanes, from left to right: pre-induction culture "T0", induced culture after 4h "T4", homogenate "H", finished IBP "IBP", and filtered IBP "IBP-F" ready for IEC. Illustration **(C)**. IEC of L10112.1 samples **(D)**, eluted from TMAE column at GuHCl molarity labelled above, after DTT treatment. The contents of lanes "L" are MWt markers with size indicated in kDa on the left.

III.4.5 The Lens IF has a limited capacity to assemble *In Vitro*

Similar attempts were made to test the assembly capacities of L10112.1 as were done with the cytotardins. After an initial 30 minute dialysis into 2mM Tris-HCl pH 8.8, some was then kept dialysing into the solution for a full hour, and some was then placed into 2mM pH 8.0. At 2mM pH 8.8 the initial morphology after 30 minutes (Fig. 5.7A) was a similar kind of aggregate seen

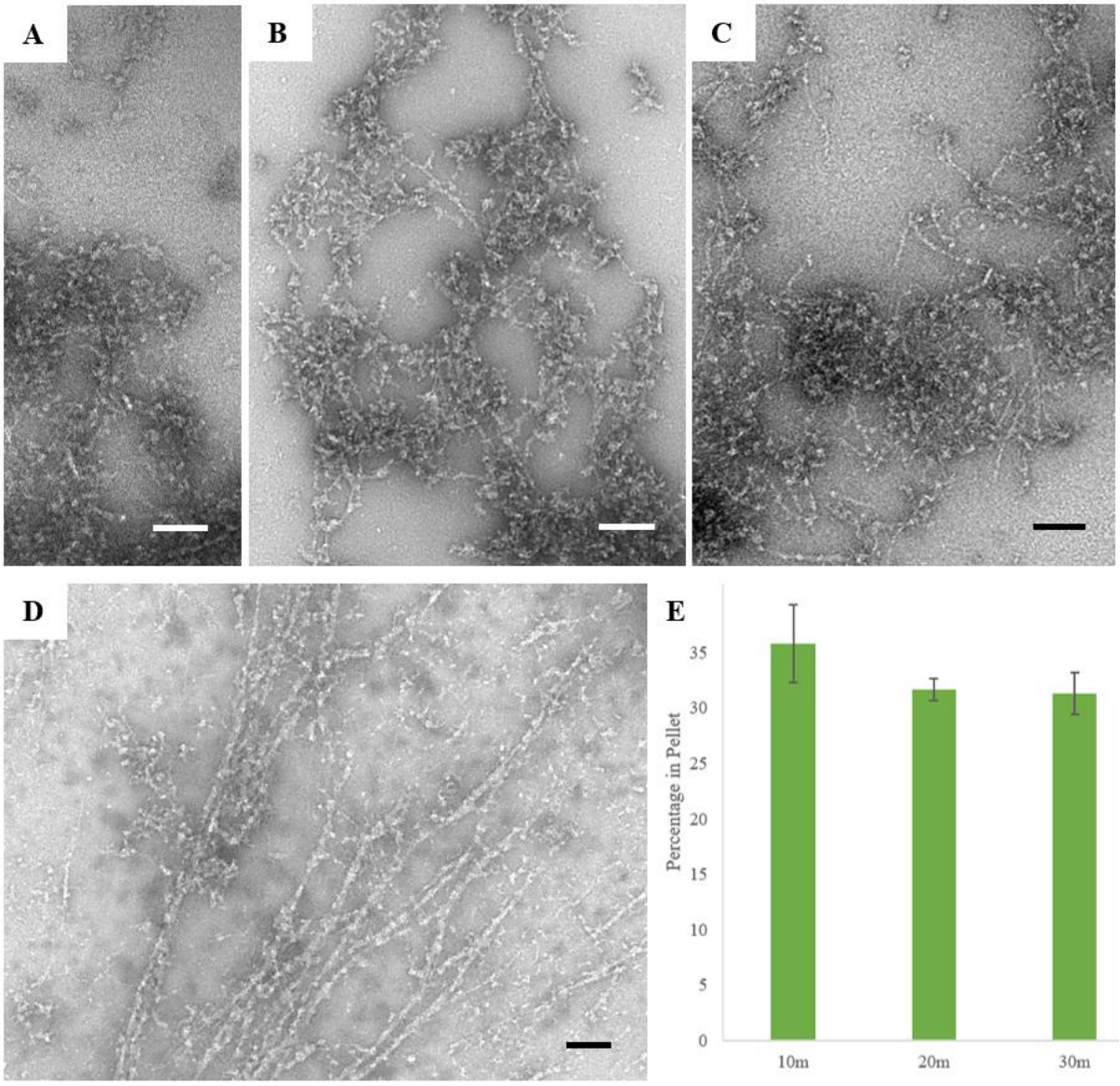

Fig. 5.7: L10112.1 was Limited to forming short rod-like Structures *in vitro*
(A) L10112.1 after initial 30 minute dialysis into 2mM Tris-HCl pH 8. **(B)** L10112.1 after 1h in 2mM pH 8.15 **(C)** Final dialysis step into 15mM Tris-HCl pH 7.7 after steps A and B. L10112.1 in 2mM Tris-HCl pH 8.8-8.0 can make short filaments **(D)**. Sedimentation Assay **(E)** of L10112.1 assembly at 2400g for 10 minutes, into 15mM Tris-HCl pH 7.6. Scale bars 100nm, error bars are standard error.

in other similar experiments, especially Fig. 4.5 at this buffer and time. After further 30 minutes dialysis into 2mM Tris8.8 L10112.1 can achieve short filamentation, and after one hour in 2mM pH 8.15 (Fig. 5.7), there was little difference from the morphology and timescale from that shown by L10112.1 in the pH 8.8 solution. After 30 minutes at 2mM pH 8.8 and 8.0, the final dialysis step into 15mM Tris-HCl pH 7.7 showed some limited change as the resultant

reticulum has clear filamentous morphology bearing some resemblance to ULFs or short, unstable filaments (Fig. 5.7).

Approaching cellular pH, at 7.4-7.7, L10112.1 appears unable to achieve extensive or long lasting linear assembly *in vitro*, whilst at higher pH the protein incurs difficulties with regular lateral assembly. Like *R. varieornatus* IFs, it was able to form *in vitro* structures across a high pH range, although the range of structures it formed were much more restricted. To quantify this TEM data, sedimentation assay of L10112.1 assembly was performed at 2400g for 10 minutes, into 15mM Tris-HCl pH 7.6, at which the sedimentation rate was significantly lower than that found in cytotardin and the LNTC mutant, but higher than the CTD mutant. The protocols from Fig. 3.2-7 appeared completely ineffective at producing paracrystals or any form of coherent structure beyond those observed in Fig. 5.7. This led to experiments where L10112.1 was dialysed directly into 2mM Tris-HCl pH 8.8, 20mM $CaCl_2$, and 2mM Tris-HCl pH 8.8, 20mM $MgSO_4$ leading to extensive aggregates which could not be effectively imaged due to their size and electron density.

III.4.6: Anti-Lens IF Serum Antibodies effectively target Cytotardin and other IFs

Among the experiments conducted by Slava Tomarev in the early 1990s, a serum antibody was produced against L10112.1. Experiments were conducted in which the proteins of interest to this study were blotted against the rabbit anti-L10112.1 serum antibody (Fig. 5.8). As a control for the western blot, repeats occurred with the addition of two MBA cell lysates provided by Drs Young, Papa and Hughes, (See Acknowledgements). These lysates, full expressions of human protein served as a control to test the range of the serum antibody, and unusually given the existing range of proteins tested, the rabbit anti-L10112.1 serum antibody showed negligeable binding. Side by side comparison of Coomassie stained SDS-PAGE and western blotted cytotardin of both wild type and mutant varieties led to the conclusion that the CTD mutant, per weight having a significantly increased antibody binding indicated that the epitope sites were not on the deleted tail region. Disruption of the LNTR region in cytotardin by the LNTC mutation also led to a protein with reduced binding by the antibody serum. This leads to the strong indication that the epitope site is near this region, as will be discussed further in this thesis.

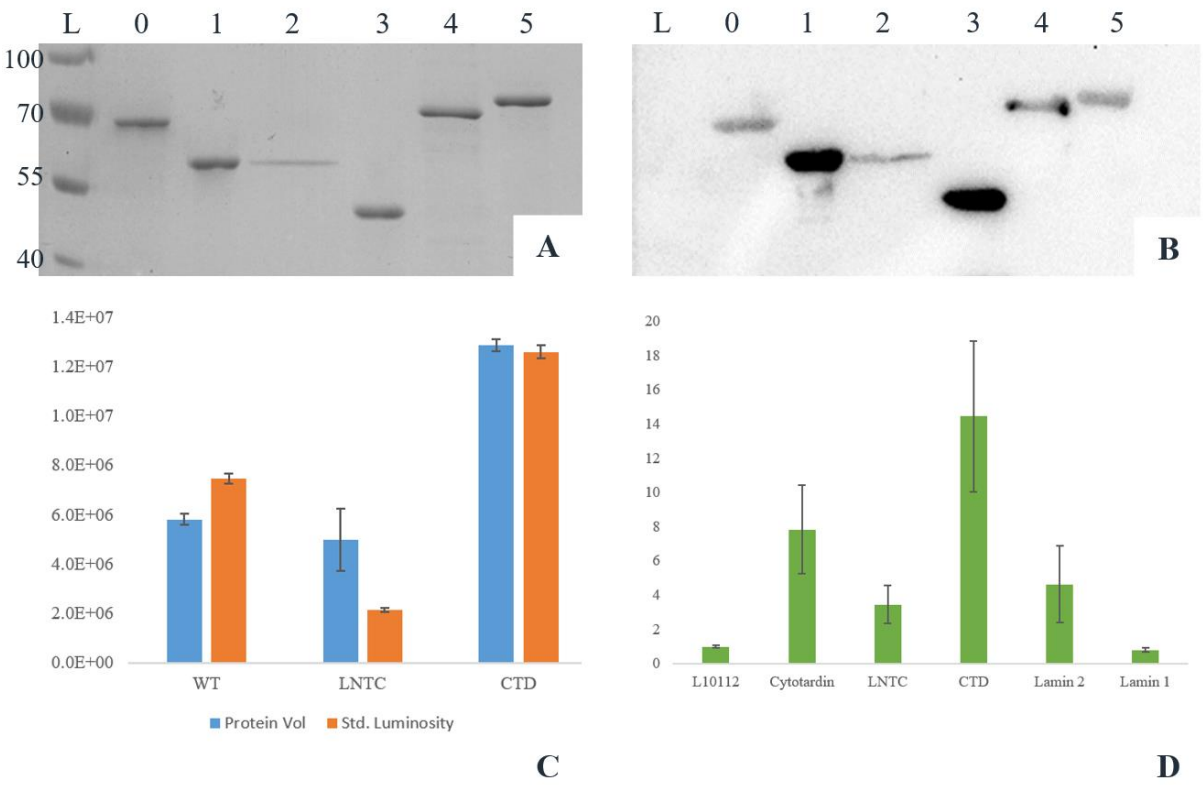

Fig. 5.8: Rabbit anti-L10112.1 Serum Antibodies show Affinity for Cytotardin

Protein samples involved in this study, from left to right: Thermo Fisher Protein Ladder, L10112.1 [0], Cytotardin [1], LNTC-Cytotardin [2], CTD-Cytotardin [3], Lamin 2 [4], Lamin 1 [5]. Coomassie stain of POI **(A)** MWt markers in kDa on the left. All blotted against the Tomarev *et al*., 1993 rabbit anti-L10112.1 serum antibody **(B)**. Digital analysis of western blots, first a single instance of serum binding to protein volume ratio for the cytotardin and variants thereof **(C)**, and then for multiple repeats of all blotted proteins **(D)**, standardised to L10112.1. Error bars are standard error.

Part IV: Discussion and Future Investigation

This study has characterised the *in vitro* assembly properties of cytotardin and lamin 2, as well as those of a novel eye lens IF. The two cytotardins of *R. varieornatus* and *H. dujardini* still relate to each other with significantly higher sequence homology than anything else, so this does not support the possibility that they evolved separately. The intermediate filament proteins of *R. varieornatus* all have this relationship to their *H. dujardini* counterparts first documented by Hering *et al*., in 2016.

IV.1 Cytotardin assembles *in vitro* faster than lamins and in a wider variety of conditions.

Existing protocols for lamin assembly (Aebi *et al*., 1986; Heitlinger *et al*., 1991, 1992; Min *et al*., 1996; Karabinos *et al*., 2003, Ben-Harush *et al*., 2009) require periods of several hours in specific conditions and cations, after separate hour long chaotrope removal and equilibration steps beforehand, to self-assemble into filaments or paracrystals. Cytotardin has the capacity to do this in a matter of minutes, forming bodies of histological scale as shown by sedimentation assay (Fig. 3.3,5,7) in across a wide range or ionic conditions shown in Section III.1. The sedimentation assay in Fig. 3.3 shows bodies of assembled cytotardin sedimenting almost entirely at RCFs of 2.14×10^5, 1.37×10^5, and 7.71×10^4 g within 30 minutes. This is calculated to have led to the sedimentation of bodies over 121S, 189S and 336S respectively, which means these protein constructs are at minimum the size of viral protein coats such as Tobacco Mosaic Virus at 175S (Freitas, 1999), and many times that of ribosomes at 70S and 80S (Slonczewski *et al*., 2009). Erickson, 2009 calculates the maximum possible Svedberg coefficient for a 50kDa protein as being 4.9S, with the maximum Svedberg coefficient for a 1000kDa body of protein being 36.1S, implying that the cytotardin constructs are much larger, denser or lower in surface area. In entering and leaving a desiccated state, the tardigrade and its cells would be exposed to massive mechanical stress from the mass transfer of water. Cytotardin has the capacity to rapidly assemble into large structures in a range of solutions including pure water (Fig 1.7), an ability that would also help protect potentially embrittled

cellular apparatus from hydrostatic pressure in the initial water influx. Sedimentation assays (Fig. 3.5, 3.7) show that both cytotardin and the lamin 2 in *Ramazzottius varieornatus* has the capacity to form networks of organelle-size that would be large enough to do so.

IV.2 Cytotardin retains a lamin-like *in vitro* assembly process

The possession by cytotardin of sequences capable of and linked to capacity for A_{CN} binding (used in the elongation phase of lamin assembly) is both theoretically predicted (Fig. 2.1) and indicated by its *in vitro* assembly properties, beginning with simple networks and ending in large paracrystals. Here major 10nm+ filaments are greatly outnumbered at the "root" by smaller, protofilament type assemblies of the sub 5nm kind observed in Turgay *et al*., 2017. The fact that some of the arginine residues linked to A_{CN} binding still remain on the LNTC mutant (Fig. 2.3) makes it possible that the mutation fails to inhibit head to tail assembly, however given the vestigial nature of A_{CN} binding sites in the wild type cytotardin tail compared to those in the coil 2-to-head potential binding regions, this is may not be significant as these would not be the primary regions for A_{CN} binding as predicted in Section III.0.7. However electron microscopy consistently showed LNTC cytotardin incapable of any form of proto-filamentation longer than 50nm, without lateral alignment, indicating that there is some connection. Furthermore, as pointed out in the previous section, this would also be significantly affected by the LNTC mutation where an acidic arginine residue is by a low polarity, weakly acidic cysteine raising the total isoelectric point of the first 20 residues of coil 1A from 9.7 to 8.18, and the first seven residues from 9.75 to 5.52. This could severely weaken the A_{CN} interactions that allow the protofilaments to elongate and explain the results of Fig. 2.7 whereby LNTC cytotardin requires significantly lower pH than the wild type to produce assemble in an ordered manner. Stalmans *et al*., 2020 also models the A_{CN} pathway assembly interaction with a partial crystallisation model of lamin A fragments. The model was accompanied by chemical crosslinks, linking regions of proximity *in vitro*, such as residues 27-76 in lamin A, which are conserved in cytotardin, including over the LNDR motif. Particularly these regions in coil two linked to the A_{CN} interaction by Stalmans *et al*., around residues 359-383 are conserved in cytotardin and cover the TYRKLLEGE motif.

Ahn *et al*., in 2019 postulates a 20nm per A_{11} or A_{22} lateral region banding pattern for lamins in its assembly model of lateral alignment, with the length of the overlap regions uncertain. This, with the A_{11} interaction regions forming tetramers with a linear lateral association compared to the clustered lateral association in the A_{22} interaction. Based on their model it is possible that the less compactly aligned A_{11} interaction-band would be more susceptible to the ingress of heavy metal staining in TEM, with the overlap regions most exclusive towards the stain due to having the highest (electron) density. However this is not reflected by the results in Fig. 4.5F, where the cysteine binding gold beads primarily bind to the less stained region of LNTC cytotardin paracrystals. Interestingly the less stained, but more gold bead sensitive region does take up nearly 20nm of the 24.9nm banding pattern, while the gold beads, and thus coil 1a domains themselves are centred in the middle of the less stained region. This implies that the A_{11}-A_{22} overlap region predicted that contains coil 1a may be at the basis for the less stained region, with the centres of either A_{11} or A_{22}-only bands being more easily stained. This tripartite model shown in that Ahn *et al*. also explains the double banding and triple banding patterns in Fig. 3.4. In banding pattern length cytotardin fits the lamin models found in (Heitlinger *et al*., 1991), whereby head-to-tail polymers associate laterally, in a near fully-staggered antiparallel formation to create IF-like protofilament assemblies with a 24-25nm banding pattern. In specific circumstances such as those illustrated in Fig. 3.3 where the cytotardin instead forms reticulated, paracrystal-like super-filaments, a ‘‘beading’’ repeat pattern can be observed. In existing *in vitro* type V IF models however, these beading lamin proto-filaments are not stable but further associate laterally into fibres and in the presence of cations, large paracrystals. Though cytotardin is capable of rapid assembly (Fig. 3.4) in a manner reminiscent of cytoplasmic IFs, the medium to long term behaviour, from proto-filamentation to paracrystallisation (Fig. 3.3-7) complete with the 25nm banding pattern (Fig. 5.3) confirms that cytotardin retains the assembly pathways intrinsic to lamins and thus validates the description of cytotardin as a Type V IF.

Given that the sedimentation assay requires aggregates of at least 168S to sediment the cytotardin, successful sedimentation of cytotardin in up to 8M urea (Fig. 3.3) leads to potential investigation of whether cytotardin shares some characteristics of ULF-led cytoplasmic IF type assembly as well as A_{CN}-led Lamin-type assembly. Results of electron microscopy appear similar to the ULF development montages shown in Strelkov *et al.*, 2003, supporting the hypothesis that cytotardin may in addition have some capacity to form ULF-like bodies in some cases. Pace *et al*., 2010 shows that some proteins, particularly those with high hydrophobicity

like IFs, not just retain solubility in solutions of close to 8M urea, but maintain a majority of their secondary structure characteristics as well. The distribution of hydrophobic residues in cytotardin, though overall thinner than those of its related lamins, is nonetheless concentrated near the conserved LNDR and TYRKLLEGE motifs (Fig. 2.2). TEM data allows the possibility that ULF-type bundles both proceed and exist alongside larger, more complex assembly (in figures 1.4 and 1.2 especially). This fits the characterisation of A-type lamins *in vivo* in Goldberg *et al*., 2008, as well as with the lesser morphological resemblance to embryonic lamin LIII of the *Xenopus laevis* embryos used to express them, although this is just a model.

IV.3 *R. varieornatus* IF Tail Regions are Important for Assembly

The A-lamin, lamin 2, carries all of the positive and negatively charged regions linked to the A_{CN} assembly mode in lamins by Kreplak *et al*., 2004 on homologous positions to those found in cytotardin, with the main alteration being on the early tail where the sequence of positively charged arginine and lysine residues is much denser. The locations and charges of many of these residues are also shared with human lamin A, which was confirmed to associate them with the A_{CN} interaction by Stalmans *et al*., in 2020 as discussed in the previous section. This suggests that like lamins, cytotardin also has an A_{CN}-guided elongation phase as the first stage of its assembly.

As for the lateral association phase of lamin assembly, cytotardin tails have relatively diffuse electrostatic attractiveness compared to their lamin counterparts and lack of Ig-like domain folds experienced by the tail region may allow it greater mobility compared to most lamins. This may contribute to the ability of cytotardin to form extensive paracrystals without the assistance of cations (Fig. 3.5-7) following models first laid out by Beck *et al*., 2012 in neurofilaments. Charged, flexible IF tail domains of neurofilaments are known to display abnormal behaviour at low salt concentrations, due to what polymer physics refer to as the “osmotic brush” effect (Zhulina and Rubinstein, 2012). When applied to the context of large scale organisation in a wider range of IFs (Kornreich *et al*., 2015) this has contributed to biophysical models of noncovalent tail crosslinks supporting large scale IF assembly even where the tail is less than 200 residues (Aufderhorst-Roberts and Koenderink, 2019).

In the osmotic brush effect, increased salt concentration leads to expansion of the charged "brush" tails and higher inter-filament adhesion. Originally applied from materials physics specifically to neurofilaments (Beck *et al*., 2010, 2012), the theory has been also applied to a range of other IFs (Kornreich *et al*., 2015). Furthermore, the tail domains of cytotardin are indicated by ExPASy PROSITE to carry 9 potential phosphorylation sites, so there is the possibility that these tail based interactions may be further augmented by phosphorylation *in vivo*, as prescribed by the bottlebrush model. The influence of the tail domain is further evidenced by how the CTD mutant appears unable to form lasting paracrystals, and those is does form are very small with less clear banding patterns (Fig. 4.3). However in the context of wild type cytotardin, where excessive aggregation has been shown as an issue with both forming ordered structures and maintaining them, the sheer number of tail-tail interactions may not be optimal for macroscopic structural integrity. When the strength of cytotardin gels was tested the NaCl free buffer produced a more viscous solution than that of NaCl containing solutions. On the other hand, were one to postulate that the low-salt conditions' thicker paracrystals (Fig. 3.7) were an indication of faster assembly speed and thus better recovery ability of the large scale structure, they may react better to the low amplitude oscillations of the time sweep in Fig. 3.8B. Alternatively, these results may be explained by Kornreich *et al*. in 2015's hypothesis that the salt conditions in the 0.1M salt buffers may have been sufficiently high that that the usual trend of salt impact on IF tail entanglement ability is reversed, as theorised to happen at relative extremes of salt concentration by Srinivasan *et al*., in 2014.

The C-Terminal Deleted mutants of cytotardin are notable as like C-Terminal deleted mutants in lamins they are unable to form sustained paracrystals (Moir *et al.*, 1991). Though it remains to be seen how N-and-C-Terminal deleted cytotardin mutants would behave, cytotardin did form remarkably similar paracrystals in Fig. 3.6 to N and C-terminal deleted lamin A mutants. Purely by the length needed by the coiled coil region, cytotardin and its lamin counterparts require at least 44.8nm going by a coiled coil length of 0.14nm per residue (Schwaiger *et al*., 2002), or 48nm by a 0.15nm per residue distance (Ahn *et al*., 2019), significantly wider than the widths of most paracrystal banding patterns. The *in vitro* assembly of the C-Terminal Deleted mutant into 10nm filaments despite lacking a tail region could also be considered an indication of lamin-type assembly in cytotardin, as experiments of lamins have shown that the A_{CN} pathway can in fact be enhanced by truncating, but not entirely removing, the tail domain (Heitlinger *et al*., 1992).

IV.4 *R. varieornatus* Lamins are also adaptable to diverse conditions

It is worth noting that the three approaches successfully used to create paracrystals with the lamin 2 (Fig. 5.2, 3.2) were designed for three different species' B-type lamins, and all of them were successful. As such, the lamin 2 of *R. varieornatus* display the capacity to self-assemble in diverse environmental conditions important for the survival of an extremophile. Comparative sedimentation assay (Fig. 3.3) indicates a far greater rate of aggregation in the lamin 1 under the conditions required to cause paracrystal assembly in the lamin 2. This implies that like lamin 2, lamin 1 may also have the ability to self-assemble in a wide pH range. Lamin 2, under viscometric testing (Fig. 5.1) also exhibited an increase in viscosity in reaction to increasing strain, or strain-stiffening, despite being in 2mM Tris-HCl solution with no cations in solution to aid assembly.

IV.5 Disruption of the LNDR site reduces cytotardin self-assembly

Arginine to cysteine mutations in the head and coil 1a regions have been widely documented in keratins, such as the first linked Epidermolysis Bullosa Simplex-linked keratin mutation, R125C, or dbSNP:rs60399023 in UniProtKB, in keratin 14 (Coulombe *et al*., 1991). This mutation is shown in cell culture to lead to poor structural integrity in the nuclear lamina and the mutant protein as prone to unstructured aggregation (Letai *et al*., 1993). This arguably ties in with results shown in Fig. 4.5 where the LNTC cytotardin aggregates in a disordered manner outside cellular pH and does not produce as many large bodies capable of sedimentation in equivalent conditions. The LNTC mutation in cytotardin is also resemblant in terms of relative position, namely at the g position of the first α-helix at the beginning of coil 1a, to the Y45C mutation in Lamin A. This mutation, linked to Emery-Dreyfuss muscular dystrophy (Bonne *et al*., 2000; Scharner *et al*., 2011) disabled binding of lamin fragments to the C-terminal of coil 2 in Lamin fragments. *In vivo*, it led to blebbing and dissolution of the nuclear lamina without the support of the chromatin. However, while the Y45C mutation inflicts a critical loss of function on the lamin, the R31C mutation in cytotardin is neither confirmed in place of an awkward interaction, nor occurs in the d amino acid of an α-helix. However, what the R31C mutation does do is replace the charged arginine with the conditionally charged cysteine, which

prefers a hydrophobic state (Iyer and Mahalakshmi, 2019). This conditional aspect of function is reflected in Fig. 4.5 where it can replicate the extensive paracrystallisation phenotype of wild type cytotardin, but only under specific conditions, whilst in all other circumstance producing disordered bodies with a quantifiably lower efficiency of aggregation than the wild type. What kind of phenotype this would result in *in vivo* has yet to be determined, and may represent a productive avenue for investigation. Point mutations producing cysteine residues in IFs are also an established tool for examining IF binding (Ahn *et al*., 2019). The reactivity and capacity for covalent bonding of the cysteine sulphuric side chain allows improved capacity for chemical modification, particularly in the case of LNTC-cytotardin where there is only a single cysteine, and this allows the residue itself to be used as a marker, for example for binding gold markers capable of being imaged via negative stain.

IV.6: Epitope sites for the rabbit Anti-Lens IF Serum

Multiple potential epitope sites exist for the polyclonal antibodies that make up the serum. Identifying these sites can be aided by several conclusions that can be drawn from figure 3.7. The relatively low affinity for L10112.1 possessed by the serum (Fig. 5.8) implies that the epitope sites in question are many times more common in the other proteins examined. Fig. 6.1 aligns and examines the potential epitope sites in L10112.1, cytotardin and the lamins. Figure 4.4 details sites of high sequence identity between the proteins of interest.

A promising area to look concerns similarity between cytotardin and Lamin 2; reasons for this include lamin 2 having a LNSR region exceedingly similar to cytotardin's LNTR. Comparing cytotardin and lamin 2 there is also another conserved sequence of 8 residues at the end of helix 2. Sequence alignment showed potential epitope sites in what the wild type cytotardin and lamin 2 shared in sequence homology on the coiled coil region. This homologous region around the LNTR is almost six residues, with the exception of a serine to threonine substitution in the third. In the less strongly bound B lamin there is an aspartate residue in this position, and this substitution may also lead to weaker binding.

A

```
Cytotardin       16 LDRVHSKDELQALNTRLAKYIDKIRNLENENVALQRQLNTAEQHTVTEVHT     66
                    |.|...|:||::||:|||.|||.||..:.|...|:|::.|.......|...
LMNA             67 LTRHQEKEELKSLNSRLAHYIDTIRAQQEEITVLRRKIETVNTQESQEATQ    117

Cytotardin      315 KDEQIRALQKQIQQLQESLQRVHEDLGDLTRQYQDLLYVKLALDAELATYN    367
                    ||..::.||:.:...|..||:.|.||.....:||.||..|:.|||||||:
LMNA            362 KDADLQRLQQLLADRQAELQKTHHDLSSQLTEYQLLLDEKIQLDAELATYH    414
```

B

```
Cytotardin      SMASSVR-------GSTAYLDRVHSKDELQALNTRLAKYIDKIRNLENENVALQRQLNTA  56
L10112.1        QLQAGVLGNISHQGVASMKLKREGEKKEMQDLNERLANFIEQARFLEAENKALRDALNKS 120
                .: :.*         ::  *.*  .*.*:* ** ***::*:: * ** ** **:  **.:

Cytotardin      LQRVHEDLGDLTRQYQDLLYVKLALDAELATYNKLLSGEEQRLGMDGSSRVTTTRTTATT 394
L10112.1        VQKLNAELEGVIKELQLLMDAKLSLELEIAAYRKLLEVEENRLCIGSMTQVVGGFRGQTE 454
                :*::: :* .: :: * *: .**:*: *:*:*.***. **:** :.. ::*.      *
```

C

```
LMNB            KSGRTESSMSINLNGNSPQNSSGSRVHSPQLSRAQEKDELHNLNDRLAKVLTQNSRYKEE 117
LMNA            ----ETRTHRTPSAGAAVPEVGGSGLAGSPLTRHQEKEELKSLNSRLAHYIDTIRAQQEE  96
Cytotardin      ------------MLSSMASSVRG---STAYLDRVHSKDELQALNTRLAKYIDKIRNLENE  45
                             .    .  *       * * :.*:**: ** ***: :      ::*

LMNB            ASETMKLYQQLMEENRELQNINTEITAELRMYDNLLKEEEIRLGIQSPTQAEPSS-RKRP 461
LMNA            LSSQLTEYQ-------LLLDEKIQLDAELATYHALLKSEEARLNMQSPPFPSTPDSARRG 441
Cytotardin      LGDLTRQYQ-------DLLYVKLALDAELATYNKLLSGEEQRLGMDGSSRVTTTRTTATT 394
                 ..    **        *   :  : ***  *. **. ** **.::.
```

Fig. 6.1: Potential rabbit anti-L10112.1 serum antibody epitope sites. Sequence comparison by CLUSTAL O(1.2.4) multiple sequence alignment

IV.7: Implications for the Evolution of Cytotardin

Lamins and cytoplasmic IFs play important roles in lending tensile strength to cellular structures (Makarov *et al*., 2019). Cytotardin assembled *in vitro* at pH between 6.5 – 9, while most organisms' cellular pH falls between 7-7.4, though human endothelial cells can reach up to pH 7.6 (Porcelli *et al*., 2005). In nematodes, revealed to be closely related to tardigrades than other *Ecdysozoa* (Hashimoto *et al.*, 2016), the 7-9 pH range also fits to many optimum enzyme pH (Platzer *et al*., 1999), and the pH range explored may also have relevance when dealing with states of oxidation that can result from environmental stress. The resilience of the cytotardin was strongly implied to be important to the tardigrade's capacity for extremophilia when the protein was first characterised, as cytotardin filaments were noted to retain their structural integrity even when the tardigrade was in its contracted "tun" state (Hering *et al*., 2016). Given that the adaptations of the *R. varieornatus* cytoplasmic IF protein demonstrate extremophilic capacity, this suggests the strong possibility that they contribute to the resilience of the overall tardigrade. *Ramazzottius varieornatus* has been documented to have superior anhydrobiotic faculties to the more extensively studied tardigrade species *H. dujardini* (Horikawa *et al*., 2008), and stronger IF networks are a potential explanation for this. It is reasonable to hypothesis that the relatively extreme environmental changes the species adapted to also prompted the radical evolution away from their fellow *Hypsibiidae* (and indeed, *Hypsibiinae*), *H. dujardini* (Yoshida *et al*., 2017; Fukuda *et al.*, 2017).

IV.8: Avenues for Further Experimentation

Having explored the *in vitro* properties of *R. varieornatus* IFs and identified a source of antibodies to bind them, the next step is a repetition of the immunofluorescence studies in Hering *et al*., 2016, to confirm their subcellular locations *R. varieornatus* IFs, especially that of cytotardin. This would allow further insights into the physiological function of cytotardin, the specifics roles of the two lamins, and the biochemical environment that the IFs are adapted to. Since the MDA-MB-231 cell line lysate did not bind to the Anti-L10112.1 antibodies found to target cytotardin (Fig.), these would represent a useful vector to recreate the Hering *et al*., 2016 exogenous expression of cytotardin. The cell lines are comparable as both MCF-7 and MDA are both epithelial cell-based, although it may be better to use MCF-7 for a more direct comparison to the original study. If further experimentation with the antibodies shows them to

be too wide-range for this line of experimentation, then there is another possibility. Confirmation of a wide range serum antibody against all three *R. varieornatus* IFs (Fig. 5.8) puts forward multiple avenues for molecular biological investigation based on which of the polyclonal antibodies can be isolated or otherwise produced monoclonally. The main possible epitope sites are common in IFs due to being near the conserved LNDR and TYRKLLEGE sites on the rod domain. Even without separation of antibodies, the serum could serve as a wide range detector of IFs for mixed protein samples and lysates.

The next most obvious avenue for further experimentation is the repetition of this study in *H. dujardini* IFs, in which the proteins of interest were initially discovered. This would answer many questions concerning the relatively high sequence divergence between the IFs of *R. varieornatus* and *H. dujardini*, and how the relatively large differences between the proteins a.a. sequences corresponds to differences in behaviour. Significant differences in behaviour, in particular at extremes of and during rapid changes in ionic composition of the solution would indicate whether the disparity in IF a.a. sequence correlates with the differences in anhydrobiotic ability between the two organisms. For example, unlike *H. dujardini*, *R. varieornatus* has the ability to enter tun state within a single hour, whereas *H. dujardini* requires up to 24 (Neves *et al*., 2020). If the differences in IF assembly speed between the species reflect this disparity, then it would support the hypothesis that the cytoplasmic IF is important for the extremophilic behaviour of the tardigrade and that extremophilic evolutionary pressure is responsible for the rapid divergence in sequence between them.

Investigation of effects on surface tension generated by cytotardin on fluid bodies it is suspended is another question in this area, as lamins are known to influence viscosity even at small concentrations (Banerjee *et al*., 2013), an effect repeatedly observed in cytotardin (Fig. 3.8). Given this effect occurs at concentrations below detectability in the bulk fluid, the surface itself may somehow promote assembly of the protein. Whilst stalagmometer methods are simplest, even in advanced forms, survismeter methods may also prove useful although this could require a high degree of precision (Chichkanov *et al*., 2002; Singh, 2008) and current survismeter technology generally does not allow for time-efficient testing.

Javadi *et al*., 2019, links concentration of IF in solution to the width of paracrystals. This could be used as a way to track relative cytotardin assembly speed, which is otherwise difficult. The speed of cytotardin assembly potentially explains the fact that significant numbers of sub-10nm

protofilament-like bodies are visible on the tail ends of cytotardin assemblies (Fig. 3.3, 3.7). The implication is that the speed of cytotardin assembly (Fig. 3.5) may restrict the supply of cytotardin material such that earlier stage forms of assembled cytotardin will be disproportionately present for lack of material to further develop them (as demonstrated conceptually by Javadi *et al*., 2019). The fact that cytotardin can do this in extreme buffer conditions (Fig. 3.7) means that could be used for a variety of such experiments without becoming assembly incompetent and could be a useful experimental model for assembly on nuclear lamins in conditions where it would not be possible to test the real thing.

IV.8.1: Chemical modification and crosslinking of cytotardin, lamins

Chemical modification may be an important mechanism for regulating *R. varieornatus* IFs *in vivo*. Phosphorylation has been demonstrated to cause IF unravelling *in vitro* (Aebi *et al*., 1988) and *in vivo* (Torvaldson *et al.,* 2015) across the IF protein family. All three *R. varieornatus* IFs have large numbers of serine and threonine residues across their structures recognised by ExPASy PROSITE as potential phosphorylation sites for this purpose.

Limited chemical modification of cytotardin has already been achieved in the LNTC mutant variant (Fig. 4.5) The situation is obscured somewhat by the evidence of breakdown products in the LNTC cytotardin caused by some interaction of the 8M urea solution and the Cu-P. The substitution of urea with guanidine hydrochloride as a chaotropes may avoid this problem. The existence of four distinct high MWt bands on the SDS-PAGE gel carries the implication of four different binding modes to the disulphide crosslinking between LNTC cytotardin monomers. This could include binding positions in a dimer-style cis-conformation and an antiparallel trans-conformation. The other two bands could be composed of either decay products still possessing the LNTC region mimicking these conformations, or by further variations in bond angles by which the disulphide cross-link could be achieved. This would provide some explanation for the variable molecular weight displayed on the SDS-PAGE.

TIPS-EBX (1-[(triisopropylsilyl)ethynyl]-1,2-benziodoxol-3(1H)-one, or Waser's reagent) - based alkynation of cytotardin and mutant variants thereof, following the protocols in Hansen *et al*., 2016, was also attempted. If successful, the alkyne group attached to either one tryptophan/cysteine or both tryptophan would form the basis of molecular labelling leading to more detailed information on the positions of cytotardin molecules within their super-molecular structures. Preliminary testing showed that efficient modification of cytotardin

requires modification of the general experimental protocol outlined in the paper, and some such research has been done by Tolnai *et al*., 2016. A potential source of problems in this procedure is potential for *R. varieornatus* proteins to retain some activity or aggregation capacity in the acetonitrile used as a secondary solvent, as the tun state, in which the cytoskeleton remains intact, is capable of protecting a tardigrade from up to 99.8% acetonitrile (Horikawa *et al*., 2008). Potentially modified cytotardin, both wild type and mutant, was found to precipitate as acetonitrile was removed from the reaction mix, though this proved useful for collecting the material.

The cysteine-bearing nature of both lamins makes them both very suitable for chemical cross-linking experiments such as in Fig. 4.5. This could even apply to a combination thereof, as disulfide cross-linking has been successfully used on heteropolymers such as in GFAP (Quinlan and Franke, 1983), vimentin and desmin (Quinlan and Franke, 1982; Quinlan *et al.*, 1986). *C. elegans*, of relatively close relation to tardigrades, also has heteropolymeric cytoplasmic IFs (Karabinos *et al*., 2019). Because tardigrade lamin 2 does not have a cysteine in the rod domain of the molecule, it was not yet possible to employ disulphide crosslinking to demonstrate the presence of two-chain 'dimer' molecules as has been done for other IF proteins (Quinlan *et al*., 1989). Given keratins 5 and 14 can be stable even in 9.5M Urea, the achievement of at least dimer formation in cytotardin at as high as 8M urea is not entirely unexpected. Given the differing mobility of crosslinked bands despite only having the opportunity to for a single crosslink per molecule excluding tetrameric crosslinking, this strongly indicates more than a single conformation in which the mutant cytotardin molecules find themselves in such close proximity. Cysteine cross-linking has been used successfully to characterise IF proteins such as keratin (Steinert *et al*., 1993a; Quinlan *et al.*, 1986), GFAP (Quinlan and Franke, 1983), vimentin and desmin (Quinlan and Franke, 1982; Quinlan *et al.*, 1986). This type of experiment shows the potential to provide further details on the assembly
Attempts at catalysis of crosslinking in Tris-HCl buffer solution without urea failed to affect the rate of disulphide crosslinking, implying that the cysteine residues in LNTC cytotardin are not accessible to each other, so Tris-urea solution was used. Disulphide crosslinks between molecules can form in significant numbers from distances at most only as far as 2nm, such that the ability for these bonds to form can be used to signify closeness of molecular arrangement between the two cysteine residues. The relatively limited nature of the crosslinked cytotardin volume implies not all configurations of interrelationship between two LNTC cytotardin may be susceptible to crosslinking.

IV.8.2: Chaperones required by Proteins of Interest

Cytotardin is a cytoplasmic IF protein that possesses the capacity for rapid organisation in conditions otherwise unsuitable for self-assembly. First documented in *H. dujardini*, (Hering *et al.*, 2016), cytotardin also appears to share aspects with other IF proteins in its capacity to form some structures whilst still exposed to urea. As in other IFs, assembly begins as before the chaotrope is fully removed from the solution, implying a high level of affinity between cytotardin at both dimer and tetramer stages typical of cytoplasmic IFs.

The capacity of cytotardin to produce globular, highly disordered reticulum in above-physiological pH, gives some indication that *in vivo*, chaperone proteins play an important role in at minimum conserving the proper shape of cytotardin for assembly, if not the assembly process itself. This is trend is repeated by cytotardin behaviour when producing paracrystals, which it forms without assistance and well in excess of the structural parameters required od an IF. Cytotardin forms paracrystals in the presence of cations (Fig. 3.4), but does not need them to do so and can form them in the presence of monovalent cations, high pH buffers or neither (Fig. 3.7). At very least the *R. varieornatus* cells would need some way of restraining the process. As with much of tardigrade biology (Neves *et al*., 2020) *R. varieornatus* IFs retain their capacities effectively to assemble *in vitro* between 5 and 25 degrees centigrade. The most complex structures and patterns can only form so long as the cytotardin is brought down in pH from 9 to 7.4 over a course of hours pH, and not left at pH 8-9 for longer than an hour (Fig. 3.3). Moreover parallels could be made to the cytoplasmic IF IFB-1 in *C elegans*, which requires Small Ubiquitin-like Modifier (or SUMO) proteins very tightly bound to its IF proteins to ensure proper behaviour and solubility in its IFB-1 cytoplasmic IF. Excessive aggregation at a µm scale has been observed in as a problem with *C. elegans* IFB-1 (Kaminsky *et al*., 2009). Potential for excessive aggregation is also abundantly clear in cytotardin, both in the form of ordered paracrystals and the inclusion bodies it forms within the bacteria used to manufacture it, so the fact that this problem in *C. elegans* only occurs upon the knockout of smo-1 responsible for SUMO chaperoning implies strongly that small chaperone proteins may have a role in moderating IF behaviour in the closely related tardigrades (Hashimoto *et al*., 2016) The lamin-like nature of cytotardin suggests that the Hsp family of chaperones might associate with it (Willsie and Clegg, 2002).

Hsp20.3 sedimented at 2400g for 5m both with cytotardin and alone (Fig. 6.2). The non-negligeable drop in cytotardin construct sedimentation occurs alongside a relative drop in Hsp20.3 sedimentation, implying that the growth of cytotardin structures may be checked by Hsp20.3. *R varieornatus* has 7 chaperone proteins in this group, and more may have preventative effects on the effects of thermal stress on cytotardin-containing structures. The non-negligeable drop in cytotardin construct sedimentation occurs alongside a relative drop in Hsp20.3 sedimentation, implying that the growth of cytotardin may be checked by Hsp20.3. Limited experimentation with Hsp20.5 was also conducted. Experimental difficulties and lack of material hampered results, but early experiments indicated that Hsp20.5 could rescue the CTD mutant phenotype's capacity to form large aggregates that it otherwise lacks compared to the wild type. If this degree of interaction can be confirmed it presents a clear avenue for investigating the role of Hsp20 chaperones in modulating the activity of cytotardin and other tardigrade IFs.

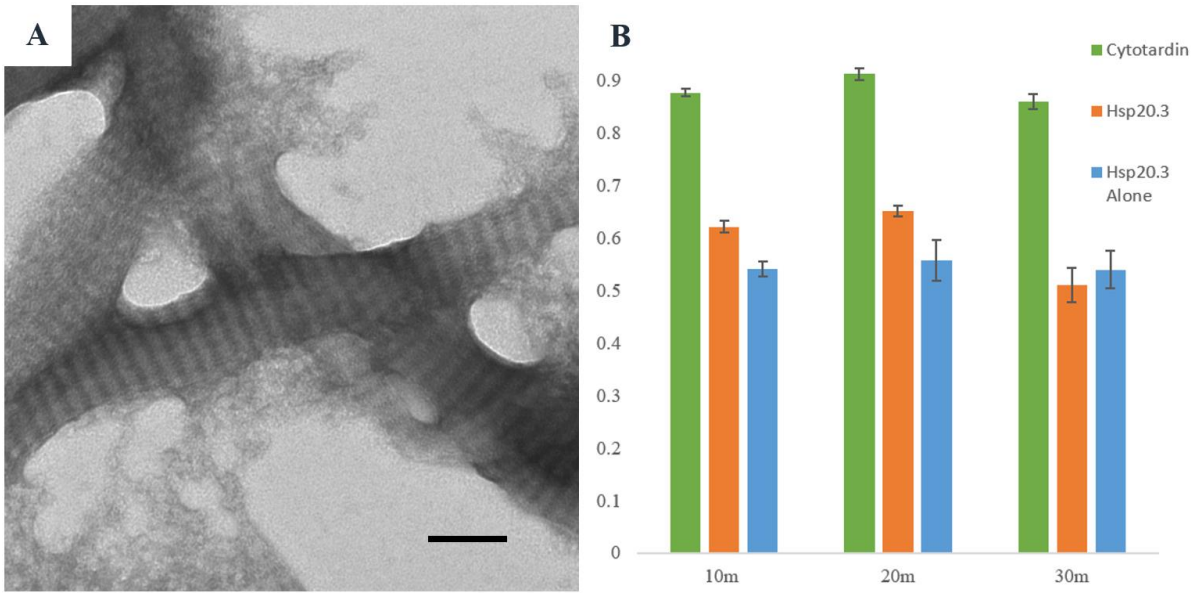

Fig. 6.2: Cytotardin with environmental stress and Hsp20 proteins

Cytotardin frozen for 1h at -20°C followed by thawing at room temperature **(A)**. Hsp20.3 sedimented at 2400g for 5m both with cytotardin and alone **(B)**. Scale bars 100nm, error bars are standard error.

The limited nature of L10112.1 structure formation (Section and Figure 3.6) also strongly implies a need for chaperone proteins, though they would not be the only IF proteins to lack the ability of self-assembly *in vivo* let alone *in vitro* (Herrmann and Aebi, 2000). The foremost

reason for this implication is that L10112.1 is an eye lens protein. Chaperone proteins such as α-crystallin, similar to small HSPs (Nicholl and Quinlan, 1994) are essential for the development of the mammalian eye lens, most densely found there, and represent an important area for further testing of L10112.1. It is a well-established capacity of chaperone proteins, for example α-B crystallin, to solubilise IF proteins (Nicholl and Quinlan, 1994). Given the tendency of suitable chaperones to solubilise IFs may lead to the effect of reducing inclusion body formation, another line of inquiry remains in co-expression of tardigrade IF and chaperone proteins (Hoffmann & Rinas, 2004) as it may prevent inclusion bodies forming to some extent and allow the proteins to be extracted in a soluble fraction of the IBP that was used in this study.

IV.8.3: *In vivo* experimentation on *R. varieornatus* IFs

Cytotardin, its mutants and the lamins form inclusion bodies when expressed in BL21 bacteria (Fig. 3.1, 4.1, 4.4), and preventing such random protein aggregation is a major function of chaperone proteins. Co-expression of *R. varieornatus* IFs alongside chaperone proteins, such as an α-B crystallin control, or the tardigrade in question's own Hsp20 chaperone proteins could provide insights into the role of such proteins, as well as potentially preventing the development of inclusion bodies (Hoffmann and Rinas, 2004).

Antibodies were purified from guinea pig and rabbit serum by Hering *et al*., in 2016 against the C-terminal regions of *H. dujardini* IFs and used for immunofluorescence staining. If those antibodies can bind *R. varieornatus* IFs, then it may show conservation of structural characteristics despite the low sequence similarity between the two. Secondly there is the possibility that similarly performing antibodies may be able to be produced from the equivalent sequences in *R. varieornatus* IFs, which would imply a functional similarity in the domains. By combining this structural and functional analysis, a more precise characterisation of the physiological and evolutionary relationship between the IFs of *R. varieornatus* and *H. dujardini* could be ascertained.

Having characterised the *in vitro* phenotypes of the two mutant varieties of *R. varieornatus* cytotardin, the question of artificially inducing those mutations in tissue cultures and even whole organisms inevitably follows. The lamins, being more widely expressed (Hering *et al*., 2016) would be easily imageable in cell culture, so potentially would also be targets for

engineering of mutations. Were these mutations to parallel those explored here, this would present an opportunity to explore the effects with additional context.

IV.8.4: Exogenous expression of *R. varieornatus* IFs

Genomic and biochemical studies have revealed that the cytoplasmic IF proteins are present in all bilaterians, with the exception of most arthropods (Bartnik and Weber, 1989; Goldstein and Gunawardena, 2000; Erber *et al*., 1998). The apparent loss of cytoplasmic IF proteins in the arthropod lineage might correlate with the acquisition of an exoskeleton (Herrmann and Strelkov, 2011; Goldstein and Gunawardena, 2000; Erber *et al*., 1998), which provides mechanical support to the arthropod epithelium in place of IFs. While isomin, the cytoplasmic IF protein of the springtail *Isotomurus maculatus* might perform a similar function to cytotardin as implied by its distribution in the intestinal epithelium in collembolans (Mencarelli *et al*., 2011), similarly to how cytotardin is distributed around the midgut in tardigrades (Hering *et al*., 2016), the localization and function of the putative lamin-derived cytoplasmic IF protein in copepods has yet to be fully understood. This ties in with the proposed function of the cytoplasmic lamins found in *C. elegans*, which have been located in potential stress sites like the internal epithelium. The transgenic cells or organism could then be tested for improved stress response. Expression of cytotardin in *I. maculatus* would serve to test cross-compatibility at a metabolic level, and would be a much closer "fit" than already successful chimeric expression experiments such as Gullmets *et al*., 2017, in which *Drosophila* displayed competence to form networks with human vimentin.

Caenorhabditis elegans is a free-living, transparent nematode model organism with 959 cells, a lifetime of 2-3 weeks, peaking about 1 mm in length. Well documented since 1974 by Sydney Brenner, this type species of its genus provides a useful benchmark and many mutated strains (Goldstein, 2018). This fellow *Ecdysozoa* to the tardigrade is the first multicellular organism to have its whole genome sequenced (Sulston *et al*., 1992), its complete cellular fate mapped (Sulston and Horvitz, 1977) and as of 2017, is the only organism to have its connectome (structure map of nervous system) completed (Hendricks and Mylonakis, 2017). *C. elegans* has cytoplasmic lamin-like proteins as well, at least four of which are vital for develop to adult stage, and another for normal adult phenotype (Karabinos *et al*., 2001). Like tardigrades, in some circumstances *C. elegans* can survive desiccation by entering dormancy (Crowe and Madin, 1974), a capacity granted to it majorly by Late Embryogenesis Abundant (LEA)

proteins (Tali *et al*., 2004; Møbjerg *et al*., 2011). *C. elegans* has long been speculated as a good comparator to tardigrade biology on account of similar sequence and insertion-deletion based phylogeny (Borner *et al*., 2014), as well as relatedness implied by 18S ribosomal DNA sequences (Aguinaldo *et al.*, 1997). *C. elegans* lamin was arguably until recently the only lamin to have been assembled into consistent 10 nm IF-like filaments *in vitro* (Karabinos *et al.*, 2003; Ben-Harush *et al.*, 2009; Grafe *et al.*, 2019). Its lamin has a relatively truncated C terminal tail domain, though not quite to the extent of cytotardin or *Ciona* Lamin, and has assembly properties which can be mimicked by the *R. varieornatus* A-type lamin in paracrystal formation (Fig. 5.2). Although requiring specific pH conditions and ions unlike cytotardin, when rapidly adjusted in those conditions in the absence of chaotropes, *C. elegans* lamin can also make rapid developments in organisation. When instantaneously adjusted to 15 mM Tris-HCl, pH 7.4, the *C. elegans* lamin assembled into short filament reticulum comparable to this in Fig. 3.3 within 5 minutes, as timescale demonstrated for cytotardin in Fig. 3.5. Addition of divalent cations showed that *C. elegans* lamin was also capable of rapidly developing paracrystals (Karabinos *et al*., 2003; Foeger *et al*., 2006). Furthermore, the Lamin of *C. elegans* has higher sequence homology to the B-lamin of *R. varieornatus* than any other than its *H dujardini* counterpart, and consequently may be a useful comparator and model to help more precisely characterise its assembly properties. Transgenic expression of *R. varieornatus* lamins and cytotardin in *C. elegans* would demonstrate of cross-compatibility between the IFs of two closely related organisms, allowing fine detail to similarities already observed *in vitro*. Not just could the *C. elegans* cells or organism be tested for altered stress response, but also improved ability to survive desiccation. Immunofluorescence using the antibodies manufactured as according to the methods of Hering *et al*., 2016 could be useful to track the locations of *R. varieornatus* IFs within the *C. elegans* cells or organism. Whether the wide-range serum antibodies examined in this study could do so, or whether they would also bind to native *C. elegans* IFs, is a line of inquiry in itself.

IV.8.5: Cryo-Electron Tomography of Cytotardin Filaments

Cryo-Electron Tomography plays an essential role in providing detailed images for IF function *in vivo* (Goldberg *et al*., 2008, Turgay *et al*., 2017). Since the location of cytotardin in tardigrades has been narrowed down to the inner epithelium by immunofluorescence when the protein was first identified (Hering *et al*., 2016), it may be possible to use techniques demonstrated in Goldberg *et al*., 2008 in order to examine the tardigrade lamin 2 *in vivo*. For

the *R. varieornatus* lamins, the *Xenopus* egg cell used in Goldberg *et al*. would be suitable, pending immunofluorescent demonstrating the lamins are incorporated into the nuclear membrane. It is not known if the structure of lamin 1 can be viewed this way, as Hering *et al*., shows lamin 1 is less tightly bound to the nuclear envelope than the lamins observed in said study. Cytotardin, associated with the inside of the cell membrane may be easier to make useable samples out of as the cell membrane may be easier to extract than nuclear envelope sections and chromatin. As a secondary options, imaging of cytotardin in tardigrade cells, or the MCF-7 cells shown in Hering *et al*. to express cytotardin could be attempted, but this would be more difficult as the procedure would have to be adapted.

IV.8.6: Partial Crystallisation of cytotardin, lamins

Crystallography is the most powerful tool for characterising the molecular structure of materials. The long, flexible nature of IFs means this was not achievable with whole molecules, but over the last 20 years a "divide and conquer" approach has been pursued in which fragments of IF proteins can be characterised.

The recent breakthroughs in exploiting the partial crystallisation of IFs follow the application of improved bioimaging and bioengineering technology (Guzenko *et al*., 2017) to principles first explored nearly 20 years ago (Strelkov *et al*., 2001). The ability to map the binding sites that enable IF assembly such as in Ahn *et al*., 2019, has led to increased understanding of the assembly processes of IFs at a molecular level. Ahn *et al*, proposed a model of lamin assembly where coiled coil formation in lamin is dictated by a combination the standard IF heptad repeat structure, kinks by bending non-helical regions, interfaced in between by hendecad repeats, 11-step extended versions of the familiar coiled-coil heptad (Parry, 2006). In Fig. 2.2 multiple potential sites for these repeats are visible and correspond as described to ends of coiled coil regions and the beginning of linker regions.

In terms of effects displayed in filament-type assembly there has been some debate about whether the A_{11} or A_{22} interaction has the major impact, though Ahn *et al*., 2019 postulates they happen near simultaneously in protofilament elongation. This interaction is postulated to occur between antiparallel pairs of dimers in Type V filaments such as Cytotardin and Lamins. Both share sequences highly similar with the 42aa sequence characteristic of IF proteins and underlying the A_{11} interaction in Lamins characterised in Lilina *et al*., 2020. The A_{11} interaction has recently been modelled by Eldirany *et al*., in 2019, using partial crystallisation of the

Keratin 1-10 heterodimer. This suggests that the molecular mechanics of the A_{11} interaction relies on hydrophobic interactions characterised by the nanoscopic morphology of the heterodimer. As such, without the relevant cryo-electron tomography to characterise such a level of structural detail in cytotardin *in vivo*, it is not yet possible to tell what exact relationship cytotardin forms observed *in vitro* bear to the *in situ* use of the protein. Likewise without partial crystallisation of cytotardin or lamin 2 fragments, the ability of the author to theorize on the characteristics of the A_{11} interaction in cytotardin is thus limited. By analysis of the residues implicated, residues 314-321 in keratin-1 forms the knob domain, 227-234 in forms the pocket domain. Cytotardin neither possesses high sequence homology to keratin 1 in its closest equivalents to the "pocket" sequence, nor in the "knob" sequence, nor generally due to the previously mentioned differences in coil 1b size between the two proteins. This fits with a contemporary model of lamin assembly in which the A_{11} interaction there is characterised as significantly weaker than in cytoplasmic IFs (Lilina *et al*., 2020). Given that guanidine hydrochloride proved especially useful in denaturing cytotardin for purification, it is possible that it may be so for the denaturation required to crystallise cytotardin fragments (Monera *et al*., 1994).

Part V: Conclusions

Expression of the IF proteins of the tardigrade *Ramazzottius varieornatus* shows three proteins; an A-type lamin 2, a B-type lamin 1 and a cytoplasmic IF discovered in 2016 called cytotardin. This protein is capable of initiating assembly in a wide variety of buffer conditions, without the need for an equilibration step to remove all chaotropes. It is shown by electron microscopy, quantified by sedimentation assay and qualified by rheometric and viscometric methods to be capable of forming multiple types of complex, mechanically impactful structure. The morphology of structures formed by cytotardin demonstrate that it is lamin-like in behaviour and self-assembly. Usually, cytotardin ultimately forms paracrystals regardless of whether cations are present, in an extreme range of environmental conditions. Cytotardin lacking all but the first 20 residues of the tail domain could not do the latter. Modification of an arginine residues in the coil 1a domain also had deleterious effects on cytotardin function and assembly. While still reliant on divalent cations for paracrystal formation, the *R. varieornatus* lamin 2 is capable of self-assembling into primitive, mechanically significant networks and paracrystals across a wide pH range. Western blot analysis shows both cytotardin and to a lesser extent the two lamins can be effectively targeted by rabbit serum antibodies against the lens IF protein, the *T. pacificus* eye lens IF L10112.1. This IF has lamin-like rod domain proportions and can self-assemble simple filaments *in vitro*. Both mutant varieties of cytotardin display altered binding to the serum, reflecting major epitope sites on the molecule. In future, the novel IFs characterised here may be of use for further experimentation in the wider field of molecular cell biology and mark further bounds as to what is possible to achieve with intermediate filaments.

Bibliography

(Aaronson and Blobel, 1975) Aaronson RP, Blobel G: Isolation of nuclear pore complexes in association with a lamina. Proc Natl Acad Sci USA. 1975, 72: 1007-1011. httpls://www.doi.org/10.1073/pnas.72.3.1007.

(Aebi *et al*., 1986) Aebi, U., Cohn, J., Buhle, L. and Gerace, L., 1986. The nuclear lamina is a meshwork of intermediate-type filaments. Nature, 323(6088), pp.560-564. https://doi.org/10.1038/323560a0

(Aebi *et al*., 1988) Aebi, U., Häner, M., Troncoso, J., Eichner, R. and Engel, A., 1988. Unifying principles in intermediate filament (IF) structure and assembly. Protoplasma, 145(2), pp.73-81.

(Aguinaldo *et al.*, 1997) Aguinaldo, A., Turbeville, J., Linford, L. *et al.* Evidence for a clade of nematodes, arthropods and other moulting animals. Nature 387, 489–493 (1997) https://doi.org/10.1038/387489a0

(Ahn *et al*., 2019) Ahn, J., Jo, I., Kang, S.M., Hong, S., Kim, S., Jeong, S., Kim, Y.H., Park, B.J. and Ha, N.C., 2019. Structural basis for lamin assembly at the molecular level. Nature communications, 10(1), pp.1-12. https://doi.org/10.1038/s41467-019-11684-x

(Angius *et al*., 2018) Angius, F., Ilioaia, O., Amrani, A., Suisse, A., Rosset, L., Legrand, A., Abou-Hamdan, A., Uzan, M., Zito, F. and Miroux, B., 2018. A novel regulation mechanism of the T7 RNA polymerase based expression system improves overproduction and folding of membrane proteins. Scientific reports, 8(1), pp.1-11. https://doi.org/10.1038/s41598-018-26668-y

(Aryal *et al*., 2006) Aryal, S., Remant, B.K.C., Dharmaraj, N., Bhattarai, N., Kim, C.H. and Kim, H.Y., 2006. Spectroscopic identification of SAu interaction in cysteine capped gold nanoparticles. *Spectrochimica Acta Part A: Molecular and Biomolecular Spectroscopy*, *63*(1), pp.160-163.

(Aufderhorst-Roberts and Koenderink, 2019) Aufderhorst-Roberts, A. and Koenderink, G.H., 2019. Stiffening and inelastic fluidization in vimentin intermediate filament networks. Soft matter, 15(36), pp.7127-7136.

(Banerjee *et al*., 2013) Banerjee A, Rathee V, Krishnaswamy R, Bhattacharjee P, Ray P, *et al*. (2013) Viscoelastic Behavior of Human Lamin A Proteins in the Context of Dilated Cardiomyopathy. PLOS ONE 8(12): e83410. https://doi.org/10.1371/journal.pone.0083410

(Beck *et al*., 2010) Beck, R., Deek, J., Choi, M.C., Ikawa, T., Watanabe, O., Frey, E., Pincus, P. and Safinya, C.R., 2010. Unconventional salt trend from soft to stiff in single neurofilament biopolymers. Langmuir, 26(24), pp.18595-18599. https://doi.org/10.1021/la103655x

(Beck *et al*., 2012) Beck, R., Deek, J. and Safinya, C.R., 2012. Structures and interactions in 'bottlebrush' neurofilaments: the role of charged disordered proteins in forming hydrogel networks. Biochemical Society Transactions, 40(5), pp.1027-1031. https://doi.org/10.1042/BST20120101

(Ben-Harush *et al*., 2009) The Supramolecular Organization of the *C. elegans* Nuclear Lamin Filament. Kfir Ben-Harush, Naama Wiesel, DaphnaFrenkiel-Krispin, Dorothee Moeller, Eyal Soreq, Ueli Aebi, Harald Herrmann, Yosef Gruenbaum, Ohad Medalia. Journal of Molecular Biology, Volume 386, Issue 5, 13 March 2009, Pages 1392-1402. https://doi.org/10.1016/j.jmb.2008.12.024

(Blobel and Gerace, 1980) Larry Gerace & Günter Blobel, The nuclear envelope lamina is reversibly depolymerized during mitosis. Cell, VOLUME 19, ISSUE 1, P277-287, JANUARY 01, 1980. https://doi.org/10.1016/0092-8674(80)90409-2

(Block, 2018) Johanna Lena Block. Stress-Strain Behavior of Single Vimentin Intermediate Filament. Göttingen Series in Biophysics; 1. January 2018. https://doi.org/ 10.17875/gup2018-1102, ISBN: 978-3-86395-373-7.

(Blumenberg, 1989) M Blumenberg, Evolution of homologous domains of cytoplasmic intermediate filament proteins and lamins., Molecular Biology and Evolution, Volume 6, Issue 1, January 1989, Pages 53–65, https://doi.org/10.1093/oxfordjournals.molbev.a040533

(Bohdan *et al*., 1992) Bohdan J. Soltys, Radhey S. Gupta. Interrelationships of endoplasmic reticulum, mitochondria, intermediate filaments, and microtubules—a quadruple fluorescence labeling study. Biochemistry and Cell Biology, 1992, 70:1174-1186, https://doi.org/10.1139/o92-163

(Bonne *et al*., 2000) Bonne, G., E. Mercuri, A. Muchir, A. Urtizberea, H. M. Becane, D. Recan, L. Merlini *et al*. "Clinical and molecular genetic spectrum of autosomal dominant Emery-Dreifuss muscular dystrophy due to mutations of the lamin A/C gene." Annals of Neurology: Official Journal of the American Neurological Association and the Child Neurology Society 48, no. 2 (2000): 170-180.

(Boothby, 2018) Boothby T.C. (2018) Molecular Biology in Tardigrades. In: Schill R. (eds) Water Bears: The Biology of Tardigrades. Zoological Monographs, vol 2. Springer, Cham

(Bramier *et al*., 2007) NucPred - Predicting Nuclear Localization of Proteins. Brameier M, Krings A, Maccallum RM. Bioinformatics, 2007. PubMed id: 17332022

(Brennich *et al*., 2014) M. E. Brennich, S. Bauch, U. Vainio, T. Wedig, H. Herrmann and S. Köster, Soft Matter, 2014, 10, 2059 —2068

(Cailleau *et al*., 1978) Cailleau R, Olive M, Cruciger QV. Long-term human breast carcinoma cell lines of metastatic origin: preliminary characterization. *In vitro*, 1978. 14(11):911– 915.

(Caprile *et al*., 2012) Caprile, L., Cossaro, A., Falletta, E., Della Pina, C., Cavalleri, O., Rolandi, R., Terreni, S., Ferrando, R., Rossi, M., Floreano, L. and Canepa, M. Interaction of L-cysteine with naked gold nanoparticles supported on HOPG: a high resolution XPS investigation. Nanoscale, 4(24), pp.7727-7734., 2012

(Chang *et al*., 2017) Chang, A.Y., Chau, V.W., Landas, J.A. and Pang, Y., 2017. Preparation of calcium competent Escherichia coli and heat-shock transformation. JEMI methods, 1, pp.22-25.

(Chapman, 1998) The Insects; Structure and Function, 4th Edition. R.F. Chapman, Cambridge University Press, 1998. ISBN 0-521-57048-4, p 403.

(Chichkanov *et al*., 2002) S.V. Chichkanov, V.E. Proskurina, V.A. Myagchenkov, "Estimation of Micelloformation, Critical Concentration for Ionogenic and Non-Ionogenic Surfactants on the Data of modified Stalagmometric Method", Butlerov Communications, vol. 3, no. 9, 2002, pp. 33–35

(Crowe, 1972) Crowe, J.H., 1972. Evaporative water loss by tardigrades under controlled relative humidities. The Biological Bulletin, 142(3), pp.407-416.

(Crowe and Madin, 1974) John H. Crowe and K. A. Madin. Transactions of the American Microscopical Society. Vol. 93, No. 4, Symposium: Perspectives on the Biology of Dormancy (Oct., 1974), pp. 513-524. https://doi.org/ 10.2307/3225155. https://www.jstor.org/stable/3225155

(Dagert and Ehrlich, 1979) Dagert, M.; Ehrlich, S. (1979). "Prolonged incubation in calcium chloride improves the competence of Escherichia coli cells". Gene. 6 (1): 23–28. https://doi.org/10.1016/0378-1119(79)90082-9. PMID 383576

(Dahlstrand *et al*., 1992) J. Dahlstrand, L.B. Zimmerman, R.D. McKay, U. Lendahl. Characterization of the human nestin gene reveals a close evolutionary relationship to neurofilaments. Journal of Cell Science 1992 103: 589-597;

(Delorenzi and Speed, 2002) MARCOIL: An HMM model for coiled-coil domains and a comparison with PSSM-based predictions. Delorenzi M, Speed T. Bioinformatics. 2002 Apr;18(4):617-25.

(Denais *et al*., 2016) Denais, C.M., Gilbert, R.M., Isermann, P., McGregor, A.L., Te Lindert, M., Weigelin, B., Davidson, P.M., Friedl, P., Wolf, K. and Lammerding, J., 2016. Nuclear envelope rupture and repair during cancer cell migration. Science, 352(6283), pp.353-358. https://www.doi.org/10.1126/science.aad7297

(Dittmer and Misteli, 2011) Dittmer, T.A., Misteli, T. The lamin protein family. Genome Biol. 2011. 12, 222. https://doi.org/10.1186/gb-2011-12-5-222

(Dodemont *et al*., 1990) H Dodemont, D Riemer, and K Weber. Structure of an invertebrate gene encoding cytoplasmic intermediate filament (IF) proteins: implications for the origin and the diversification of IF proteins. EMBO J. 1990 Dec; 9(12): 4083–4094. PMCID: PMC552181, PMID: 2249666

(Döring and Stick, 1990) Döring, V. and Stick, R. (1990), Gene structure of nuclear lamin LIII of *Xenopus laevis*; a model for the evolution of IF proteins from a lamin-like ancestor.. The EMBO Journal, 9: 4073-4081. https://doi.org/10.1002/j.1460-2075.1990.tb07629.x

(Doyère, 1842) Doyère, P.L.N. 1842. Memoires sur le tardigrade. Sur le facilité possedent les tardigrades, les rotifers, les anguilleles des toit et quelques autres animacules, de renvenir à la vie après été complement déssechées. Ann. Sci. Nat., 18: 5.

(Drozdetskiy *et al*., 2015) Alexey Drozdetskiy, Christian Cole, James Procter, Geoffrey J. Barton, JPred4: a protein secondary structure prediction server, Nucleic Acids Research, Volume 43, Issue W1, 1 July 2015, Pages W389–W394, https://doi.org/10.1093/nar/gkv332

(Elbein *et al*., 2003) Elbein AD, Pan YT, Pastuszak I, Carroll D (April 2003). "New insights on trehalose: a multifunctional molecule". Glycobiology. 13 (4): 17R–27R. https://doi.org/10.1093/glycob/cwg047. PMID 12626396

(Eldirany *et al*., 2019) Eldirany, S.A., Ho, M., Hinbest, A.J., Lomakin, I.B. and Bunick, C.G., 2019. Human keratin 1/10-1B tetramer structures reveal a knob-pocket mechanism in intermediate filament assembly. The EMBO journal, 38(11), p.e100741.

(Eldirany *et al*., 2021) Eldirany, S.A., Lomakin, I.B., Ho, M. and Bunick, C.G., 2021. Recent insight into intermediate filament structure. Current opinion in cell biology, 68, pp.132-143.

(Erber *et al*., 1999) Erber A, Riemer D, Hofemeister H, Bovenschulte M, Stick R, Panopoulou G, Lehrach H, Weber K: Characterization of the Hydra lamin and its gene: a molecular phylogeny of metazoan lamins. J Mol Evol. 1999, 49: 260-271. 10.1007/PL00006548.

(Erickson, 2009) Erickson, Harold P. “Size and shape of protein molecules at the nanometer level determined by sedimentation, gel filtration, and electron microscopy.” Biological procedures online vol. 11 32-51. 15 May. 2009, https://doi.org/10.1007/s12575-009-9008-x

(Fenelon *et al*., 2017) Fenelon, Jane C.; Renfree, Marilyn B. (2017-09-15). "The enigma of embryonic diapause". Development. 144 (18): 3199–3210. https://doi.org/10.1242/dev.148213. ISSN 1477-9129. PMID 28928280.

(Feng *et al*., 2013) Feng, X., Zhang, H., Margolick, J.B. and Coulombe, P.A., 2013. Keratin intracellular concentration revisited: implications for keratin function in surface epithelia. The Journal of investigative dermatology, 133(3), p.850.

(Fisher *et al*., 1986) Fisher DZ, Chaudhary N, Blobel G: cDNA sequencing of nuclear lamins A and C reveals primary and secondary structural homology to intermediate filament proteins. Proc Natl Acad Sci USA. 1986, 83: 6450-6454. 10.1073/pnas.83.17.6450.

(FitzGerald *et al*., 1991) Paul G. FitzGerald & Dcbra Graham (1991) Ultrastructural localization of aA-crystallin to the bovine lens fiber cell cytoskeleton, Current Eye Research, 10:5, 417-436, https://doi.org/10.3109/02713689109001750

(Foeger *et al.*, 2006) Solubility properties and specific assembly pathways of the B-type lamin from Caenorhabditis elegans. Nicole Foeger, Naama Wiesel, Dorothee Lotsch, Norbert Mücke, Laurent Kreplak, Ueli Aebid, Yosef Gruenbaum, Harald Herrmann. Journal of Structural Biology, Volume 155, Issue 2, August 2006, Pages 340-350 https://doi.org/10.1016/j.jsb.2006.03.026

(Foisner and Gerace 1993) Roland Foisner and Larry Gerace. Cell, Volume 73, Issue 7, 2 July 1993, Pages 1267-1279, Cell Integral membrane proteins of the nuclear envelope interact with lamins and chromosomes, and binding is modulated by mitotic phosphorylation. https://doi.org/10.1016/0092-8674(93)90355-T

(Freitas, 1999) Robert A. Freitas Jr., Nanomedicine, Volume I: Basic Capabilities, Landes Bioscience, Georgetown, TX, 1999

(Fukuda *et al.*, 2017) Fukuda, Y., Miura, Y., Mizohata, E. and Inoue, T., 2017. Structural insights into a secretory abundant heat-soluble protein from an anhydrobiotic tardigrade, Ramazzottius varieornatus. FEBS letters, 591(16), pp.2458-2469.

(Fukuda *et al.*, 2020) Fukuda, Y., Kim, J. and Inoue, T., 2020. Structure of cytochrome b 5 unique to tardigrades. Protein Science, 29(8), pp.1829-1835.

(Gabler *et al*., 2020) Protein Sequence Analysis Using the MPI Bioinformatics Toolkit. Gabler F, Nam SZ, Till S, Mirdita M, Steinegger M, Söding J, Lupas AN, Alva V. Curr Protoc Bioinformatics. 2020 Dec;72(1):e108. https://doi.org/ 10.1002/cpbi.108.

(Galiova *et al*., 2008) Galiova G, Bartova E, Raska I, Krejci J, Kozubek S: Chromatin changes induced by lamin A/C deficiency and the histone deacetylase inhibitor trichostatin A. Eur J Cell Biol. 2008, 87: 291-303. 10.1016/j.ejcb.2008.01.013.

(Georgatos and Blobel, 1987) Georgatos, S. D. and Blobel, G. (1987). Lamin B constitutes an intermediate filament attachment site at the nuclear envelope. J. Cell Biol. 105, 117-125. https://doi.org/10.1083/jcb.105.1.117

(Gerace *et al*., 1978) Gerace L, Blum A, Blobel G: Immunocytochemical localization of the major polypeptides of the nuclear pore complex-lamina fraction. Interphase and mitotic distribution. J Cell Biol. 1978, 79: 546-566. 10.1083/jcb.79.2.546.

(Giesler *et al.*, 1985) N. Geisler, E. Kaufmann, K. Weber. Antiparallel orientation of the two double-stranded coiled-coils in the tetrameric protofilament unit of intermediate filaments. J. Mol. Biol., 182 (1985), pp. 173+

(Glass and Gerace, 1990) Glass JR, Gerace L. Lamins A and C bind and assemble at the surface of mitotic chromosomes. J Cell Biol. 1990 Sep;111(3):1047-57. https://doi.org/ 10.1083/jcb.111.3.1047. PMID: 2202732; PMCID: PMC2116261.

(Godsel *et al*., 2008) Godsel, L.M., Hobbs, R.P. and Green, K.J., 2008. Intermediate filament assembly: dynamics to disease. Trends in cell biology, 18(1), pp.28-37.

(Gold and Fahrney, 1964) Gold AM, Fahrney D (1964). "Sulfonyl Fluorides as Inhibitors of Esterases. II. Formation and Reactions of Phenylmethanesulfonyl α-Chymotrypsin". Biochemistry. 3 (6): 783–791. https://doi.org/10.1021/bi00894a009. PMID 14211616

(Goldberg *et al*., 2008) Martin W. Goldberg, Jindriska Fiserova, Irm Huttenlauch, Reimer Stick; A new model for nuclear lamina organization. Biochem Soc Trans 1 December 2008; 36 (6): 1339–1343. https://doi.org/10.1042/BST0361339

(Goldstein, 2018) Goldstein, B., 2018. The emergence of the tardigrade *Hypsibius exemplaris* as a model system. Cold Spring Harbor Protocols, 2018(11), pp.pdb-emo102301.

(Grafe *et al.*, 2019) Grafe, Marianne; Batsios, Petros; Meyer, Irene; Lisin, Daria; Baumann, Otto; Goldberg, Martin W.; Gräf, Ralph. 2019. "Supramolecular Structures of the Dictyostelium Lamin NE81" Cells 8, no. 2: 162. https://doi.org/10.3390/cells8020162

(Grafe *et al.*, 2020) Grafe, Marianne; Hofmann, Phillip; Batsios, Petros; Meyer, Irene; Gräf, Ralph. 2020. "*In vivo* Assembly of a Dictyostelium Lamin Mutant Induced by Light, Mechanical Stress, and pH" Cells 9, no. 8: 1834. https://doi.org/10.3390/cells9081834

(Greven, 2018) Greven, H., 2018. From Johann August Ephraim Goeze to Ernst Marcus: A ramble through the history of early tardigrade research (1773 until 1929). In Water bears: The biology of tardigrades (pp. 1-55). Springer, Cham.

(Gross and Mayer, 2019) Gross Vladimir and Mayer Georg 2019 Cellular morphology of leg musculature in the water bear *Hypsibius exemplaris* (*Tardigrada*) unravels serial homologies. R. Soc. open sci.6191159. http://doi.org/10.1098/rsos.191159

(Gullmets *et al*., 2017) Gullmets, J., Torvaldson, E., Lindqvist, J., Imanishi, S.Y., Taimen, P., Meinander, A. and Eriksson, J.E. (2017), Internal epithelia in Drosophila display rudimentary competence to form cytoplasmic networks of transgenic human vimentin. Faseb, 31: 5332-5341. https://doi.org/10.1096/fj.201700332R

(Guo *et al.*, 2014) Guo, Y., Kim, Y., Shimi, T., Goldman, R.D. and Zheng, Y., 2014. Concentration-dependent lamin assembly and its roles in the localization of other nuclear proteins. Molecular biology of the cell, 25(8), pp.1287-1297.

(Gupta *et al.*, 2018) Gupta, S., Rawat, S., Arora, V. *et al*. An improvised one-step sucrose cushion ultracentrifugation method for exosome isolation from culture supernatants of mesenchymal stem cells. Stem Cell Res Ther 9, 180 (2018). https://doi.org/10.1186/s13287-018-0923-0

(Guzenko *et al*., 2017) Guzenko D., Chernyatina A.A., Strelkov S.V. (2017) Crystallographic Studies of Intermediate Filament Proteins. In: Parry D., Squire J. (eds) Fibrous Proteins: Structures and Mechanisms. Subcellular Biochemistry, vol 82. Springer, Cham

(Hansen *et al*., 2016) Hansen, M.B., Hubálek, F., Skrydstrup, T. and Hoeg-Jensen, T., 2016. Chemo-and regioselective ethynylation of tryptophan-containing peptides and proteins. Chemistry–A European Journal, 22(5), pp.1572-1576.

(Hashimoto *et al*., 2016) Hashimoto, T., Horikawa, D.D., Saito, Y., Kuwahara, H., Kozuka-Hata, H., Shin, T., Minakuchi, Y., Ohishi, K., Motoyama, A., Aizu, T. and Enomoto, A., 2016. Extremotolerant tardigrade genome and improved radiotolerance of human cultured cells by tardigrade-unique protein. Nature communications, 7(1), pp.1-14. https://doi.org/10.1038/ncomms12808

(Heitlinger *et al*., 1991) E Heitlinger, M Peter, M Häner, A Lustig, U Aebi, E A Nigg; Expression of chicken lamin B2 in Escherichia coli: characterization of its structure, assembly, and molecular interactions. J Cell Biol 1 May 1991; 113 (3): 485–495. https://doi.org/10.1083/jcb.113.3.485

(Heitlinger *et al*., 1992) E.Heitlinger M.Peter A.Lustig W.Villiger E.A.Nigg U.Aebi. The role of the head and tail domain in lamin structure and assembly: Analysis of bacterially expressed chicken Lamin A and truncated B2 lamins. Journal of Structural Biology, Volume 108, Issue 1, January–February 1992, Pages 74-91. https://doi.org/10.1016/1047-8477(92)90009-Y

(Hendricks and Mylonakis, 2017) Gabriel Hendricks & Eleftherios Mylonakis (2017) Expanding the nematode model system: The molecular basis of inflammation and infection recovery in C. elegans, Virulence, 8:3, 244-245, https://doi.org/ 10.1080/21505594.2016.1239011 PMID 838129

(Hengherr *et al*., 2008) Steffen Hengherr, Arnd G. Heyer, Heinz-R. Köhler Ralph O. Schill. Trehalose and anhydrobiosis in tardigrades – evidence for divergence in responses to dehydration. FEBS J 275: 281–288. First published: 14 December 2007 https://doi.org/10.1111/j.1742-4658.2007.06198.x

(Hering *et al*., 2016) Hering, L., Bouameur, J.E., Reichelt, J., Magin, T.M. and Mayer, G., 2016. Novel origin of lamin-derived cytoplasmic intermediate filaments in tardigrades. Elife, 5, p.e11117. https://doi.org/10.7554/eLife.11117.001

(Herrmann and Aebi, 2000) Herrmann, H. and Aebi, U., 2000. Intermediate filaments and their associates: multi-talented structural elements specifying cytoarchitecture and cytodynamics. Current opinion in cell biology, 12(1), pp.79-90.

(Herrmann and Aebi, 2004) Herrmann, H. and Aebi, U., 2004. Intermediate filaments: molecular structure, assembly mechanism, and integration into functionally distinct intracellular scaffolds. Annual review of biochemistry, 73(1), pp.749-789.

(Herrmann *et al.*, 1996) Herrmann, H., Häner, M., Brettel, M., Müller, S.A., Goldie, K.N., Fedtke, B., Lustig, A., Franke, W.W. and Aebi, U., 1996. Structure and assembly properties of the intermediate filament protein vimentin: the role of its head, rod and tail domains. Journal of molecular biology, 264(5), pp.933-953.

(Herrmann *et al*., 2004) Herrmann H, Kreplak L, Aebi U. 2004. Isolation, characterization, and *in vitro* assembly of intermediate filaments. Methods Cell Biol 78:3–24.

(Herrmann *et al*., 2007) Herrmann, H., Bar, H., Kreplak, L., Strelkov, S. V. \& Aebi, U. Intermediate filaments: from cell architecture to nanomechanics. Nat. Rev. Mol. Cell Biol. 8, 562–573 (2007).

(Herrmann *et al*., 2009) H. Herrmann, S.V. Strelkov, P. Burkhard, U. Aebi, Intermediate filaments: primary determinants of cell architecture and plasticity. J. Clin. Invest., 119, (2009), 1772– 1783.

(Hoffmann and Rinas, 2004) Hoffmann F., Rinas U. Roles of Heat-Shock Chaperones in the Production of Recombinant Proteins in Escherichia coli. In: Physiological Stress Responses in Bioprocesses. Advances in Biochemical Engineering, vol 89. Springer, Berlin, Heidelberg

(Horikawa *et al*., 2008) Daiki D. Horikawa, Takekazu Kunieda, Wataru Abe, Masahiko Watanabe, Yuichi Nakahara, Fumiko Yukuhiro, Tetsuya Sakashita, Nobuyuki Hamada, Seiichi Wada, Tomoo Funayama, Chihiro Katagiri, Yasuhiko Kobayashi, Seigo Higashi, and Takashi Okuda. Establishment of a rearing system of the extremotolerant tardigrade Ramazzottius varieornatus: a new model animal for astrobiology. Astrobiology, 8(3), pp.549-556. Astrobiology. Jun 2008.ahead of print, http://doi.org/10.1089/ast.2007.0139

(Hua *et al*., 2014) Hua, B., Han, K.Y., Zhou, R., Kim, H., Shi, X., Abeysirigunawardena, S.C., Jain, A., Singh, D., Aggarwal, V., Woodson, S.A. and Ha, T., 2014. An improved surface passivation method for single-molecule studies. Nature methods, 11(12), pp.1233-1236.

(Hutchison *et al*., 1994) C.J. Hutchison, J.M. Bridger, L.S. Cox, I.R. Kill. Weaving a pattern from disparate threads: lamin function in nuclear assembly and DNA replication. Journal of Cell Science 1994 107: 3259-3269

(Iyer and Mahalakshmi, 2019) Iyer, B.R. and Mahalakshmi, R., 2019. Hydrophobic characteristic is energetically preferred for cysteine in a model membrane protein. Biophysical journal, 117(1), pp.25-35.

(Jagadeesh *et al*., 2018) Jagadeesh, M.K., Roszkowska, M. and Kaczmarek, Ł., 2018. Tardigrade indexing approach on exoplanets. Life sciences in space research, 19, pp.13-16.

(Javadi *et al*., 2019) Javadi, A., Söderholm, N., Olofsson, A., Flärdh, K. and Sandblad, L., 2019. Assembly mechanisms of the bacterial cytoskeletal protein FilP. Life science alliance, 2(3).

(Oh *et al.*, 2009) Oh, Richard E. Lenski, F. William Studier, Patrick Daegelen, Jihyun F. Kim. Genome Sequences of Escherichia coli B strains REL606 and BL21(DE3). Journal of Molecular Biology, Volume 394, Issue 4, 2009, Pages 644-652, ISSN 0022-2836,
https://doi.org/10.1016/j.jmb.2009.09.052.

(Ji *et al*., 2019) Ji, X., Yu, Y., Ni, P. *et al*. Genome-wide identification of small heat-shock protein (HSP20) gene family in grape and expression profile during berry

development. BMC Plant Biol 19, 433 (2019) https://doi.org/10.1186/s12870-019-2031-4

(Jönsson and Persson, 2010) Jönsson KI, Persson O (2010) Trehalose in three species of desiccation tolerant tardigrades. Open Zool J 3: 1–5.

(Kamilari *et al*., 2019) Kamilari, M., Jørgensen, A., Schiøtt, M., & Møbjerg, N. (2019). Comparative transcriptomics suggest unique molecular adaptations within tardigrade lineages. BMC genomics, 20(1), 607. https://doi.org/10.1186/s12864-019-5912-x

(Kaminsky *et al*., 2009) Kaminsky, R., Denison, C., Bening-Abu-Shach, U., Chisholm, A.D., Gygi, S.P. and Broday, L., 2009. SUMO regulates the assembly and function of a cytoplasmic intermediate filament protein in C. elegans. Developmental cell, 17(5), pp.724-735.

(Kang *et al*., 2018) Kang, S.M., Yoon, M.H. and Park, B.J., 2018. Laminopathies; Mutations on single gene and various human genetic diseases. BMB reports, 51(7), p.327.

(Karabinos *et al*., 1998) Karabinos, Anton, Riemer, Dieter, Erber, Andreas and Weber, Klaus, Homologues of vertebrate type I, II and III intermediate filament (IF) proteins in an invertebrate: the IF multigene family of the cephalochordate *Branchiostoma*, FEBS Letters, 437, Published 1998. https://doi.org/ 10.1016/S0014-5793(98)01190-9

(Karabinos *et al*., 2001) Karabinos A, Schmidt H, Harborth J, Schnabel R, Weber K: Essential roles for four cytoplasmic intermediate filament proteins in Caenorhabditis elegans development. Proc Natl Acad Sci USA. 2001, 98: 7863-7868. 10.1073/pnas.121169998.

(Karabinos *et al*., 2003) Anton Karabinos, Jürgen Schünemann, Michael Meyer, Ueli Aebi, Klaus Weber, The Single Nuclear Lamin of Caenorhabditis elegans Forms *In vitro* Stable Intermediate Filaments and Paracrystals with a Reduced Axial Periodicity. Journal of Molecular Biology, Volume 325, Issue 2, 2003, Pages 241-247. ISSN 0022-2836, https://doi.org/10.1016/S0022-2836(02)01240-8.

(Karabinos *et al*., 2019) Karabinos, A., 2019. Intermediate filament (IF) proteins IFA-1 and IFB-1 represent a basic heteropolymeric IF cytoskeleton of nematodes: A molecular phylogeny of nematode IFs. Gene, 692, pp.44-53.

(Kaufmann *et al*., 1983) Kaufmann SH, Gibson W, Shaper JH. Characterization of the major polypeptides of the rat liver nuclear envelope. J Biol Chem 1983; 258:2710-9

(Kaufmann *et al.*, 1985) Kaufmann, E., Weber, K., and Geisler, N., Intermediate filament forming ability of desmin derivatives lacking either the amino-terminal 67 or the carboxy-terminal 27 residues. J. Mol. Biol., 185, 733–742 (1985).

(Kazuhiro *et al.*, 2007) Kazuhiro ISOBE, Rumi GOHARA, Toshihisa UEDA, Yozo TAKASAKI & Shoji ANDO (2007) The Last Twenty Residues in the Head Domain of Mouse Lamin A Contain Important Structural Elements for Formation of Head-to-Tail Polymers *in vitro*, Bioscience, Biotechnology, and Biochemistry, 71:5, 1252-1259, https://doi.org/ 10.1271/bbb.60674

(Kitten and Nigg, 1991) G T Kitten, E A Nigg; The CaaX motif is required for isoprenylation, carboxyl methylation, and nuclear membrane association of lamin B2.. J Cell Biol 1 April 1991; 113 (1): 13–23. https://doi.org/10.1083/jcb.113.1.13

(Kobashi, 1968) Kobashi, K., 1968. Catalytic oxidation of sulfhydryl groups by o-phenanthroline copper complex. Biochimica et Biophysica Acta (BBA)-General Subjects, 158(2), pp.239-245.

(Koenig and Gross, 2020) Koenig KM, Gross JM. Evolution and development of complex eyes: a celebration of diversity. Development. 2020 Oct 13;147(19):dev182923. https://doi.org/10.1242/dev.182923. PMID: 33051250; PMCID: PMC7578360.

(Kollmar, 2015) Martin Kollmar. Polyphyly of nuclear lamin genes indicates an early eukaryotic origin of the metazoan-type intermediate filament proteins. PMCID: PMC4448529, PMID: 26024016, Sci Rep. 2015; 5: 10652. Published online 2015 May 29. https://doi.org/10.1038/srep10652

(Kornreich *et al*., 2015) Kornreich, Micha, Avinery, Ram, Malka-Gibor, Eti, Laser-Azogui, Adi and Beck, Roy (2015), Order and disorder in intermediate filament proteins, FEBS Letters, 589, https://doi.org/10.1016/j.febslet.2015.07.024

(Kreplak *et al*., 2004) Kreplak, L., Aebi, U. and Herrmann, H., Molecular mechanisms underlying the assembly of intermediate filaments. Experimental cell research, 2004, 301(1), pp.77-83. https://doi.org/10.1016/j.yexcr.2004.08.021

(Krimm *et al*., 2002) Krimm, I., Östlund, C., Gilquin, B., Couprie, J., Hossenlopp, P., Mornon, J.P., Bonne, G., Courvalin, J.C., Worman, H.J. and Zinn-Justin, S., 2002. The Ig-like structure of the C-terminal domain of lamin A/C, mutated in muscular dystrophies, cardiomyopathy, and partial lipodystrophy. Structure, 10(6), pp.811-823.

(Krüger *et al*., 2012) Anne Krüger, Petros Batsios, Otto Baumann, Eva Luckert, Heinz Schwarz, Reimer Stick, Irene Meyer, and Ralph Gräf. Characterization of NE81, the first lamin-like nucleoskeleton protein in a unicellular organism. Molecular Biology of the CellVol. 23, No. 2. Published 2012

(Laemmli, 1970) Laemmli UK (August 1970). "Cleavage of structural proteins during the assembly of the head of bacteriophage T4". Nature. 227 (5259): 680–685. https://doi.org/10.1038/227680a0. PMID 5432063

(Lamitina and Strange, 2005) Transcriptional targets of DAF-16 insulin signalling pathway protect *C. elegans* from extreme hypertonic stress. S. Todd Lamitina and Kevin Strange. American Journal of Physiology-Cell Physiology 2005 288:2, C467-C474

(Laumer *et al*., 2019) Laumer Christopher E., Fernández Rosa, Lemer Sarah, Combosch David, Kocot Kevin M., Riesgo Ana, Andrade Sónia C. S., Sterrer Wolfgang, Sørensen Martin V. and Giribet Gonzalo 2019. Revisiting metazoan phylogeny with genomic sampling of all phylaProc. R. Soc. B.2862019083120190831. https://doi.org/10.1098/rspb.2019.0831

(Letai *et al*., 1993) Letai, A., Coulombe, P.A., McCormick, M.B., Yu, Q.C., Hutton, E. and Fuchs, E., 1993. Disease severity correlates with position of keratin point mutations in patients with epidermolysis bullosa simplex. Proceedings of the National Academy of Sciences, 90(8), pp.3197-3201.

(Lewis *et al*., 1986) S A Lewis, N J Cowan. Anomalous placement of introns in a member of the intermediate filament multigene family: an evolutionary conundrum. Molecular and Cellular Biology May 1986, 6 (5) 1529-1534; https://doi.org/ 10.1128/MCB.6.5.1529

(Li *et al.*, 2009) Li, Z., Li, X., Yu, Q. *et al*. The small heat shock protein (sHSP) genes in the silkworm, *Bombyx mori*, and comparative analysis with other insect sHSP genes. BMC Evol Biol 9, 215 (2009) https://doi.org/10.1186/1471-2148-9-215

(Lin and Worman, 1993) Lin F, Worman HJ: Structural organization of the human gene encoding nuclear lamin A and nuclear lamin C. J Biol Chem. 1993, 268: 16321-16326.

(Lin and Worman, 1995) Lin F, Worman HJ: Structural organization of the human gene (LMNB1) encoding nuclear lamin B1. Genomics. 1995, 27: 230-236. 10.1006/geno.1995.1036.

(Lin *et al*., 2010) Lin, Y.C., Yao, N.Y., Broedersz, C.P., Herrmann, H., MacKintosh, F.C. and Weitz, D.A., 2010. Origins of elasticity in intermediate filament networks. Physical review letters, 104(5), p.058101.

(Lilina *et al*., 2020) Anastasia V.Lilina, 1Anastasia A.Chernyatina1DmytroGuzenkoSergei V.Strelkov Lateral A_{11} type tetramerization in lamins. Journal of Structural Biology, Volume 209, Issue 1, 1 January 2020, 107404, Journal of Structural Biology. https://doi.org/10.1016/j.jsb.2019.10.006

(Listgarten, 1974) Listgarten, M.A., 1974. The double hemidesmosome: A new intercellular junction. American Journal of Anatomy, 141(1), pp.133-138.

(Liu *et al*., 2000) Liu, J., Ben-Shahar, T.R., Riemer, D., Treinin, M., Spann, P., Weber, K., Fire, A. and Gruenbaum, Y., 2000. Essential roles for Caenorhabditis elegans lamin gene in nuclear organization, cell cycle progression, and spatial organization of nuclear pore complexes. Molecular biology of the cell, 11(11), pp.3937-3947.

(Loewinger and McKeon, 1988) Loewinger, L. and McKeon, F. (1988), Mutations in the nuclear lamin proteins resulting in their aberrant assembly in the cytoplasm. The EMBO Journal, 7: 2301-2309. https://doi.org/10.1002/j.1460-2075.1988.tb03073.x

(Lourim and Lin 1989) Lourim D, Lin JJ. Expression of nuclear lamin A and muscle-specific proteins in differentiating muscle cells *in ovo* and *in vitro*. J Cell Biol. 1989 Aug;109(2):495-504. https://doi.org/ 10.1083/jcb.109.2.495. PMID: 2668298; PMCID: PMC2115726.

(Lowry *et al*., 1951) Lowry, O.H., Rosebrough, N.J., Farr, A.L. and Randall, R.J., 1951. Protein measurement with the Folin-phenol reagent. biol. Chem. 193, 265, 275.

(Luby-Phelps, 2000) Luby-Phelps K. Cytoarchitecture and physical properties of cytoplasm: volume, viscosity, diffusion, intracellular surface area. Int Rev Cytol. 2000 192: 189-221. p.195. PubMed ID10553280

(Ludwiczak *et al*., 2019) DeepCoil - a fast and accurate prediction of coiled-coil domains in protein sequences. Ludwiczak J, Winski A, Szczepaniak K, Alva V, Dunin-Horkawicz S. Bioinformatics. 2019 Aug 15;35(16):2790-2795.

(Lupas *et al*., 1991) Lupas, A., Van Dyke, M. and Stock, J., 1991. Predicting coiled coils from protein sequences. Science, pp.1162-1164.

(MacGowan *et al*. 2019) MacGowan, S.A., Madeira, F., Britto-Borges, T., Warowny, M., Drozdetskiy, A., Procter, J.B. and Barton, G.J., 2020. The Dundee resource for sequence analysis and structure prediction. Protein Science, 29(1), pp.277-297. https://doi.org/10.1002/pro.3783

(Maaroufi and Tanguay, 2013) Maaroufi H, Tanguay RM (2013) Analysis and Phylogeny of Small Heat Shock Proteins from Marine Viruses and Their Cyanobacteria Host. PLOS ONE 8(11): e81207. https://doi.org/10.1371/journal.pone.0081207

(Majzik *et al*., 2010) Majzik A, Fülöp L, Csapó E, Bogár F, Martinek T, Penke B, Bíró G, Dékány I. Functionalization of gold nanoparticles with amino acid, beta-amyloid peptides and fragment. *Colloids Surf B Biointerfaces*. 2010 Nov 1;81(1):235-41. https://doi.org/10.1016/j.colsurfb.2010.07.011. Epub 2010 Jul 13. PMID: 20674288.

(Makarov *et al*., 2019) Makarov, A.A., Zou, J., Houston, D.R., Spanos, C., Solovyova, A.S., Cardenal-Peralta, C., Rappsilber, J. and Schirmer, E.C., 2019. Lamin A molecular compression and sliding as mechanisms behind nucleoskeleton elasticity. Nature communications, 10(1), pp.1-17. https://doi.org/10.1038/s41467-019-11063-6

(Marisch *et al*., 2013) Marisch K, Bayer K, Scharl T, Mairhofer J, Krempl PM, Hummel K, Razzazi-Fazeli E, Striedner G. A comparative analysis of industrial Escherichia coli K-12 and B strains in high-glucose batch cultivations on process-, transcriptome- and proteome level. PLoS One. 2013 Aug 8;8(8):e70516. https://doi.org/10.1371/journal.pone.0070516. PMID: 23950949; PMCID: PMC3738542.

(McKeon *et al*., 1986) McKeon FD, Kirschner MW, Caput D. Homologies in both primary and secondary structure between nuclear envelope and intermediate filament proteins. Nature 1986; 319:463-8. https://doi.org/10.1038/319463a0

(McKeon, 1991) McKeon FD. Nuclear lamin proteins: Domains required for nuclear targeting assembly and cell-cycle-regulated dynamics. Curr Opin Cell Biol 1991; 3:82-6

(Min *et al*., 1996) Min, G.W., Tong, X.J., Chen, B., Zhang, B., Liu, Z.F., Ding, M.X. and Zhai, Z.H., 1996. Assembly of lamins in vitro. Cell Research, 6(1), pp.11-22.. https://doi.org/10.1038/cr.1996.2

(Mencarelli *et al*., 2011) Mencarelli C, Ciolfi S, Caroti D, Lupetti P, Dallai R Isomin: a novel cytoplasmic intermediate filament protein from an arthropod species. BMC Biol 9, 17. 2011.

(Meier *et al*., 1991) J. Meier, K.H. Campbell, C.C. Ford, R. Stick, C.J. Hutchison. The role of lamin LIII in nuclear assembly and DNA replication, in cell-free extracts of *Xenopus* eggs. Journal of Cell Science 1991 98: 271-279;

(Milo *et al*., 2010) Milo, R., Jorgensen, P., Moran, U., Weber, G. and Springer, M., 2010. BioNumbers—the database of key numbers in molecular and cell biology. Nucleic acids research, 38(suppl_1), pp.D750-D753.

(Møbjerg *et al*., 2011) Møbjerg, N., Halberg, K.A., Jørgensen, A., Persson, D., Bjørn, M., Ramløv, H. and Kristensen, R.M., 2011. Survival in extreme environments–on the current knowledge of adaptations in tardigrades. Acta Physiologica, 202(3), pp.409-420.

(Moir *et al*., 1991) R.D. Moir, A.D. Donaldson, M. Stewart. Expression in Escherichia coli of human lamins A and C: influence of head and tail domains on assembly properties and paracrystal formation. Journal of Cell Science 1991 99: 363-372; https://doi.org/10.1242/jcs.99.2.363

(Monera *et al*., 1994) Monera, O.D., Kay, C.M. and Hodges, R.S. (1994), Protein denaturation with guanidine hydrochloride or urea provides a different estimate of stability depending on the contributions of electrostatic interactions. Protein Science, 3: 1984-1991. https://doi.org/10.1002/pro.5560031110

(Monkos, 1996) Monkos, K., 1996. Viscosity of bovine serum albumin aqueous solutions as a function of temperature and concentration. International journal of biological macromolecules, 18(1-2), pp.61-68.

(Neves *et al*., 2020) Neves, R.C., Hvidepil, L.K.B., Sørensen-Hygum, T.L. *et al*. Thermotolerance experiments on active and desiccated states of *Ramazzottius varieornatus* emphasize that tardigrades are sensitive to high temperatures. Sci Rep 10, 94 (2020). https://doi.org/10.1038/s41598-019-56965-z

(Nicholl and Quinlan, 1994) lain D.Nicholl and Roy A. Quinlan, The EMBO Journal vol.13 no.4 pp.945-953, 1994. Chaperone activity of α-crystallins modulates
intermediate filament assembly. Department of Biochemistry, The University, Dundee DD1 4HN, UK

(Nikolova *et al*., 2004) Nikolova V, Leimena C, McMahon AC, Tan JC, Chandar S, Jogia D, Kesteven SH, Michalicek J, Otway R, Verheyen F, Rainer S, Stewart CL, Martin D, Feneley MP, Fatkin D: Defects in nuclear structure and function promote dilated cardiomyopathy in lamin A/C-deficient mice. J Clin Invest. 2004, 113: 357-369.

(Omary *et al*., 2004) Omary, M.B., Coulombe, P.A. and McLean, W.I., 2004. Intermediate filament proteins and their associated diseases. New England Journal of Medicine, 351(20), pp.2087-2100. https://doi.org/10.1056/NEJMra040319

(Pace *et al*., 2010) C Nick Pace,1,2,* Beatrice M P Huyghues-Despointes,2 Hailong Fu,1 Kazufumi Takano,3,4 J Martin Scholtz,1,2 and Gerald R Grimsley. Urea denatured state ensembles contain extensive secondary structure that is increased in hydrophobic proteins. Protein Sci. 2010 May; 19(5): 929–943. Published online 2010 Mar 2. https://doi.org/ 10.1002/pro.370. PMCID: PMC2868236. PMID: 20198681

(Parry *et al*., 1977) Parry, D.A.D., Crewther, W.G., Fraser, R.D.B. and MacRae, T.P., 1977. Structure of α-keratin: structural implication of the amino acid sequences of the type I and type II chain segments. Journal of molecular biology, 113(2), pp.449-454.

(Parry, 2006) Parry, D.A., 2006. Hendecad repeat in segment 2A and linker L2 of intermediate filament chains implies the possibility of a right-handed coiled-coil structure. Journal of structural biology, 155(2), pp.370-374.

(Parry and Steinert, 1999) Parry, D.A. and Steinert, P.M., 1999. Intermediate filaments: molecular architecture, assembly, dynamics and polymorphism. Quarterly reviews of biophysics, 32(2), pp.99-187.

(Pekny and Lane, 2007) Milos Pekny, E. Birgitte Lane, Intermediate filaments and stress, Experimental Cell Research. Volume 313, Issue 10, 2007, Pages 2244-2254, ISSN 0014-4827. https://doi.org/10.1016/j.yexcr.2007.04.023.

(Perng *et al*., 1999) Perng, M.D., Cairns, L., Van Den IJssel, P., Prescott, A., Hutcheson, A.M. and Quinlan, R.A., 1999. Intermediate filament interactions can be altered by HSP27 and alphaB-crystallin. Journal of cell science, 112(13), pp.2099-2112. https://doi.org/10.1242/jcs.112.13.2099

(Perng *et al*., 2004) Perng, M.D., Wen, S.F., van den IJssel, P., Prescott, A.R. and Quinlan, R.A., 2004. Desmin aggregate formation by R120G αB-crystallin is caused by altered filament interactions and is dependent upon network status in cells. Molecular biology of the cell, 15(5), pp.2335-2346. https://doi.org/10.1091/mbc.e03-12-0893

(Pilato *et al*., 2011) Pilato, G., Kiosya, Y., Lisi, O., Inshina, V. and Biserov, V., 2011. Annotated list of *Tardigrada* records from Ukraine with the description of three new species. Zootaxa, 3123(1), pp.1-31.

(Platzer *et al*., 1999) Platzer, E.G., Wang, W., Thompson, S.N. and Borchardt, D.B., 1999. Arginine kinase and phosphoarginine, a functional phosphagen, in the rhabditoid nematode *Steinernema carpocapsae*. The Journal of parasitology, pp.603-607.

(Pol *et al*., 2012) Edwin van der Pol, Anita N. Böing, Paul Harrison, Augueste Sturk and Rienk Nieuwland. 2012. Vescicles in Health and Disease. Pharmacological Reviews July 1, 2012, 64 (3) 676-705; https://doi.org/10.1124/pr.112.005983

(Porcelli *et al*., 2005) Porcelli AM, Ghelli A, Zanna C, Pinton P, Rizzuto R, Rugolo M. pH difference across the outer mitochondrial membrane measured with a green fluorescent protein mutant. Biochem Biophys Res Commun. 2005 Jan 28 326(4):799-804. p.801 right column 2nd paragraph and p.802 fig.3PubMed ID15607740

(Powers *et al*., 2002) Powers JC, Asgian JL, Ekici OD, James KE (2002). "Irreversible inhibitors of serine, cysteine, and threonine proteases". Chem. Rev. 102 (12): 4735–4736. https://doi.org/10.1021/cr010182v. PMID 12475205.

(Quinlan and Franke, 1982) R A Quinlan, W W Franke. Heteropolymer filaments of vimentin and desmin in vascular smooth muscle tissue and cultured baby hamster kidney cells demonstrated by chemical crosslinking. Proceedings of the National Academy of Sciences Jun 1982, 79 (11) 3452-3456; https://doi.org/10.1073/pnas.79.11.3452

(Quinlan and Franke, 1983) QUINLAN, R.A. and FRANKE, W.W. (1983), Molecular Interactions in Intermediate-Sized Filaments Revealed by Chemical Cross-Linking. European Journal of Biochemistry, 132: 477-484. https://doi.org/10.1111/j.1432-1033.1983.tb07386.x

(Quinlan *et al.*, 1986) Quinlan, R.A., Hatzfeld, M., Franke, W.W., Lustig, A., Schulthess, T. and Engel, J., 1986. Characterization of dimer subunits of intermediate filament proteins. Journal of molecular biology, 192(2), pp.337-349.

(Quinlan *et al*., 1989) Quinlan, R.A., Moir, R.D. and Stewart, M.U.R.R.A.Y., 1989. Expression in Escherichia coli of fragments of glial fibrillary acidic protein: characterization, assembly properties and paracrystal formation. Journal of Cell Science, 93(1), pp.71-83.

(Quinlan *et al*., 1996) Quinlan, R.A., Carte, J.M., Sandilands, A. and Prescott, A.R., 1996. The beaded filament of the eye lens: an unexpected key to intermediate filament structure and function. *Trends in cell biology*, *6*(4), pp.123-126. https://doi.org/10.1016/0962-8924(96)20001-7

(Reuner *et al*., 2010) Reuner, A., Hengherr, S., Mali, B. *et al.* Cell Stress and Chaperones (2010) 15: 423. https://doi.org/10.1007/s12192-009-0158-1

(Riemer *et al*., 1994) Riemer D, Weber K: The organization of the gene for Drosophila lamin C: limited homology with vertebrate lamin genes and lack of homology versus the Drosophila lamin Dmo gene. Eur J Cell Biol. 1994, 63: 299-306.

(Riemer and Weber, 1994) Riemer D, Weber K: The organization of the gene for Drosophila lamin C: limited homology with vertebrate lamin genes and lack of homology versus the Drosophila lamin Dmo gene. Eur J Cell Biol. 1994, April, 63: 299-306.

(Riemer and Weber, 1998) Riemer D, Weber K: Common and variant properties of intermediate filament proteins from lower chordates and vertebrates; two proteins from the tunicate Styela and the identification of a type III homologue. J Cell Sci. 1998, 111: 2967-2975.

(Rodgers *et al.*, 1996) Rogers, K.R., Herrmann, H. and Franke, W.W., 1996. Characterization of disulfide crosslink formation of human vimentin at the dimer, tetramer, and intermediate filament levels. Journal of structural biology, 117(1), pp.55-69.

(Ruan *et al*., 2012) Crystal structures of the coil 2B fragment and the globular tail domain of human lamin B1. Ruan J, Xu C, Bian C, Lam R, Wang JP, Kania J, Min J, Zang J. FEBS Lett. 586, 314-8, (2012). View articlePMID: 22265972

(Sawada *et al*., 1995) K. Sawada, J. Agata, G. Eguchi, Roy Quinlan & H. Maisel (1995) The predicted structure of chick lens CP49 and a variant thereof, CP49ins, the first vertebrate cytoplasmic intermediate filament protein with a lamin-like insertion in helix 1B, Current Eye Research, 14:7, 545-553, https://doi.org/10.3109/02713689508998401

(Scharner *et al*., 2011) Scharner, J., Brown, C.A., Bower, M., Iannaccone, S.T., Khatri, I.A., Escolar, D., Gordon, E., Felice, K., Crowe, C.A., Grosmann, C. and Meriggioli, M.N., 2011. Novel LMNA mutations in patients with Emery-Dreifuss muscular dystrophy and functional characterization of four LMNA mutations. Human mutation, 32(2), pp.152-167.

(Schwaiger *et al*., 2002) Schwaiger, I., Sattler, C., Hostetter, D. *et al*. The myosin coiled-coil is a truly elastic protein structure. Nature Mater 1, 232–235 (2002). https://doi.org/10.1038/nmat776

(Shiraishi, n.d., ret. 2020) Shiraishi, H. (n.d.). Transformation of *E. coli* by calcium chloride method. http://kuchem.kyoto-u.ac.jp/seika/shiraishi/protocols/competent_cell.html

(Siezen, 1982) Siezen, R.J., 1982. Squid lens cytoskeleton and membrane proteins. Current eye research, 2(9), pp.579-590.

(Singh, 2008) Singh, M., Survismeter for simultaneous viscosity and surface tension study for molecular interactions. Surf. Interface Anal. 2008, 40: 15-21. https://doi.org/10.1002/sia.2663

(Slonczewski *et al*., 2009) Slonczewski, Joan; Foster, John Watkins (2009). Microbiology: An Evolving Science. New York: W.W. Norton. ISBN 9780393978575

(Smith and Seegan, 1984) Smith, C.A. and Seegan, G.W., 1984. The pleated sheet: an unusual negative-staining method for transmission electron microscopy of biological macromolecules. Journal of ultrastructure research, 89(2), pp.111-122.

(Smith *et al*., 1985) Smith, P.E., Krohn, R.I., Hermanson, G.T., Mallia, A.K., Gartner, F.H., Provenzano, M., Fujimoto, E.K., Goeke, N.M., Olson, B.J. and Klenk, D.C., 1985. Measurement of protein using bicinchoninic acid. Analytical biochemistry, 150(1), pp.76-85.

(Smithies, 1965) Smithies O. Disulfide-bond cleavage and formation in proteins. Science. 1965 Dec 17;150(3703):1595-8. https://doi.org/10.1126/science.150.3703.1595. PMID: 5866656.

(Soellner *et al.*, 1985) Soellner, P., Quinlan, R.A. and Franke, W.W., 1985. Identification of a distinct soluble subunit of an intermediate filament protein: tetrameric vimentin from living cells. Proceedings of the National Academy of Sciences, 82(23), pp.7929-7933.

(Stalmans *et al*., 2020) Stalmans, G., Lilina, A.V., Vermeire, P.J., Fiala, J., Novák, P. and Strelkov, S.V., 2020. Addressing the molecular mechanism of longitudinal lamin assembly using chimeric fusions. Cells, 9(7), p.1633. https://doi.org/10.3390/cells9071633

(Steinert and Roop, 1988) Steinert, P.M. and Roop, D.R., 1988. Molecular and cellular biology of intermediate filaments. Annual review of biochemistry, 57(1), pp.593-625.

(Steinert *et al*., 1983) Steinert, P.M., Rice, R.H., Roop, D.R., Trus, B.L. and Steven, A.C., 1983. Complete amino acid sequence of a mouse epidermal keratin subunit and implications for the structure of intermediate filaments. Nature, 302(5911), pp.794-800.

(Steinert *et al*., 1993a) Steinert, P.M., Marekov, L.N., Fraser, R.B. and Parry, D.A., 1993. Keratin intermediate filament structure: crosslinking studies yield quantitative information on molecular dimensions and mechanism of assembly. Journal of molecular biology, 230(2), pp.436-452.

(Steinert *et al*., 1993b) Steinert, P.M., Marekov, L.N. and Parry, D.A., 1993. Diversity of intermediate filament structure. Evidence that the alignment of coiled-coil molecules in vimentin is different from that in keratin intermediate filaments. Journal of Biological Chemistry, 268(33), pp.24916-24925.

(Stick, 1988) Stick R. cDNA cloning of the developmentally regulated lamin L-III of Xenuopus laevis . EMBO J 1988; 7:3189-97

(Stick, 1992) Stick R: The gene structure of *Xenopus* nuclear lamin A: a model for the evolution of A-type from B-type lamins by exon shuffling. Chromosoma. 1992, 101: 566-574. 10.1007/BF00660316.

(Strelkov *et al*., 2001) Strelkov, S.V., Herrmann, H., Geisler, N., Lustig, A., Ivaninskii, S., Zimbelmann, R., Burkhard, P. and Aebi, U., 2001. Divide-and-conquer crystallographic approach towards an atomic structure of intermediate filaments. Journal of molecular biology, 306(4), pp.773-781.

(Strelkov *et al*., 2003) Sergei V. Strelkov, Harald Herrmann, Ueli Aebi. “Molecular architecture of intermediate filaments”, 20 February 2003 https://doi.org/10.1002/bies.10246

(Strelkov *et al*., 2004) Sergei V. Strelkov, Jens Schumacher, Peter Burkhard, Ueli Aebi, Harald Herrmann. Crystal Structure of the Human Lamin A Coil 2B Dimer: Implications for the Head-to-tail Association of Nuclear Lamins. Volume 343, Issue 4, 29 October 2004, Pages 1067-1080. Journal of Molecular Biology. https://doi.org/10.1016/j.jmb.2004.08.093

(Sullivan *et al*., 1999) Sullivan T, Escalante-Alcalde D, Bhatt H, Anver M, Bhat N, Nagashima K, Stewart CL, Burke B: Loss of A-type lamin expression compromises nuclear envelope integrity leading to muscular dystrophy. J Cell Biol. 1999, 147: 913-920. 10.1083/jcb.147.5.913.

(Sulston and Horvitz, 1977) J.E.Sulston, H.R.Horvitz. Post-embryonic cell lineages of the nematode, Caenorhabditis elegans. Developmental Biology Volume 56, Issue 1, March 1977, Pages 110-156 https://doi.org/10.1016/0012-1606(77)90158-0

(Sulston *et al*., 1992) Sulston, J., Du, Z., Thomas, K., Wilson, R., Hillier, L., Staden, R., Halloran, N., Green, P., Thierry-Mieg, J., Qiu, L. and Dear, S., 1992. The C. elegans genome sequencing project: a beginning. Nature, 356(6364), pp.37-41.

(Taimen *et al*., 2009) Pekka Taimen,a,1 Katrin Pfleghaar,a,1 Takeshi Shimi,a Dorothee Möller,b Kfir Ben-Harush,c Michael R. Erdos,d Stephen A. Adam,a Harald Herrmann,b Ohad Medalia,c Francis S. Collins,d,2 Anne E. Goldman,a and Robert D. Goldmana. A progeria mutation reveals functions for lamin A in nuclear assembly, architecture, and chromosome organization. Proc Natl Acad Sci U S A. 2009 Dec 8; 106(49): 20788–20793. Published online 2009 Nov 19. PMCID: PMC2779830, PMID: 19926845, Cell Biology. https://doi.org/ 10.1073/pnas.0911895106

(Takahashi *et al*., 1981) TAKAHASHI, M.A., TAKANO, M. and ASADA, K., 1981. Tris-induced cross-linking of thylakoid peptides; thiol oxidation catalyzed by Tris-Cu2+ complexes as a possible mechanism. The Journal of Biochemistry, 90(1), pp.87-94.

(Tali *et al*., 2004) Tali Z. Gal Itamar Glazer Hinanit Koltai. “An LEA group 3 family member is involved in survival of *C. elegans* during exposure to stress”, First published: 06 October 2004. https://doi.org/10.1016/j.febslet.2004.09.049, PMID 15527756

(Tauber *et al*., 1986) Tauber, M.J., Tauber, C.A., Masaki, S. (1986) Seasonal Adaptations of Insects. Oxford University Press

(Tenga and Medalia, 2020) Tenga, R. and Medalia, O., 2020. Structure and unique mechanical aspects of nuclear lamin filaments. Current Opinion in Structural Biology, 64, pp.152-159.

(Thermo Scientific, 2013) Thermo Scientific Web Archive March 23 2013. https://web.archive.org/web/20130323022558/http://phadia.com/en/Allergen-information/ImmunoCAP-Allergens/Food-of-Animal-Origin/Mollusks/Pacific-Flying-Squid

(Thermo Fisher, 2021) https://www.thermofisher.com/uk/en/home/brands/thermo-scientific/molecular-biology/thermo-scientific-nucleic-acid-electrophoresis-purification/dna-electrophoresis-thermo-scientific/dna-ladders-thermo-scientific/generuler-dna-ladders.html#guide. Retrieved 2021.

(Thompson *et al*., 2012) Journal of Endodontics Volume 38, Issue 1, January 2012, Pages 62-65. Inhibition of Endogenous Dentin Matrix Metalloproteinases by Ethylenediaminetetraacetic Acid. Jeremy M. Thompson, Kelli Agee, Stephanie Sidow, Kathleen McNally, Kimberly Lindsey, James Borke, Mohammed Elsalanty, Franklin R. Tay, David H. Pashley, https://doi.org/10.1016/j.joen.2011.09.005

(Tolnai *et al*., 2016) Tolnai, G.L., Brand, J.P. and Waser, J., 2016. Gold-catalyzed direct alkynylation of tryptophan in peptides using TIPS-EBX. Beilstein journal of organic chemistry, 12(1), pp.745-749.

(Tomarev and Zinovieva, 1990) Tomarev S.I., Zinovieva R.D. (1990) Gene Families Coding for the Eye Lens Proteins of Cephalopods. In: Harris J.R., Zbarsky I.B. (eds) Nuclear Structure and Function. Springer, Boston, MA. https://doi.org/10.1007/978-1-4613-0667-2_28

(Tomarev *et al*., 1993) Tomarev, S.I., Zinovieva, R.D. and Piatigorsky, J., 1993. Primary structure and lens-specific expression of genes for an intermediate filament protein and a β-tubulin in cephalopods. Biochimica et Biophysica Acta (BBA)-Gene Structure and Expression, 1216(2), pp.245-254. https://doi.org/ 10.1016/0167-4781(93)90151-3. PMID: 8241265.

(Torvaldson *et al*., 2015) Elin Torvaldson, Vitaly Kochin & John E Eriksson (2015) Phosphorylation of lamins determine their structural properties and signaling functions, Nucleus, 6:3, 166-171, https://doi.org/ 10.1080/19491034.2015.1017167

(Traub *et al*., 1986) Traub, P., Perides, G., Schimmel, H. and Scherbarth, A., 1986. Interaction in vitro of nonepithelial intermediate filament proteins with total cellular lipids, individual phospholipids, and a phospholipid mixture. Journal of Biological Chemistry, 261(23), pp.10558-10568.

(Tumanov *et al*., 2020) Tumanov, D.V., 2020. Integrative redescription of Hypsibius pallidoides Pilato *et al*., 2011 (*Eutardigrada: Hypsibioidea*) with the erection of a new genus and discussion on the phylogeny of Hypsibiidae. European Journal of Taxonomy, (681).

(Turgay *et al*., 2017) Yagmur Turgay, Matthias Eibauer, Anne E. Goldman, Takeshi Shimi, Maayan Khayat, Kfir Ben-Harush, Anna Dubrovsky-Gaupp, K. Tanuj Sapra, Robert D. Goldman & Ohad Medalia. 2017. The molecular architecture of lamins in somatic cells. Nature 543, 261–264.

(Valentine *et al*., 1968) Valentine, R.C., Shapiro, B.M. and Stadtman, E.R., 1968. Regulation of glutamine synthetase. XII. Electron microscopy of the enzyme from Escherichia coli. Biochemistry, 7(6), pp.2143-2152.

(Vergnes *et al*., 2004) Vergnes, L., Péterfy, M., Bergo, M.O., Young, S.G. and Reue, K., 2004. Lamin B1 is required for mouse development and nuclear integrity. *Proceedings of the National Academy of Sciences*, *101*(28), pp.10428-10433.

(Wang *et al*., 2000) Wang, J., Karabinos, A., Schünemann, J., Riemer, D. and Weber, K., 2000. The epidermal intermediate filament proteins of tunicates are distant keratins; a polymerisation-competent hetero coiled coil of the Styela D protein and Xenopus keratin 8. European journal of cell biology, 79(7), pp.478-487. https://doi.org/10.1078/0171-9335-00069

(Weber *et al.*, 1989) Weber, K., Plessmann, U. and Ulrich, W. (1989), Cytoplasmic intermediate filament proteins of invertebrates are closer to nuclear lamins than are vertebrate intermediate filament proteins; sequence characterization of two muscle

proteins of a nematode. The EMBO Journal, 8: 3221-3227. https://doi.org/10.1002/j.1460-2075.1989.tb08481.x

(Welnicz *et al*., 2011) Welnicz, W., Grohme, MA., Kaczmarek, L., Schill, RO., and Frohme, M. (2011), 'Anhydrobiosis in Tardigrades- The Last Decade', Journal of Insect Physiology, vol. 57, pp. 577-583

(Wessel and Flügge, 1984) Wessel, D.M. and Flügge, U.I., 1984. A method for the quantitative recovery of protein in dilute solution in the presence of detergents and lipids. Analytical biochemistry, 138(1), pp.141-143.

(Westh and Ramløv, 1991) Westh P, Ramløv H (1991) Trehalose accumulation in the tardigrade *Adorybiotus coronifer* during anhydrobiosis. Journal of Experimental Zoology 258: 303–311.

(Wilfinger *et al*., 1997) William W. Wilfinger, Karol Mackey, and Piotr. Chomczynski, Effect of pH and Ionic Strength on the Spectrophotometric Assessment of Nucleic Acid Purity: BioTechniques 22:474-481 (March 1997.)

(Willsie and Clegg, 2002) Julia K. Willsie James S. Clegg. Small heat shock protein p26 associates with nuclear lamins and HSP70 in nuclei and nuclear matrix fractions from stressed cells. 09 January 2002 https://doi.org/10.1002/jcb.10040

(Wood *et al*., 2003) Wood, P., Baty, D.U., Lane, E.B. and McLean, W.H., 2003. Long-range polymerase chain reaction for specific full-length amplification of the human keratin 14 gene and novel keratin 14 mutations in epidermolysis bullosa simplex patients. The Journal of investigative dermatology, 120(3), pp.495-497.

(Wright, 2001) Jonathan C. Wright, Cryptobiosis 300 Years on from van Leuwenhoek: What Have We Learned about Tardigrades?, Zoologischer Anzeiger - A Journal of Comparative Zoology, Volume 240, Issues 3–4, 2001, Pages 563-582, ISSN 0044-5231, https://doi.org/10.1078/0044-5231-00068.

(Worman, 2012) Worman, H. J. (2012). Nuclear lamins and laminopathies. J. Pathol. 226, 316-325. https://doi.org/10.1002/path.2999

(Yamaguchi *et al*., 2012) Yamaguchi A, Tanaka S, Yamaguchi S, Kuwahara H, Takamura C, Imajoh-Ohmi S, *et al.* (2012) Two Novel Heat-Soluble Protein Families Abundantly Expressed in an Anhydrobiotic Tardigrade. PLoS ONE 7(8): e44209. https://doi.org/10.1371/journal.pone.0044209

(Yoshida *et al*., 2017) Comparative genomics of the tardigrades *Hypsibius dujardini* and Ramazzottius varieornatus. Yoshida Y, Koutsovoulos G, Laetsch DR, Stevens L, Kumar S, *et al*. (2017) Comparative genomics of the tardigrades *Hypsibius dujardini* and Ramazzottius varieornatus. PLOS Biology 15(7): e2002266. https://doi.org/10.1371/journal.pbio.2002266

(Zaner *et al.*, 1982) Zaner KS, Stossel TP. Some perspectives on the viscosity of actin filaments. J Cell Biol. 1982 Jun;93(3):987-91. https://doi.org/ 10.1083/jcb.93.3.987. PMID: 6889602; PMCID: PMC2112123.

(Zimek *et al*., 2002) Zimek, A. and Weber, K., 2002. The gene for a cytoplasmic intermediate filament (IF) protein of the hemichordate *Saccoglossus kowalevskii*; definition of the unique features of chordate IF proteins. Gene, 288(1-2), pp.187-193.

(Zimmerman *et al*., 2018) Zimmermann L, Stephens A, Nam SZ, Rau D, Kübler J, Lozajic M, Gabler F, Söding J, Lupas AN, Alva V. A Completely Reimplemented MPI Bioinformatics Toolkit with a New HHpred Server at its Core. J Mol Biol. 2018 Jul 20. S0022-2836(17)30587-9.

(Zhang *et al*., 2015) Zhang, Z., Kuipers, G., Niemiec, Ł. *et al*. High-level production of membrane proteins in *E. coli* BL21(DE3) by omitting the inducer IPTG. Microb Cell Fact 14, 142 (2015). https://doi.org/10.1186/s12934-015-0328-z

(Zhou *et al*., 2014) Zhou Jun, Hailing Liu, Yile Chen, Jiye Wen, Long Li and Xiaoying Wu, 2014. Expression and significance of VEGF and miR-205 and target proteins Ezrin and Lamin A / C in ovarian cancer. Journal of Central South University (Medical Science), 39 (2), pp.142-150.

(Zhou *et al*., 2021) Zhou, X., Lin, Y., Kato, M., Mori, E., Liszczak, G., Sutherland, L., Sysoev, V.O., Murray, D.T., Tycko, R. and McKnight, S.L., 2021. Transiently structured head domains control intermediate filament assembly. Proceedings of the National Academy of Sciences, 118(8). https://doi.org/10.1073/pnas.2022121118